MOLETRACK SCARPS TO MOUNTAINS: QUATERNARY TECTONICS OF THE

CENTRAL ALASKA RANGE

by

SEAN PATRICK BEMIS

A DISSERTATION

Presented to the Department of Geological Sciences
and the Graduate School of the University of Oregon
in partial fulfillment of the requirements
for the degree of
Doctor of Philosophy

March 2010

University of Oregon Graduate School

Confirmation of Approval and Acceptance of Dissertation prepared by:

Sean Bemis

Title:

"Moletracks Scarps to Mountains: Quaternary Tectonics of the Central Alaska Range"

This dissertation has been accepted and approved in partial fulfillment of the requirements for the Doctor of Philosophy degree in the Department of Geological Sciences by:

Ray Weldon, Chairperson, Geological Sciences
Joshua Roering, Member, Geological Sciences
David Schmidt, Member, Geological Sciences
Douglas Kennett, Outside Member, Anthropology

and Richard Linton, Vice President for Research and Graduate Studies/Dean of the Graduate School for the University of Oregon.

March 20, 2010

Original approval signatures are on file with the Graduate School and the University of Oregon Libraries.

An Abstract of the Dissertation of

Sean Patrick Bemis   for the degree of   Doctor of Philosophy

in the Department of Geological Sciences

to be taken   March 2010

Title: MOLETRACK SCARPS TO MOUNTAINS: QUATERNARY TECTONICS OF

THE CENTRAL ALASKA RANGE

Approved: _____

Dr. Ray J. Weldon

Deformation across plate boundaries often occurs over broad zones with relative

motions between plates typically accommodated by faults of different styles acting

together in a complex system. Collision of the Yakutat microplate within the Alaskan

portion of the Pacific–North America plate boundary drives deformation over 600 km

away where the Denali fault divides predominantly rigid crustal block motions of

southern Alaska from distributed deformation in central Alaska. Quaternary geologic

mapping along the Nenana River valley and the Japan Hills of the northern foothills of

the Alaska Range defines zones of Quaternary thrust faulting recorded in the progressive

deformation of Pleistocene fluvial terraces. I use topographic profiles of these terraces

and paleoseismic trenching of fault scarps to characterize the Quaternary activity and

constrain the subsurface geometry of these faults. Radiocarbon and cosmogenic exposure

dating methods provide age control on the stratigraphy in the trenches and landforms

offset by these faults. These observations define a 1 - 1.5 mm/yr slip rate for the Gold King fault which changes laterally from a north-vergent thrust into a north and south vergent thrust wedge that uplifts the Japan Hills. Along the Nenana River valley, the progressive deformation of Pleistocene surfaces defines a north-vergent critically-tapered thrust wedge. The geometry of progressive uplift and folding requires a near planar, south-dipping basal thrust fault with two major north-dipping backthrusts. All three faults were active simultaneously on a scale of 10^4 yrs with slip rates of 0.25 - 1 mm/yr, until the late Pleistocene when we infer the retreat of glacial ice from the main axis of the Alaska Range caused a change in thrust wedge dynamics. I use the orientation of Quaternary deformation north of the Denali fault to show that strain is highly partitioned and establish geologic constraints on the regional horizontal stress orientation. North of the Denali fault, fault-normal principal shortening accommodates 3-5 mm/yr of strain transfer across the Denali fault system. Two appendices contain additional results of paleoseismic trenching and neotectonic investigations across 4 active faults near the Nenana River.

This dissertation includes previously unpublished co-authored material.

CURRICULUM VITAE

NAME OF AUTHOR: Sean Patrick Bemis

PLACE OF BIRTH: Bremerton, Washington

DATE OF BIRTH: January 28, 1979

GRADUATE AND UNDERGRADUATE SCHOOLS ATTENDED:

    University of Oregon
    University of Alaska Fairbanks

DEGREES AWARDED:

    Doctor of Philosophy in Geological Sciences, 2010, University of Oregon
    Master of Science in Geology, 2004, University of Alaska Fairbanks
    Bachelor of Science in Geology, 2001, University of Alaska Fairbanks

AREAS OF SPECIAL INTEREST:

    Neotectonics and Paleoseismology
    Structural Geology

PROFESSIONAL EXPERIENCE:

    Graduate Teaching Fellow, University of Oregon, Sep 2004 – Dec 2009

    Engineering Geology Intern, Alaska Division of Geological & Geophysical
        Surveys, Jun 2007 – Dec 2009

    Student Support Technician, Alaska Division of Geological & Geophysical
        Surveys, Sep 2008 – Jan 2009

    Engineering Geology Intern, Alaska Division of Geological & Geophysical
        Surveys, Jul 2004 – Aug 2004

    Teaching Assistant, University of Alaska Fairbanks, Sep 2001 – Dec 2004

GRANTS, AWARDS AND HONORS:

Geological Society of America, Student Research Grant, 2002, 2006
Thayer Scholarship, Dept. of Geological Sciences, University of Oregon, 2005
Arco Alaska Scholarship, Dept. of Geology and Geophysics, University of Alaska
    Fairbanks, 2004
Student Travel Grant, Geophysical Institute, University of Alaska Fairbanks, 2003
Travel Grant, Graduate School, University of Alaska Fairbanks, 2003
Student Research Grant, Alaska Geological Society, 2002, 2003
Brian R. Zelenka Memorial Scholarship, Dept. of Geology and Geophysics,
    University of Alaska Fairbanks, 2002
BP-Amoco Scholarship, Dept. of Geology and Geophysics, University of Alaska
    Fairbanks, 2002

PUBLICATIONS:

Carver, G.A., Bemis, S.P., Solie, D.N., Castonguay, S., and Obermiller, K.E., in revision,
Active and potentially active faults in or near the Alaska Highway corridor, Dot
Lake to Tetlin Junction, Alaska: Alaska Division of Geological & Geophysical
Surveys Preliminary Interpretive Report 2010-XX.

Philibosian, B., Fumal, T.E., Weldon, R.J., Kendrick, K.J., Scharer, K.M., Bemis, S.P.,
Burgette, R.J., and Wisely, B.A., 2009, Photomosaics and Logs of Trenches on
the San Andreas Fault near Coachella, California: U.S. Geological Survey, 2
sheets.

Carver, G.A., Bemis, S.P., Solie, D.N., and Obermiller, K.E., 2008, Active and
potentially active faults in or near the Alaska Highway corridor, Delta Junction to
Dot Lake, Alaska: Alaska Division of Geological & Geophysical Surveys
Preliminary Interpretive Report 2008-3D, 32 p.

Bemis, S.P., and Wallace, W.K., 2007, Neotectonic framework of the north-central
Alaska Range foothills, *in* Ridgway, K., Trop, J., Glen, J., and Fisher, M. eds.,
Tectonic Growth of a Collisional Continental Margin: Crustal Evolution of
Southern Alaska, Geological Society of America Special Paper 431, p. 549-572.

ACKNOWLEDGMENTS

This dissertation would have been impossible without the invaluable field support of many individuals: Nate Pamperin, Jim Hunter, Dave Pott, Evan Thoms, Ben Mackey, Sammy Castonguay, Patty Craw, Allison Payne, Nick and Nyle Weldon, Gregg Vinger, and Alec Duncan. Also providing vital logistical support: Kelly Mansfield, Sam and Jarrod Decker, Dan Jordan, Larry at Windy Creek, Robert Kohlsdorf, and Jon Nierenberg. I thank Usibelli Coal Mine and the Alaska Railroad for access to their properties.

Over the years, my research in the Alaska Range has benefited greatly from the ideas, support, encouragement of the following friends and colleagues (in addition to people mentioned above): Wes Wallace, Gary Carver, Peter Haeussler, David Schwartz, Gordon Seitz, Jeff Benowitz, Ken Ridgway, and many others.

I feel that I left my committee members, Josh, David, and Doug, criminally underutilized during much of this project. If I could express one minor regret, it is that I did not incorporate them more into the research early on, or seek them out when I struggled with concepts. I thank them for their time and encouragement, and hope we can continue as colleagues as I pursue some of the new ideas out of this dissertation in the near future. Ray has been a fantastic advisor. I am still astounded by his focus, determination, and his way of thinking through problems more carefully and

systematically than I can ever imagine. Maybe we can put together another snowmobile-supported spring field excursion in Alaska in a few years.

My parents and family provided me with the well-balanced, supportive foundation on which I have built my life. I thank you so much for the support, love, and encouragement. Really, I cannot say thank you enough.

And if there is one thing that made leaving Alaska to come to Eugene entirely worth it, that would be Shannon. A lot of life has happened in the few years since we met here, and there is so much ahead of us. She continually amazes me, and I look forward to every moment with her.

TABLE OF CONTENTS

LIST OF FIGURES

Figure   Page

LIST OF TABLES

LIST OF PLATES

CHAPTER I

INTRODUCTION

1.1 Motivation

The term "moletrack" is used informally in neotectonic and paleoseismic research to describe a fault scarp that is both relatively sinuous in plan view, and in cross-section forms a mound such that the crest of the surface rupture is higher than either side . This type of scarp is often associated with both strike-slip and thrust fault surface ruptures and in general is the result of the complex interaction of the discrete displacement during an earthquake at depth with unconsolidated material at the earth's surface. In thrust fault settings, the moletrack can become a persistent topographic feature as it grows through successive earthquakes, illustrating that, in other words, the growth of any mountain range begins with a single earthquake. Thus the title phrase "moletrack scarps to mountains" is used to describe the range of scales of investigation utilized in this dissertation to examine fault systems and fault interactions to better document and understand the growth of continental orogenic belts.

This research was initially motivated by the results of the Alaska workshop for the USGS National Seismic Hazard Mapping Project in May 2005. At this meeting, we discussed how, despite having more shallow crustal earthquakes than an equivalent region of the contiguous United States, Alaska has only a fraction of the known Quaternary active faults. Given this discrepancy, there is a limited framework within which to model seismic hazards for the state, and very few faults are characterized in sufficient detail to include as individual seismogenic sources. As a result of the low population density of Alaska, there is a lower vulnerability to immediate impacts of large earthquakes; however, significant risks still exist. A primary risk is to transportation corridors and national defense facilities. Pipelines, railroads and highways cross multiple active fault zones as they traverse from interior to southern Alaska. Several proposed

natural gas pipeline corridors intersect zones of active faulting that remain largely uncharacterized for seismic engineering. An additional risk is the seasonal influence on potential impacts from earthquake damage. Major disruptions to transportation and energy supplies during a typical winter in interior Alaska could cause significant secondary damage threats to much of the population as a result of extreme cold. Therefore, through these studies, I could significantly advance the understanding of active faults in interior Alaska and use the unique geologic/geomorphic setting of these faults to ask fundamental questions about tectonic processes.

1.2   Organization

Because the typical earthquake cycle is well beyond the range of the average human lifespan, we must employ geologic markers that record the deformation of the earth's crust at a temporal resolution suitable for the geologic question posed. The chapters of this dissertation examine tectonic deformation and fault interaction at the local scale, across a fold-thrust belt, and across a portion of a plate boundary. Although these chapters are presented separately, each study is informed by the insights provided by the others.

Chapter II, *Quaternary geology and neotectonics of the Japan Hills – Gold King Creek area, central Alaska: Identification of active thrust faults and related late Cenozoic deformation*, presents a 1:25,000 scale Quaternary geologic map of the Japan Hills – Gold King Creek region on the northern margin of the central Alaska Range. This mapping identified numerous landforms indicative of young tectonic deformation and the locations of several Quaternary/Holocene active thrust faults. Profiles of progressively deformed fluvial terraces constrain the geometry of the thrust faults in the subsurface. Appendix A provides basic age control on a prominent terrace level that is used to infer correlations with the regional glacial chronologies for Pleistocene deposits. This chapter will be published with co-authors Ray Weldon, Evan Thoms, and Patty Burns.

Chapter III, *Progressively deformed geomorphic surfaces constrain the balance between thrust wedge thickening and foreland propagation in a basement-involved fold-thrust belt*, addresses the question of how faults within an orogenic wedge interact through time by analyzing the progressive deformation across a fold-thrust belt recorded

by fluvial terraces and an early Pleistocene geomorphic surface. The geometry of progressive folding defines the geometry of faults in the subsurface, and the sequence of offset landforms constrains the slip rates for each structure. The results show that the faults were all active during much of the Quaternary, and thus simultaneously thickening the orogenic wedge and propagating the wedge tip. However, a decrease in slip rate and lack of offset on latest Pleistocene surfaces across the basal thrust suggests a change in wedge dynamics that we infer to result from the loss of glacial ice along the main axis of the Alaska Range since the late Pleistocene. This chapter will be published with co-author Ray Weldon.

Chapter IV, *Strain-partitioning on the Denali fault and Quaternary growth of the Alaska Range: Transpressive deformation along a curved fault*, examines the relationship of the Denali fault with the thrust system of the central Alaska Range and addresses the question of how a mountain range can grow out of a major strike-slip fault. I use the distribution and orientation of Quaternary faults and folds in the Alaska Range north of the Denali fault to show that the principal shortening direction driving growth of the Alaska Range is oriented normal to the Denali fault. Estimates of the shortening rate across the northern Alaska Range and the previously determined slip rates for the Denali fault are used to define the motions of adjacent crustal blocks, revising the tectonic model of central Alaska. This chapter will be published with co-authors Ray Weldon and Gary Carver.

Chapter V, *Conclusion*, presents a summary of the results and implications of each chapter. Appendix A presents trench logs and basic paleoseismic interpretations from 6 excavations across fault scarps along the Nenana River valley in central Alaska. These document the first paleoearthquake data for the region north of the Denali fault and west of the Delta River. Although more work is required on each fault, I include these results for the disclosure of data relevant to critical infrastructure and the additional insight into the Quaternary activity of the faults in the central Alaska Range they provide. Appendix B provides data from radiocarbon analyses and in-situ terrestrial cosmogenic nuclide surface exposure dating from this research, with basic models for the surface exposure ages.

CHAPTER II

QUATERNARY GEOLOGY AND NEOTECTONICS OF THE JAPAN HILLS – GOLD

KING CREEK AREA, CENTRAL ALASKA: IDENTIFICATION OF ACTIVE

THRUST FAULTS AND RELATED LATE CENOZOIC DEFORMATION

This chapter has been prepared for submission as a Preliminary Interpretive Report for publication by the Alaska Division of Geological & Geophysical Surveys (ADGGS) and was co-authored with my faculty advisor Ray Weldon, Evan Thoms (U.S. Geological Survey), and Patty Burns (formerly with ADGGS). As the lead author, I conducted fieldwork with assistance provided by all three co-authors. I was responsible for data collection, analysis, and interpretation, and preparation of the complete map and report. Evan Thoms provided important insights into the stratigraphic relationships and Patty Burns helped to improve my mapping strategy and provided fundamental logistical support. Ray Weldon provided mentoring and input during data analysis and interpretation and provided important comments on previous drafts of this chapter.

2.1   Introduction

The M7.9 2002 Denali fault earthquake sequence was the most recent of 5 earthquakes of >M7 to occur in central Alaska in the past 100 years (Ruppert et al., 2008). These large earthquakes are accompanied by a high level of shallow crustal seismicity in interior Alaska, and a diffuse, lower level of seismicity in the northern Alaska Range (Ruppert et al., 2008). Despite this elevated level of crustal seismicity, little is known about the faults associated with these earthquakes. Furthermore, only recently have researchers begun to identify the framework of active faults that are accommodating the modern uplift of the Alaska Range (Bemis and Wallace, 2007; Carver et al., 2006; Carver et al., 2008) and the associated seismic hazards.

As a part of ongoing investigations of active faulting and the timing/style of uplift

in the northern foothills of the Alaska Range, we selected the Japan Hills – Gold King
Creek area as a promising target for neotectonic investigations due to the widespread
occurrence of Quaternary landforms commonly used in neotectonic studies (Figure 2.1).
It is also near the epicenter of a M7.2 earthquake in 1947 that had a reverse fault focal
mechanism (Fletcher and Christensen, 1996), although no surface rupture has been
documented for this event. The Japan Hills are the northernmost topographic element of
the Alaska Range, and occurs as a broad, east-west trending, low-relief dome a few
kilometers north of the main east-west topographic escarpment that forms the northern
margin of the Alaska Range for ~150 km (Figure 2.1). Our map area is covered by the
1:63,360-scale Fairbanks A-2 quadrangle, which Wahrhaftig (1970a) mapped as part of a
series of eight 1:63,360 scale geologic maps that cover much of the northern foothills of
the Alaska Range (Wahrhaftig, 1970a; b; c; d; e; f; g; h).
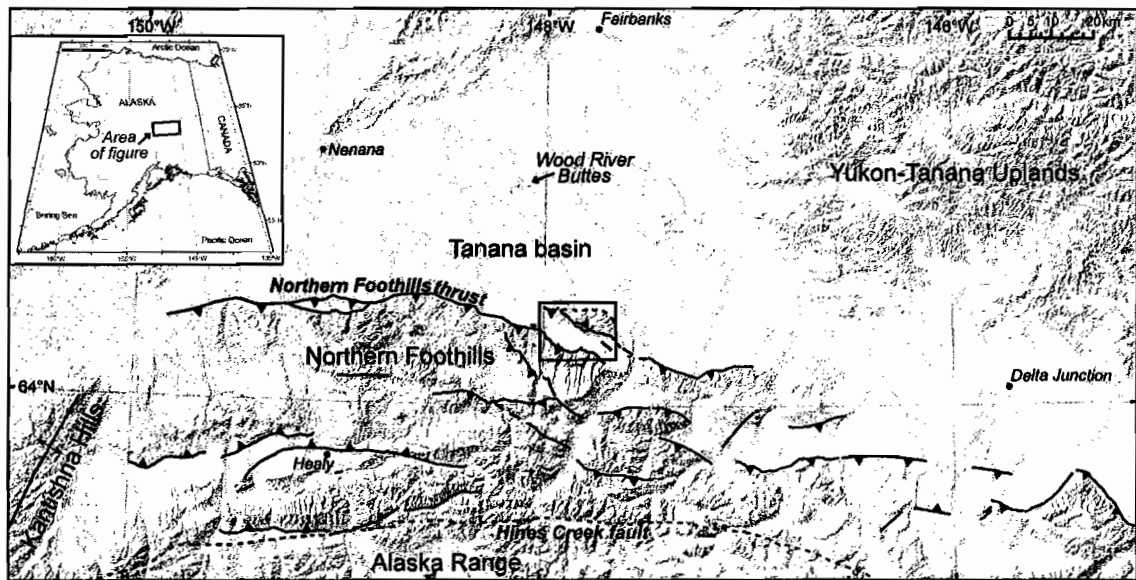
Figure 2.1. Shaded-relief image of interior Alaska showing mapped faults with Quaternary displacement.
Area of figure shown on inset map of Alaska, study area shown by the black outline on the shaded relief
image. Major communities of interior Alaska shown in black italics, streams mentioned in text labeled in
white italic font. Faults shown are the simplified traces of active Quaternary faults as mapped by Bemis
and Wallace (2007), Carver et al. (2006; 2008) and Chapter IV.

We mapped the Quaternary geology and landforms of this region at 1:25,000
scale using a combination of air photo analysis and field traverses, with supplementary

data collected by differential GPS surveying of key landforms. Our map depicts the distribution of surficial geologic units and landforms, including the surface expression of faulting and folding. This report supplements the map (Plate 2.1; all plates are located in pocket inside back cover) with a general discussion of geologic units and a detailed discussion on the evidence for active faults. Measurements of deformed landforms supplement the rare structural attitudes on geologic units and we present two north-south cross-sections interpreted from these data.

2.2   Neotectonic Setting

Active faults in central Alaska are part of the broad Pacific – North America plate boundary and respond to stresses imposed by the subduction and collision of the Yakutat Microplate in southeast Alaska (e.g. Haeussler, 2008). The Denali fault is a major continental right-lateral strike-slip fault that separates the predominantly block motions of south-central Alaska from the zones of diffuse deformation of central Alaska (e.g. Haeussler, 2008; Freymueller et al., 2008; Chapter IV). This diffuse deformation occurs as two distinct zones, the belt of Denali fault-parallel thrust faults that comprise the Alaska Range north of the Denali fault, and three NNE-trending left-lateral seismic zones north of the Alaska Range. Recent neotectonic investigations in the Alaska Range have recognized a continuous system of active thrust faults and fault-related folds along its northern flank (Carver et al., 2006; Bemis and Wallace, 2007; Carver et al., 2008; Chapter IV).

As part of the northern foothills fold-thrust belt, Bemis (2004) and Bemis and Wallace (2007) inferred late Cenozoic faults and folds in the Japan Hills – Gold King area based on interpretations of the geology presented by (Wahrhaftig, 1970a), and reconnaissance-level air photo interpretation. These faults include the Northern Foothills thrust, a south-dipping thrust fault that extends east-west continuously for approximately 150 km, forming the topographic boundary between the Alaska Range and Tanana basin for most of its length. Bemis and Wallace (2007) inferred another south-dipping thrust fault, named the Japan Hills Splay, as a northern splay from the Northern Foothills thrust, with the Japan Hills anticline forming as a fault-related fold in the hanging-wall of the thrust fault.

2.3 Field Investigations and Mapping

Mapping the Quaternary geology of this region consisted of initial reconnaissance-level air photo mapping, a 3 week field season in summer 2006, detailed mapping on stereo air photos in ArcGIS (aided by the ERDAS Stereo Analyst extension), an 8 day field season in early spring 2007, and incorporation of the field and air photo observations into a the final version of the map. Imagery used for mapping included scans of 1940's and 50's black and white, ~1:40,000 scale air photos, and false-color infrared, ~1:63,360 scale air photos from August 1981. Final map assembly and geologic interpretations were aided by 2.5 m resolution, false-color, orthorectified SPOT satellite imagery (obtained from <www.alaskamapped.org>).

As with many successful Quaternary mapping projects in Alaska (e.g. Reger et al., 2008), most of the mapping of contacts was done on air photos, with field investigations accommodating the checking of critical contacts and unit descriptions. Field mapping included field checking units mapped on air photos, describing units, and defining criteria for mapping additional units on the air photos. Natural geologic exposures are rare in the field area, so we examined a few deposits with small test pits, and many more by probing with a 1.2 m frost probe. Frost probing facilitated rapid identification of surficial fine-grained deposits and identifying permafrost depth. Two small trenches were excavated on potential fault scarps, but exposed no evidence of tectonic deformation. Plant species and vegetation patterns of the different surficial units often provided an important diagnostic tool for the differentiation of units on air photos. As a result of our approach to mapping, we incorporate a variety of contact, fault, fold axis, and structural attitude symbology in order to appropriately represent the level of uncertainty in the mapped relations. On Plate 2.1, designation as "Certain" is used to indicate features that were either identified in the field or occur as sharp features in air photos and are located to within less than 10-20 m. "Approximately located" indicates a feature was not seen in the field, but is obvious on air photos, though can only be located to within a 100-200 meters. "Inferred" is typically used where the feature was not seen in the field, is not obvious on air photos, but due to other obvious map/field relations, the feature that is depicted appears to be required. Additional details provided in the legend on Plate 2.1.

We also selected the accessible, well-preserved fluvial terraces along Gold King Creek and a small drainage on the north flank of the Japan Hills (Plate 2.1 and Figure 2.1) to survey the longitudinal profiles of the terrace treads. There surveys were performed with a Trimble GeoXH (Series 2005) hand-held differential GPS, with a survey point spacing of 75-100 m with closer spacing where deformation was apparent. Except for these deformed zones, points were only collected where the unmodified terrace tread was visually obvious by the simultaneous occurrence of a locally planar surface, appropriate vegetation patterns, and a nearby terrace riser crest (Figure 2.2). As we collected these surveys in early spring with snow still on the ground, we were unable to assess the thickness of the loess and organic mat on top of the terrace gravels, but based on summer field observations, we assume that these deposits did not change significantly along the length of individual profiles and so the relative shape of the profile is unaffected. The GPS survey data was post-processed against 3 continuous GPS stations within a 120 km radius to correct for ionospheric and internal GPS errors, resulting in a GPS positional uncertainty for most points of <1 m.
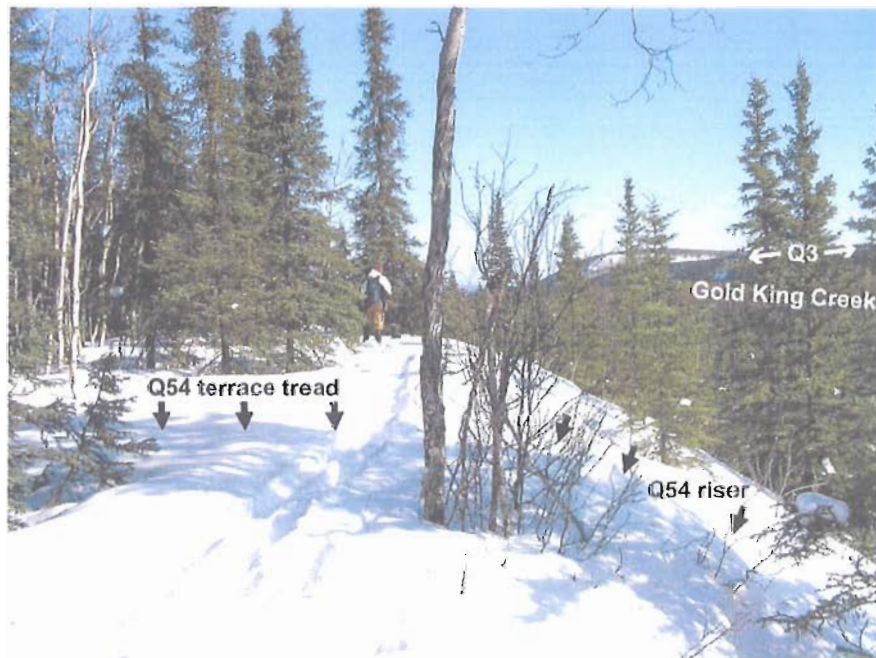
Figure 2.2. Surveying the Gold King Creek terraces. Nyle Weldon collects a data point on the surface of Q54 next to the sharp riser crest with the Q55 terrace surface visible below. View is to the north with the Gold King Creek drainage to the right and well below the Q3 terrace surface across the creek.

For age control on the fluvial terraces, we collected 5 depth profiles for in-situ terrestial cosmogenic nuclide (TCN) surface exposure age dating. For these samples, we tried to select relatively fresh riser surfaces where we exposed a section from the top of the terrace tread down to 2-3 meters. From the exposed sections, we collected 4 or 5, one liter samples of the undisturbed terrace gravels spaced ~50 cm vertically. We logged the exposed section, taking note of the thickness and geometry of the overlying loess and documenting the depth of cryoturbation. To establish constraints on the timing and rate of loess accumulation on the terrace treads, we collected charcoal samples from the loess wherever possible. We analyzed one of these depth profiles and the results are shown in Appendix B.

2.4   Stratigraphy

The stratigraphy of the Japan Hills – Gold King Creek is similar to much of the northern foothills of the Alaska Range (north of the Hines Creek fault, Figure 1)) in that it can be subdivided into 3 primary components, 1) crystalline basement composed of metamorphic rocks, 2) Neogene terrestrial sedimentary deposits, 3) Quaternary alluvial and colluvial deposits and landforms that are broadly correlative with major climatic events. General descriptions of the units and groups of units are provided here, with more detailed descriptions provided on the map sheet (Plate 2.1).

2.4.1   *Crystalline Bedrock Unit - Br*

Wahrhaftig (1970a) mapped the central region of the Japan Hills as Totatlanika Schist(?), which in the northern foothills of the Alaska Range, is predominantly bimodal meta-igneous unit with associated carbonaceous and metasedimentary rocks (Wahrhaftig, 1968; Dusel-Bacon et al., 2004). Dusel-Bacon and others (2004) report a Middle Devonian – early Mississippian age for the protolith of the Totatlanika Schist. Due to difficult access, poor geologic exposure, and our focus on the Quaternary stratigraphy and deformation, this study does not present any new data on this unit.

2.4.2   *Neogene Terrestrial Sedimentary Deposits*

In the northern foothills of the Alaska Range there are two widespread Neogene sedimentary formations, the Usibelli Group, and the Nenana Gravel. The Usibelli Group, described in detail by Wahrhaftig et al. (1969) and Ridgway et al. (1999; 2007), is a coal-

bearing sequence of fluvial and lacustrine sediments, that is formally divided into 5 separate formations. The age of this unit spans most of the Oligocene and Miocene (Ridgway et al., 2007). This unit was deposited directly on the crystalline bedrock by dominantly south and southwest-flowing streams (Ridgway et al., 2007). Despite the occurrence of a thick section of the Usibelli Group about 10 km south of the map area, we did not find any exposures of this unit in contact with the bedrock exposed in the Japan Hills.

The Pliocene Nenana Gravel represents an major reversal of drainage direction, and is recognized as the coarse-grained foreland deposits derived from the initiation of the growth of the Alaska Range immediately to the south (Wahrhaftig, 1987; Thoms, 2000; Ridgway et al., 1999; 2007). The unit is up to 1200 m thick at its type section near Healy (Figure 2.1), and thins northward to 500 m or less near the modern range front (Thoms, 2000; Ridgway et al., 2007). Previously, the deposition of the Nenana Gravel was interpreted to have ceased by approximately 2.8 Ma (Wahrhaftig, 1970g; Wahrhaftig, 1987), but new $^{40}Ar/^{39}Ar$ dates in Athey and others (2006) move this constraint to ~1 Ma. Bemis and Wallace (2007) argue that the end of the Nenana Gravel occurred due to the propagation of thrust faults that uplifted the northern foothills above the base level of the Tanana basin. Thus, the upper surface of the Nenana Gravel is the former Tanana basin floor and as such provides an important structural marker and constraint on cumulative deformation, deformation rates, and structural geometry. However, the age of this surface is only loosely constrained at one location, and it is unknown if the onset of uplift of this surface was synchronous throughout the Alaska Range.

2.4.3 Quaternary Deposits

The oldest of the post-Nenana Gravel (and thus Quaternary) deposits is the unit Qfco. It only occurs on the northern flanks of the Japan Hills and isolated locations on the southern range front. In its outcrop pattern, it can be difficult to differentiate from the Nenana Gravel, but is most obvious where the upper surface of the Nenana Gravel can be continuously traced to lie unconformably underneath these deposits. Therefore, Qfco was deposited on top of the Nenana Gravel, but due to the widespread preservation of the upper surface of the Nenana Gravel, this deposition must have only occurred locally,

perhaps as growth strata on the flanks of a growing fold (Figure 2.3). The age of this unit is inferred to be close to the age of the cessation of Nenana Gravel deposition because the deposit is deformed nearly the same as the underlying Nenana Gravel, and much more than the late Quaternary deposits.
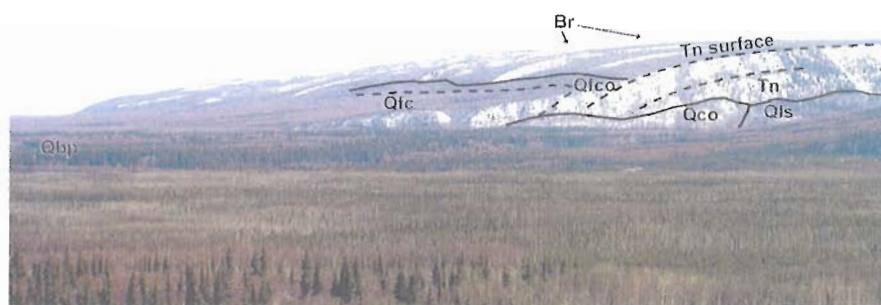
Figure 2.3. View of the northern flank of the Japan Hills, looking ESE across Bonnifield Creek. This view illustrates the folding and uplift of the Nenana Gravel, defined by the deformation of the upper surface and bedding within the unit, and highlighted by black dashed lines. As the Japan Hills grew, sediments accumulated in the Tanana basin, offlapping the upper surface of the Nenana Gravel. Note how the bedrock is exposed on the horizon, suggesting that at the highest point the bedrock is above the projection of the surface of the Nenana Gravel, as it is also shown in Figure 2.7.

We divide the remaining Quaternary units into three general categories, alluvial, colluvial, and paludal deposits (Correlation Chart on Plate 2.1). Most of the alluvial deposits younger than Qfco are likely associated with climatic cycles during the mid to late Pleistocene, as recognized throughout the Alaska Range, particularly along the Nenana and Delta rivers (e.g. Wahrhaftig, 1958; Reger et al., 2008; Thorson, 1986). Through mapping of cross-cutting relations and altitudinal differences above the downcutting streams, we established a relative age chronology (Correlation Chart on Plate 2.1) that is tied to absolute ages based on a 50,730 ± 3200 BP (likely infinite) radiocarbon age from within the Q3 fluvial deposits (location (B) on Plate 2.1), and an absolute minimum age of ~82 ± 7 ka modeled from a cosmogenic radionuclide depth-concentration profile for the Q3 tread (location (C) on Plate 2.1; dating details in Appendix B). This indicates that Q3 is older than Marine Isotope Stage (MIS) 4, and likely correlative with MIS 6 or 8 (Gibbard and Cohen, 2009).

Gold King Creek is the only perennial stream in the map area, and Bonnifield Creek only carries surface flow during periods of extended heavy rain. Despite this difference, both drainages have a flight of fluvial terraces. Based on morphology and cross-cutting relationships, we identify 3 discrete periods of aggradation, separated by subsequent incision, that lead to the emplacement of suites of terraces. The oldest of these, Q3, consists of a large, triangular surface between Gold King and Bonnifield creeks, as well as a narrow strip along the south side of the Japan Hills on the footwall of the Gold King fault Section B, where it is largely covered by colluvium (unit Qco; Plate 2.1). The Q4 and Q5 sets of terraces are inferred to have been emplaced by two subsequent regional glacial advances, the Healy and Riley Creek advances (respectively) of the Nenana River valley glacial sequence (e.g. Wahrhaftig, 1958; Thorson, 1986; Dortch, 2006). Relationships between these terraces are best preserved on the west side of Gold King Creek, where each advance has a distinct fill terrace surface, and 2-4 cut terraces. These cut terraces probably represent climatic fluctuations during the glacial advances, resulting in punctuated downcutting of the stream superimposed on the uplift of the terraces. Many of the smaller drainages also have terraces associated with them, but their extent is limited and correlation to the other terraces is dubious.

With the regional drainage direction to the north, the most extensive sets of alluvial fans are preserved on the north-flowing drainages (units Qfaa and Qjfa). While we are able to establish relative ages within individual sets of alluvial fans, there is no morphological basis for correlating the alluvial fans on the north side of the Japan Hills with the fans adjacent to the southern range front. Therefore, we map these as separate sequences with different nomenclature, although these sequences likely overlap in time. Unit Qfc is an alluvial deposit that occurs as a variety of indistinct, permafrost-dominated surfaces that probably span a significant period of time. Map relations suggest this unit is older than the sequences of alluvial fans (units Qfaa and Qjfa) and is clearly emplaced below the Q5 terraces, suggesting that the entire sequence of alluvial fans could be latest Pleistocene and younger.

Colluvial deposits are widespread on low-gradient hillslopes and form an apron along the base of steeper hillslopes. Paludal, or swamp, deposits are restricted to flat

regions without local drainage so that a significant thickness of silt and peat could accumulate in a bog. Where the surface has been disturbed and the permafrost melted, these can form thaw ponds over 1-2 meters deep.

2.5 Active and Potentially Active Faults

The first-order observation that indicates recent fault-related deformation of the Japan Hills – Gold King area is the presence of two major antecedent drainages that cut directly across the topographic high of the Japan Hills themselves (Plate 2.1). The fluvial terraces along these drainages were former floodplains of the streams, but now project higher than the elevation of the basin downstream. In addition, the upper surface of the Nenana Gravel is uplifted and folded across the Japan Hills (Figure 2.3) and across the range front. This upper surface of the Nenana Gravel and large-scale bedding observed in the uppermost portion of the Nenana Gravel defines three different folds: 1) a north-vergent monocline on the south margin of the map area, 2) a south-vergent monocline on the south side of the Japan Hills, and 3) broad folding across the crest of the Japan Hills with a distinct monoclinal 'kink' on the northern limb. These folds are all associated with the late Quaternary faults in the study area (Plate 2.1).

2.5.1 Northern Foothills Thrust

The trace of the Northern Foothills thrust as shown on Plate 2.1 varies only slightly from the mapped trace of Bemis and Wallace (2007). Through air photo mapping, we identified intermittent scarps and vegetation lineaments along the base of the range front, although these intermittent features could not be linked by a continuous fault trace. We accessed the fault scarps in several locations between Gold King Creek and the second drainage east from Bonnifield Creek (Plate 2.1). There are prominent scarps preserved in the older Qco and Qfc deposits, but we did not identify any scarps crossing the younger alluvial deposits. In particular, at the projection of the fault trace in unit Qfaa3 on the east side of Bonnifield Creek (location (D) on Plate 2.1), there is a continuous latest Pleistocene(?) fill terrace approximately 4-5 meters above the modern stream elevation that shows no discernible deformation within several hundred meters of the projection of the fault trace.

2.5.2   Gold King Fault

The Gold King fault supercedes the interpretation of the "Japan Hills splay" of Bemis and Wallace (2007). Where the Japan Hills splay was inferred to be a north-vergent, south-dipping thrust fault underlying the Japan Hills, we found a north-vergent south-dipping thrust west of Gold King Creek and a south-vergent, north-dipping thrust fault east of Bonnifield Creek (Plate 2.1). We will discuss the Gold King fault in these two sections.

2.5.2.1 Section A

West of Gold King Creek, the Gold King fault forms an abrupt north-facing scarp where it crosses Q5 terraces (Figure 2.4). On Q54, the fault forms a approximately 2 m tall scarp with a steep forelimb and a 10-15 m wide flat, slightly south-tilted backlimb (location (E) on Plate 1). This panel is the terrace surface that has been backtilted relative to the gradient of the rest of the terrace, and several small linear gullies have incised across the scarp to accommodate surface drainage of the terrace tread (Figure 2.5). A couple of these gullies are less than 1 m deep and end abruptly at the scarp, indicating these formed after previous earthquake ruptures, and were abandoned following the most recent event(s). We do not have direct constraints on the age of this terrace, but it is clearly no older than late Pleistocene given the stratigraphic position relative to the other terraces and the elevation relative to Gold King Creek. There has certainly been two, and likely no more than 3 surface-rupturing earthquakes to form this scarp, and the fresh morphology of the scarp face indicates that at least the most recent event was probably during the late Holocene.

Where the Gold King fault scarp cuts across the Q53 terrace, it maintains a similar morphology, but at a larger scale. The scarp is approximately 15 m tall, but only 10 m of this offset is the cumulative offset of the terrace tread, and an additional 5 m of scarp height results from the complex hanging wall deformation that creates a similar back-tilted panel as Q54 (Figure 2.5; location (F) on Plate 1). However, at the location of our GPS profile, the back-tilted panel is 35-40 m long and dips approximately 5° south (Figure 2.4). The Q53 terrace riser has an essentially linear projection across the fault, indicating displacement on this fault is predominantly dip-slip.
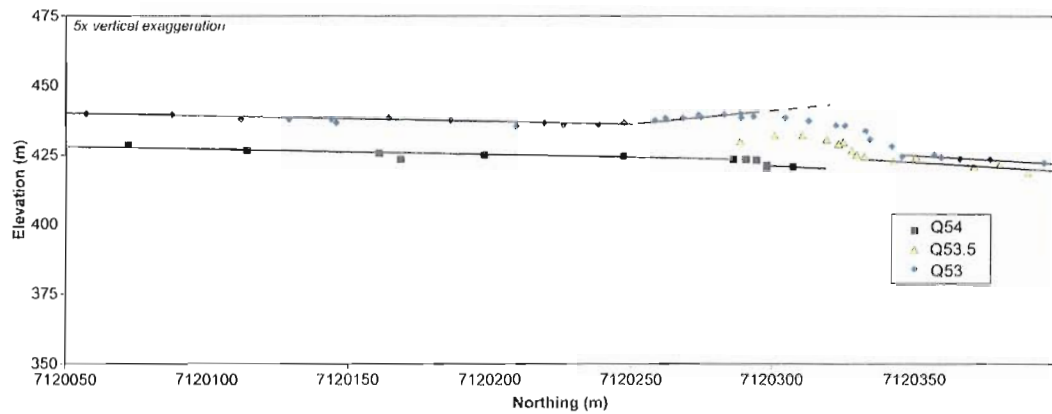
Figure 2.4. Topographic profiles across the Gold King fault Section A scarp, west of Gold King Creek. The scarp offsets three terraces at this location, two of which (Q53 and Q54) are shown on Figure 2.10. Q53.5 is an intermediate terrace remnant that does not appear beyond this survey and is offset an intermediate amount between the higher and lower scarps. This progressive change of scarp shape across older surfaces indicates that the length and dip of the back-tilted panel increases with increasing displacement and scarp height. Evidence for deformation in addition to the brittle offset producing the fault scarp is shown by the steeper dip of the footwall surfaces of Q53 and Q53.5 and the elevation above the modern stream profile as shown on Figure 2.10.

Figure 2.5. View to the northwest along the westernmost segment of the Gold King fault, showing the prominent scarp on Q53. Antecedent channels (white arrows), back-tilted terrace surface (between black arrows) and abrupt scarp face illustrate the geometry and progressive growth of the fault scarp over multiple earthquake cycles.

We did not identify a recent fault scarp in the Gold King Creek floodplain, but a 2 m scarp (similar size to the scarp on Q54) occurs in unit Qco to the north of the large Q3 surface (location (G) on Plate 2.1). The portion of the Q3 surface immediately south of this scarp also has a similar large-scale scarp morphology to Q53 and Q55, but the back-tilted panel appears to have been eroded early in the history of the surface. There is a distinct change in the nature of the fault that corresponds with the location of the small, north-flowing drainage to the east of the landing strip on the Q3 surface (Plate 2.1).

2.5.2.2 Section B

Despite visually obvious deformation of the upper surface of the Nenana Gravel, air photo and field investigations did not reveal a fault scarp on the northern flank of the Japan Hills. However, evidence of ongoing deformation is shown by northward tilting of the Nenana Gravel and a sequence of alluvial surfaces (Figure 2.6; location (H) of Plate 2.1)). This dramatic folding is direct evidence of active faulting at depth.
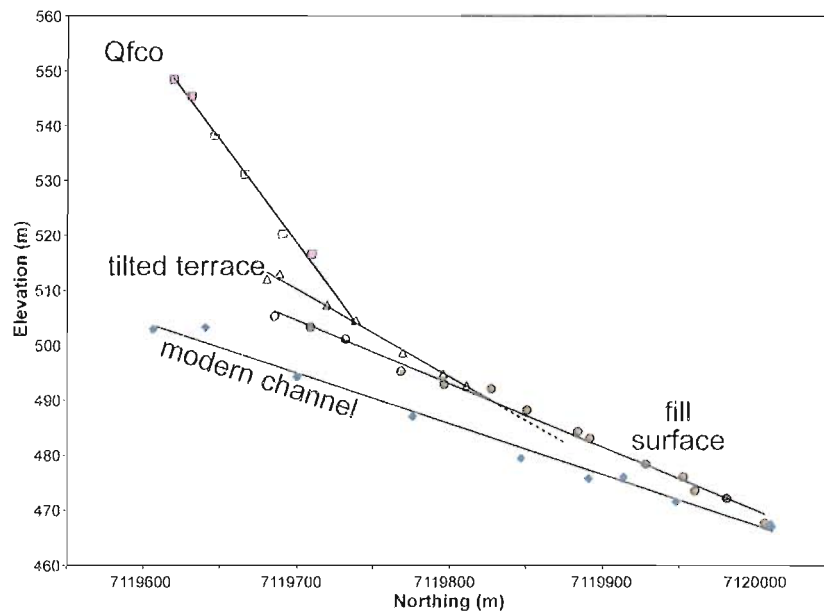
Figure 2.6. Profiles of landforms across the abrupt Japan Hills northern range front. The profiles, in addition to traverses up and downstream from this survey, demonstrated the lack of a surface trace of a fault along this portion of the northern flank of the Japan Hills. The profile labeled "modern channel" is an ephemeral stream which has incised into the surface of an alluvial fan whose profile is labeled as "fill surface". This fill surface aggraded over the tilted terrace, as observed by field relations and represented by the dashed line projected below the fill surface. Qfco is likely early Pleistocene and dips ~21° N.

The eastern end of Section B corresponds to an alignment of landforms and vegetation lineaments near the north-flowing drainage between locations (G) and (I) on Plate 2.1. Immediately east of the drainage is an isolated knob (location (I) on Plate 2.1) composed of Nenana Gravel. The southwest margin of this knob aligns with vegetation lineaments and a deflection of the drainage by a small scarp-like feature.

On the south side of the Japan Hills, evidence exists for a surface-rupturing fault trace where large-scale bedding in the uppermost Nenana Gravel defines a sharp monoclinal fold (Figure 2.7, location (J) on Plate 2.1). Uplift of the Nenana Gravel and the relatively sinuous nature of the Nenana Gravel monocline indicate this is a north-dipping, south-vergent thrust fault that underlies the main topography of the Japan Hills. However, the elevation of the Q3, Q4, and Q5 terraces and deposits above the modern floodplain indicates that this region, despite being in the footwall of this section of the Gold King fault, is experiencing uplift relative to the Tanana basin.
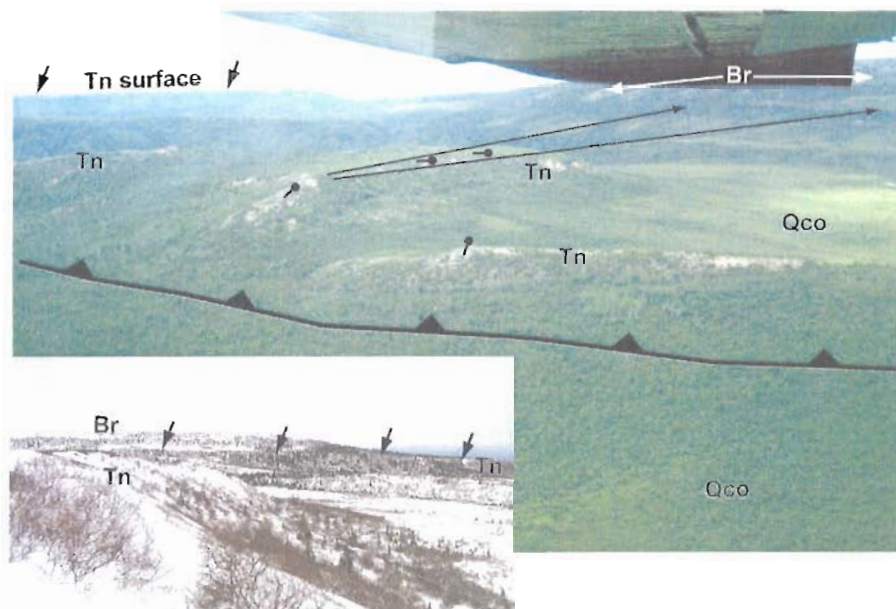
Figure 2.7. Oblique photo of the monoclinal fold that defines the surface trace of the Gold King fault Section B. View is to the NW. Location of fold in center of photo indicated as location (J) on Plate 2.1. Dip tadpoles depict the abrupt steepening of the Nenana Gravel beds towards the fault trace. Thin black arrows illustrate how the horizontal beds project to the lineation on the bedrock in the core of the Japan Hills anticline. These arrows also show the view of the inset picture that looks along those horizontal beds, showing the alignment of these beds with the vegetation lineament and topographic break (highlighted with short arrows) across the valley, indicating that the Nenana Gravel onlapped onto what would have been a bedrock knob protruding from the basin floor prior to uplift.

2.5.2.3 NW-striking faults on eastern margin of map

Two northwest-trending, parallel lineaments that are defined by a combination of linear patches of vegetation, aligned ponds, and topographic scarps occur on the southeastern edge of the map area (Figure 2.8, Plate 1). These lineaments appear to be two faults, with unknown, but likely steep dip due to their linear map trace. Due to the lack of significant relief across these faults, they appear to be predominantly strike-slip. Of these two faults, the southwestern fault is the least distinct, having just a short 0.8 – 1 km segment that appears to be a fault scarp, with an additional 0.5 to 1.2 km of fault trace interpreted from aligned streams, ponds and vegetation. The northeastern fault has a prominent trace for approximately 7 km, extending from the eastern end of the Gold King fault southeast to the Wood River. There is one visually-compelling laterally offset stream channel indicating right-lateral slip, and a complex configuration of stream channels and terrace risers shown in Figure 2.8 providing additional evidence for right-lateral slip. This right-lateral relative motion on this fault is consistent with the direction of shortening across the Gold King fault Section B. Furthermore, the topographic relief of the Japan Hills ends to the north of these faults suggesting these faults represent a change in the mode of deformation, and perhaps act to transfer strain from the Northern Foothills thrust east of the Wood River (Figure 2.1) to the Gold King fault.

2.6 Quaternary Deformation From Deformed Geomorphic Surfaces

Instead of relying upon sparse structural attitudes and sometimes poorly constrained bedrock contacts to construct a cross-section for the study area, we use the preserved geomorphic surfaces as kinematic markers to construct the geometry of these faults at depth. In our map area we have two types of widely preserved geomorphic surfaces – the upper surface of the Nenana Gravel and fluvial terraces. As the uplifted Tanana basin surface, the upper surface of the Nenana Gravel represents a widespread, formerly planar structural datum. The fluvial terraces each represent the former floodplain of the associated stream, which was abandoned as the stream incised. With the length of our analysis very short relative to the full stream profile, we can approximate the stream profiles and terraces as representing linear structural markers.
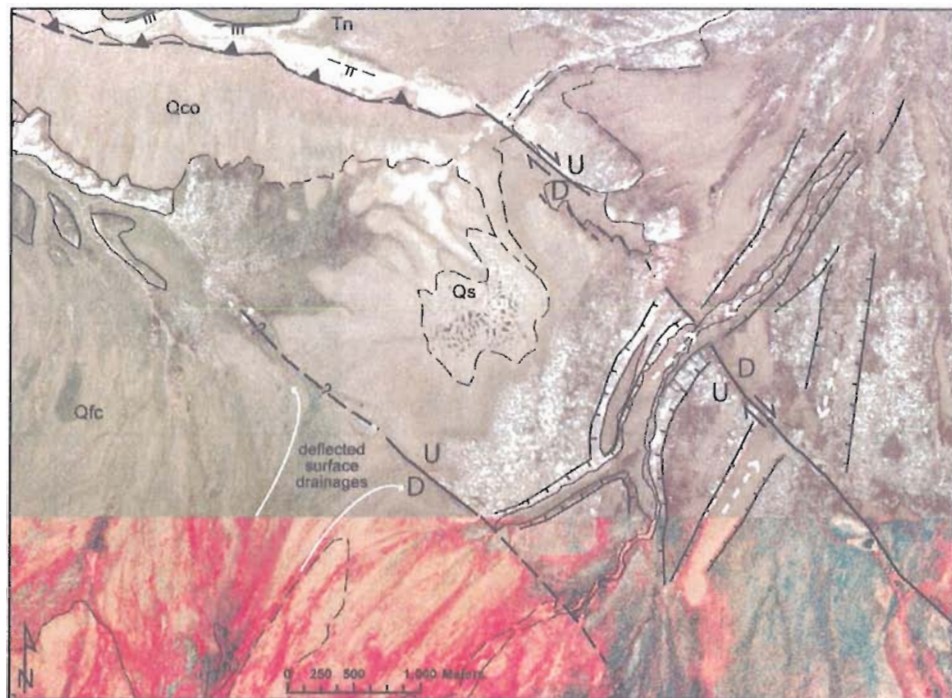
Figure 2.8. Northwest-striking faults on the east edge of the map area. Mapped geologic contacts, fault traces, terrace risers, and structural symbols same as Plate 2.1. The area of this figure extends ~2 km east of the Plate 2.1 map area. The western fault does not exhibit any clearly lateral offsets, but the narrow linear trace and control on local surface drainage indicates the presence of a brittle structure. The eastern fault has a very distinct trace with multiple offset landforms. A compelling right-lateral stream offset occurs just west of where this fault merges with the Gold King fault. This right-lateral offset and other possible stream channel offsets are shown by dashed white arrow, and by the pattern of right-laterally displaced terrace risers. Base imagery is a combination of orthorectified false-color infrared air photos and false-color SPOT imagery (obtained from <www.alaskamapped.org>).

Tectonic deformation of fluvial terraces can consist of uplift, abrupt offsets, tilting, and folding – the same types of deformation that could be seen in traditional structural geology studies. However, using a sequence of fluvial terraces has the advantage of preserving the progressive deformation of the structure since discrete moments in the past, such that any structural model not only has to fit the instantaneous constraints presented by the modern geometry, but also explain the evolution of the terraces over the time since formation. Using the detailed GPS surveys of terrace treads, and projecting the surveyed points to a plane perpendicular to the trace of the fault, we identify panels, separated by fold hinges, that have each experienced the same deformational pathway.

2.6.1 Pre-uplift Configuration

During the deposition of the Nenana Gravel during the Pliocene, the Japan Hills existed as a low-relief bedrock knob protruding above the basin floor in a similar manner to the modern Wood River Buttes (Figure 2.1). The position the Nenana Gravel surface relative to the elevation of the bedrock and the correspondence of geomorphic features shows that the alluvial deposits of the Nenana Gravel onlapped onto the bedrock high (Figure 2.7). Whether this bedrock knob was uplifting prior to cessation of the Nenana Gravel deposition or was simply a topographic high is unknown because geologic exposures of the Nenana Gravel are not sufficient to identify any possible occurrence of growth folding in syntectonic strata. Previous studies (Wahrhaftig, 1970a; Bemis and Wallace, 2007) assumed that the Nenana Gravel once completely buried the bedrock, which would have produced an overestimated cumulative uplift.

2.6.2 Section A-A'

Most of the stream-parallel terraces were surveyed along Gold King Creek and are positioned within a swath extending about 3 km in east-west width (Figure 2.9). We project the survey data onto a N-S plane, which is schematically shown by the line of section A-A' on Plate 2.1. Figure 2.10 shows the compiled terrace profiles relative to the profile of Gold King Creek. Although not all the terraces are continuous across the zone, the pattern of deformation is clearly defined by the sequence of surfaces. From these profiles, we delineate 4 distinct deformational panels on these profiles, each separated by a relatively narrow hinge zone (Figure 2.10). From ~1 km north of the NFT, the terraces appear where they have been progressively rotated away from the stream gradient to form a downstream-divergent fanning of surfaces. North of the divergent terraces, the terraces are parallel to one another for the rest of the distance to the Gold King fault; however, only the northernmost ~1.6 km of these terraces are also parallel to the Gold King Creek (our approximation for paleo-stream gradient). The ~1.3 km segment in the middle of the profiles consist of parallel terraces that are back-tilted relative to the stream gradient. The fourth deformation zone is defined by a short panel of backtilted terraces that forms the backlimb of the fault scarp and the hummocky roll-over to the steep forelimb of the fault scarp. To extend the structural control south of the Gold King Creek terraces and across

21

the Northern Foothills thrust, we use the upper surface of the Nenana Gravel (where preserved) and 2 bedding attitudes measured in the field (Plate 2.1, Figure 2.10).
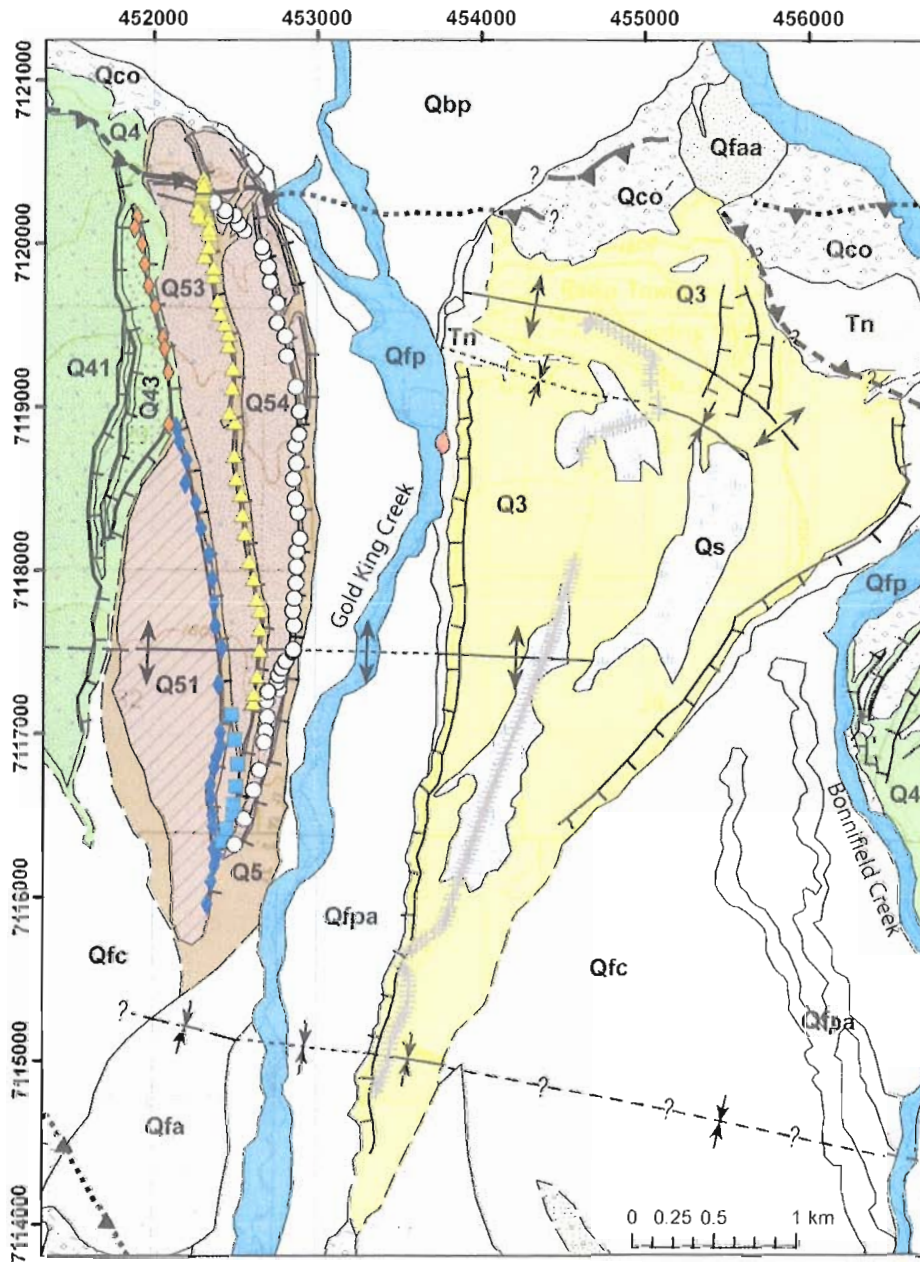
Figure 2.9. Geologic map showing GPS survey points for the terrace profiles on Figure 2.10. Note how the structures begin to curve to the southeast on Q3 due to the apparent interaction with the south-vergent Section B of the Gold King fault, causing the apparent misalignment of the scarp on the north end of the Q3 profile on Figure 2.10.
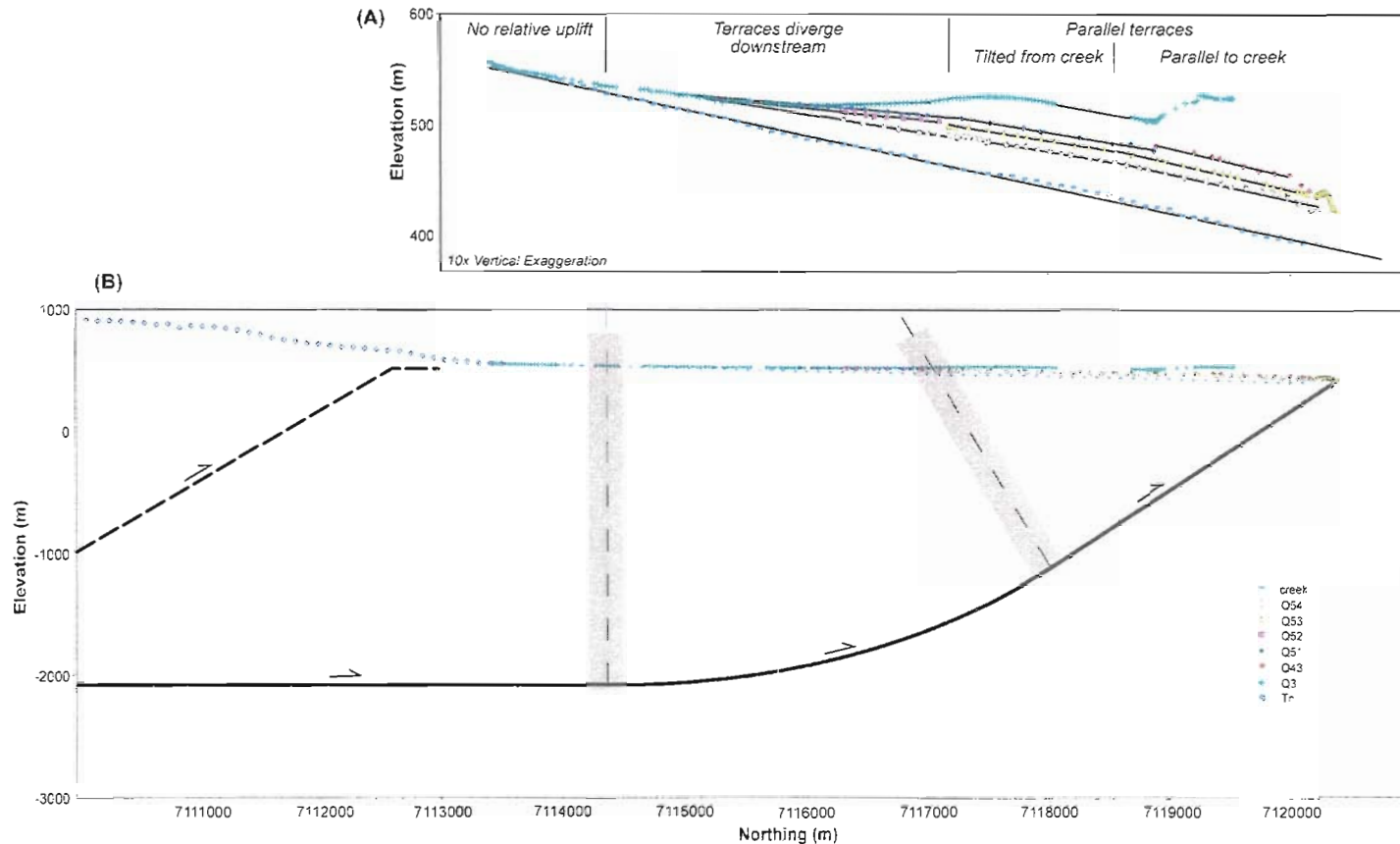
Figure 2.10. Surveyed terrace profiles (A) and cross-sectional interpretation (B) along section A-A' (Plate 2.1). In (A) the solid black lines are linear regressions fit to individual segments of the survey data in order to delineate different deformational panels, with the unique characteristic of each panel noted above. The Q4 and Q5 terraces are the primary data source for defining the style of deformation, and Q3 is shown to further highlight the pattern but cannot be projected accurately into the northern end of the profile because the uplift of Q3 is oblique to the section. (A) and (B) are vertically aligned, so the fault geometry can be matched with the exaggerated profiles. The symbols for survey points are the same for (A) and (B). The NFT is dashed because of the uncertainty in dip, but the location near the surface is accurate with a couple hundred meters. The thin dashed lines in (B) are the hinges that define the transition from planar fault to curved fault and intersect the hinges in the terraces. The broad gray zones around these dashed lines represent uncertainty in the exact location of the hinge and the minor geometric space problem that occurs at a fault transition like this.

The point at which the terraces converge in the upstream direction represents a boundary where no relative uplift occurs between this convergence point and the Northern Foothills thrust. This indicates that the underlying thrust fault is essentially horizontal south of that point. In addition, the downstream divergent and parallel terraces require different structural geometries to accommodate the different styles of progressive deformation. The parallel terraces can be fit by a simple south-dipping, planar fault. The downstream divergent terraces occur as a transition between a horizontal fault and a dipping fault. Because a narrow fault bend at depth would create a fault-bend fold (e.g. Suppe, 1983) at the surface, this fault transition and pattern of progressive tilting at the surface is better fit by a listric thrust fault. We determined the depth and radius of curvature for this listric segment using the geometric constraints of the locations of hinges, the location of the Gold King fault surface trace, and the requirement of a horizontal thrust plane south of the terraces. However, this geometry does not accommodate the hinge separating the two panels of self-parallel terraces. Because these terraces are all parallel to one another, and the only deviation is from the creek, it appears that this tilting occurred as a result of a post-Q54 change in fault geometry at depth. Specifically, this suggests a larger radius of curvature for the listric segment of the fault. The transition from planar to curved fault planes creates a geometric complication at the hinge zone. However, due to the low cumulative slip and the relatively near surface occurrence of the hinges, this relatively minor space problem could easily be accommodated by the development of localized, low-displacement shear zones.

The dip of the NFT is unconstrained, but the sinuous surface trace and the presence of the nearly 15 km long panel of essentially planar uplift of the Nenana Gravel surface south of the map area (Figure 2.1) indicate it certainly dips less than 45° to the south, and likely 30° or less. The Gold King fault must merge with the NFT at depth a short distance south of our cross-section.

2.6.3 Section B-B'

The nearly continuous preservation of the Nenana Gravel surface and the occurrence of Quaternary terraces on the flanks of the Japan Hills are the primary structural markers along the B-B' line of section. Figure 2.11 shows the composite

profile across the Japan Hills and the Northern Foothills thrust, constructed using elevation data from differential GPS surveys, attitudes generated by photogrammetric techniques, and profiles made from points extracted from the USGS 30 m DEM. GPS surveys across the northern flank of the Japan Hills (Figure 2.6) provide more detail on the geometry of deformation that is not visible at the scale of Figure 2.11. The Nenana Gravel upper surface is very broadly warped across the crest of the Japan Hills into a box-like fold with two angular hinges and it is truncated on the southern side of hills by the Gold King fault section B. This Nenana Gravel surface appears again on the south end of the section where it begins south of the NFT with steep north dips and gradually shallowing to the south. In between the NFT and Gold King faults are a swath of terrace remnants that are tentatively correlated with Q3 and Q5 based on relative elevations above the active streams. The Q5 terraces merge with unit Qfc across the syncline in a region suggesting no relative uplift of this zone, in a similar manner to Section A-A' to the west (Figure 2.10).

With only the Nenana Gravel extensively preserved along much of the line of section, there are fewer geometric constraints for Section B-B' than Section A-A'. However, the south-vergent surface trace requires a north-dipping fault beneath the Japan Hills, but because there is also relative uplift on the footwall of this segment of the Gold King fault, there must also be a south-dipping fault in the subsurface, forming a thrust wedge at depth. The location of the tip of the wedge is constrained by the folding of the northern flank of the Japan Hills where the ~20° N dipping panel of Nenana Gravel (Figure 2.11) and the offlapping relationships suggested by the Figure 2.6 show the progressive folding due to this structure at depth. The Gold King fault daylights as one or two traces along section B, and due to the subtle kink in the Nenana Gravel surface across the crest of the Japan Hills (Figure 2.11) it is likely that the southern trace is the more recently active strand. Cutting off the northern strand to a lower angle at depth could produce a fault bend, resulting in the folding of the upper surface. The subsurface geometry of Figure 2.11 does not fully produce the geometry of folding defined by the Nenana Gravel deformation, but defines a representative framework of the style of faulting and magnitudes of displacement required for the observed surface deformation.
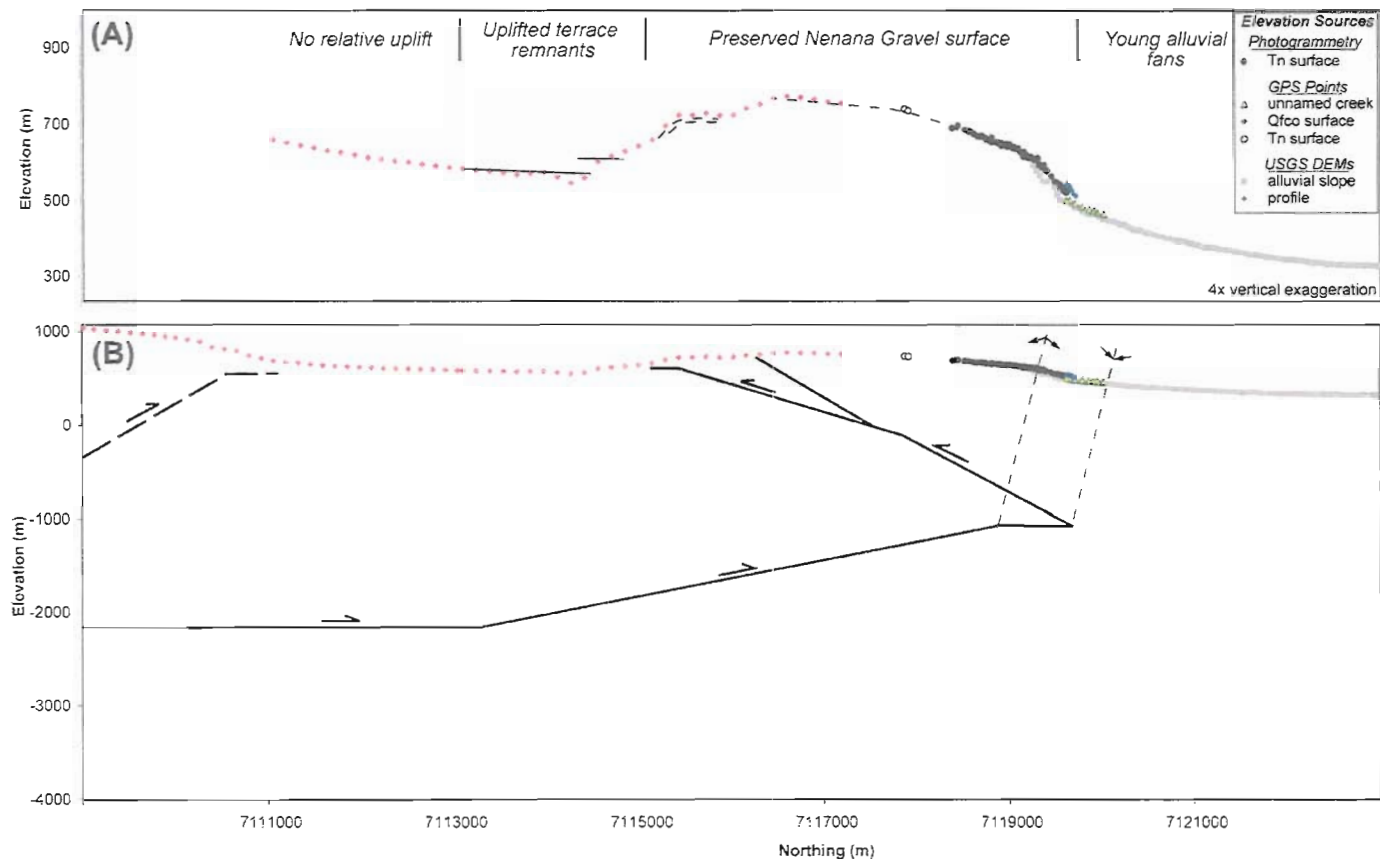
Figure 2.11. Topographic profile (A) and cross-sectional interpretation (B) along section B-B' (Plate 2.1). Preserved remnants of the Nenana Gravel surface are projected to the line of section to establish this surface as our primary structural datum. The profile data is derived from multiple sources, with photogrammetric and GPS survey data (including the data from Figure 2.6) used to defined the deformation on the north side of the Japan Hills anticline. The solid black lines in (A) show the position and approximate projection of the Q3 and Q5 surfaces. Thin dashed black lines depict the occurrence and approximate geometry of resistant beds that occur in the uppermost Nenana Gravel. In (B), the thick black lines indicate the interpreted fault geometry, with dashed lines represent poorly constrained dips. We schematically represent the monoclinal folds at the surface trace of the NFT and Gold King fault as a ramp-flat fault-bend fold.

2.6.4 Synthesis of Regional Deformation

Figure 2.12 presents our picture of how the faults in our study area fit in to the framework of range-bounding structures. Morphologically-young scarps demonstrate the Holocene activity of the Northern Foothills thrust beyond our map area (Carver et al., 2006), but not on the segment south of the Gold King fault. Instead we argue that most of the strain across the range front is accommodated by the Gold King fault. The NW-trending faults appear to accommodate some of this strain transfer from the Northern Foothills thrust to the Gold King fault. We depict the NW-striking faults as strike-slip, but it likely has a complex oblique component as well, as shown by an alternating pattern of which side of the fault is relatively up or down.
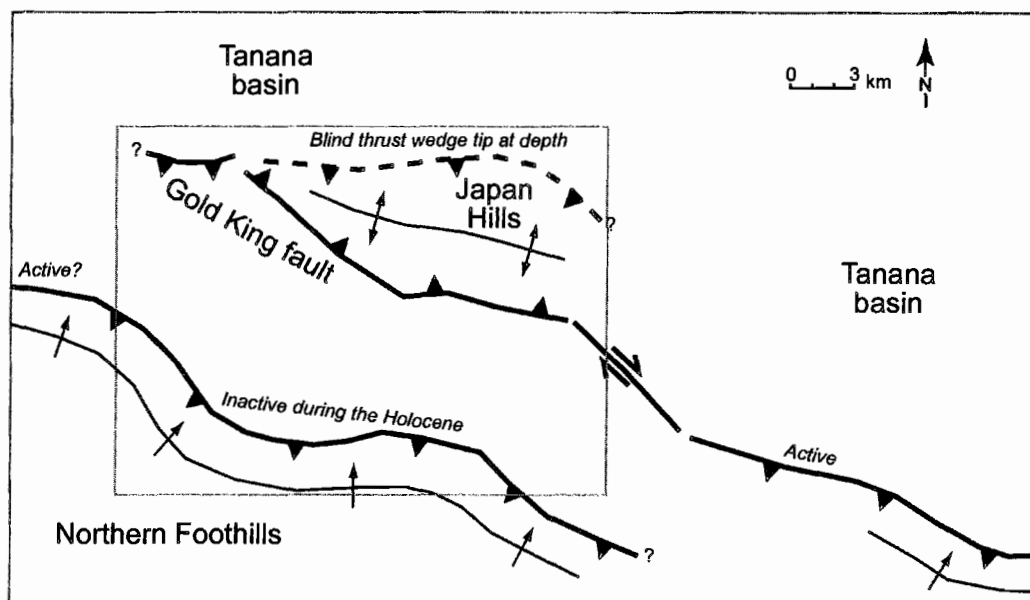
Figure 2.12. Schematic framework of the Japan Hills – Gold King structures as part of the northern Alaska Range thrust system. The Plate 2.1 map area is shown by the gray outline. The Gold King fault accommodates most of the recent deformation across this portion of the northern foothills range front, and the NW-striking fault on the east edge of the map area is a lateral structure that appears to accommodate the transfer of strain from the Northern Foothills thrust onto the Gold King fault.

2.7 Conclusions

Mapping and field investigations in the Japan Hills – Gold King Creek area on the south margin of the Tanana basin document the local Quaternary stratigraphy and deformation related to the Northern Foothills thrust and the Gold King fault. The Gold

King fault is a revision of the previously inferred "Japan Hills splay" (Bemis and Wallace, 2007) and displays clear evidence of late Pleistocene and likely Holocene surface displacement. The Northern Foothills thrust is a major thrust that dramatically displaces the Pliocene Nenana Gravel, but there is no evidence of Holocene offset on this fault within the map area and few late Pleistocene markers to assess its recent activity. Two additional active faults occur on the east margin of the map area and at least one acts as a structural linkage between the Northern Foothills thrust and the Gold King fault. Progressive deformation of geomorphic surfaces constrain the complex subsurface geometry of the Gold King fault that consists of a south-dipping thrust fault at depth, but forms a thrust wedge at depth underneath the Japan Hills where it breaches the surface as a north-dipping thrust.

This study highlights the importance of surficial geologic mapping and analysis of landforms in the investigation of active faults in Alaska and the potential for detailed structural analyses without the benefit of additional subsurface data. The sub-arctic climate and position beyond the glacial ice limits of the Pleistocene glacial advances appears to contribute to extensive preservation of Pleistocene landforms in this region, but the recent deformation recorded by landforms is still subtle due to the low slip rates of these faults. Therefore, in similar settings of poor geologic exposure, low slip rates, and particularly with a younger landscape or lower geomorphic preservation potential, the approach used here may be the only way to identify active faults.

2.8   Bridge

The previous chapter focuses on using the surficial geology and geomorphology of the Japan Hills – Gold King area of the northern margin of the Alaska Range to identify active thrust faults and constrain their subsurface geometry. Use of a sequence of progressively deformed landforms above a thrust fault provides unique constraints on fault geometry and evolution and is particularly important in this region of poor geologic exposure.

Chapter III employs this same technique of deriving subsurface thrust fault geometry from the progressive deformation of geomorphic surfaces, but applies it to a transect across the fold-thrust belt of the northern Alaska Range. I use the rates of displacement determined from individual surfaces offset across multiple faults within an orogenic wedge system to show that all the major faults in the system were active simultaneously through most of the Quaternary. However, the range-bounding thrust fault (the orogenic wedge tip) has experienced reduced activity over the most recent major glacial-interglacial cycles, and has not ruptured the surface since at least ~26 ka. I speculate that glacial loading during the Quaternary glacial advances increases the topographic slope for this portion of the Alaska Range orogenic wedge, promoting fault activity of the range-bounding faults during glacial advances and shifting fault activity to structures internal to the wedge during interglacial times.

CHAPTER III

PROGRESSIVELY DEFORMED GEOMORPHIC SURFACES CONSTRAIN THE

BALANCE BETWEEN THRUST WEDGE THICKENING AND FORELAND

PROPAGATION IN A BASEMENT-INVOLVED FOLD-THRUST BELT

This manuscript is co-authored with my faculty advisor, Ray Weldon. As lead author, I led data collection in the field and conducted the data compilation, analysis, interpretations, and manuscript preparation. Ray Weldon provided assistance with field data collection, interpretations, and critical reviews on drafts of this chapter.

3.1 Introduction

Basement-involved fold and thrust belts commonly accommodate shortening and mountain growth in intracontinental orogens (e.g. the Tien Shan in central Asia and the eastern Andes in South America). These differ from accretionary wedges and other thin-skinned fold and thrust belts through the incorporation of crystalline basement rocks as part of the internal structure of the fold and thrust belt instead of the deformation predominantly occurring within a sedimentary sequence detached from basement rocks. Although thin-skinned fold and thrust belts were the basis for the development of critical wedge theory (Chapple, 1978), where it can be shown that a gently dipping fault underlies a basement-involved belt, the same basic principles should also apply, though the deformation mechanisms that maintain the wedge may differ.

Critical coulomb wedge theory describes a deforming mountain belt as a wedge in equilibrium between frictional stresses on a basal fault and gravitational loading from the overlying topography. As a result, a balance between the thickening of the orogenic wedge (through internal deformation) and the foreland propagation of this wedge is predicted. However, there is no explicit constraint from the model that dictates whether thickening and propagation occur as alternating episodes or synchronously. Observations

of subduction zone earthquakes suggest that in accretionary wedges, much of the internal deformation occurs in association with megathrust earthquakes, often during aftershocks (e.g. Wang and Hu, 2006; Henstock et al., 2006; Fisher et al., 2007). Thus, the motion on the basal thrust occurs essentially simultaneous with wedge thickening, maintaining critical taper of the accretionary wedge. Simultaneous wedge thickening and propagation has also been observed by Price (2001) in the southern Canadian Rockies and in analogue modeling (e.g. Dixon and Liu, 1992). However, the equilibrium could also be maintained through alternating episodes of thickening and advancement of the wedge towards the foreland, such as is observed by Uba et al. (2009) in the Bolivian Subandes and through discrete element modeling (Naylor and Sinclair, 2007).

To evaluate the short-term (10^4-10^6 yr) balance of wedge thickening and propagation in continental belts, we need to examine geologic features present across the fold and thrust belt that represent a discrete period of time and record the deformation across the entire zone. This type of analysis would be difficult in ancient fold and thrust belts, as markers of sufficient temporal and spatial distribution to test short-term critical wedge behavior are uncommon. Thermochronologic methods have potential in ancient settings, but presumably would require a dense sampling strategy to differentiate between exhumation of the entire fold and thrust belt versus exhumation of local zones, and then the temporal resolution would be limited to time scales greater than ~10^5 yrs (Carrapa, 2009). Studies of the geometry of growth stratigraphy can provide robust constraints for the geometry of subsurface faults, and hold great promise for understanding the temporal relationships of faults within a fold-thrust belt, but is limited to areas of dense subsurface data or where there is abundant geologic exposure with well-dated stratigraphic sections. For active fold-thrust belts, neotectonic investigations of active structures and the progressive deformation of geomorphic surfaces across the deforming zone can provide constraints on thrust belt geometry and on individual fault activity on 10^2 to 10^6 yr time scales. These markers do not require significant geologic exposure and may be most useful in zones with relatively low shortening rates, perhaps on the order of <5 mm/yr. In this chapter, the term geomorphic surfaces represents all landforms which can be approximated to represent a formerly planar surface, including regional aggradational

alluvial surfaces and fluvial terraces.

In most active fold and thrust belts, fluvial terraces are often found along major streams emanating from the axis of the mountain belt. These surfaces are the abandoned floodplains of a stream and generally form as a result of the interaction between ongoing uplift and the punctuated/cyclic climatic changes of the late Cenozoic (e.g. Molnar et al., 1994). Because the contractional structures of a fold and thrust belt are typically the primary control on the topographic growth of the mountain belt, the major streams often flow across the structural grain. Therefore, in settings where fluvial terraces are well-preserved along a stream, these landforms behave as kinematic markers that record the cumulative fold and thrust belt deformation since the time of terrace formation. As Quaternary climate has experienced cyclic changes, multiple fluvial terraces are often preserved along a given stream, recording the progressive evolution of individual structures and the fold and thrust belt as a whole.

To examine the temporal balance of thickening and propagation of an orogenic wedge, we examine the active fold-thrust belt that occurs in the northern foothills of the central Alaska Range (Bemis, 2004; Bemis and Wallace, 2007) (Figure 3.1). This basement-involved thrust belt is comprised of east-west striking thrust faults and fault-related folds, and the widespread uplift of an extensive Plio-Pleistocene geomorphic surface indicates that a basal thrust underlies the entire deforming region. Therefore, using the unique constraints provided by the progressive deformation of sequences of geomorphic surfaces preserved across the western portion of this thrust belt, we will present 1) a structural cross-section for the region between the Nenana and Teklanika rivers, 2) evidence for simultaneous activity of multiple faults within the fold-thrust belt, 3) estimates of Quaternary slip rates for two faults as recorded by multiple geomorphic surfaces, and 4) evidence for a change in thrust wedge behavior in the mid-late Pleistocene. This approach will demonstrate the utility of the progressive deformation of geomorphic features for defining structures and the mechanical relationships between faults.
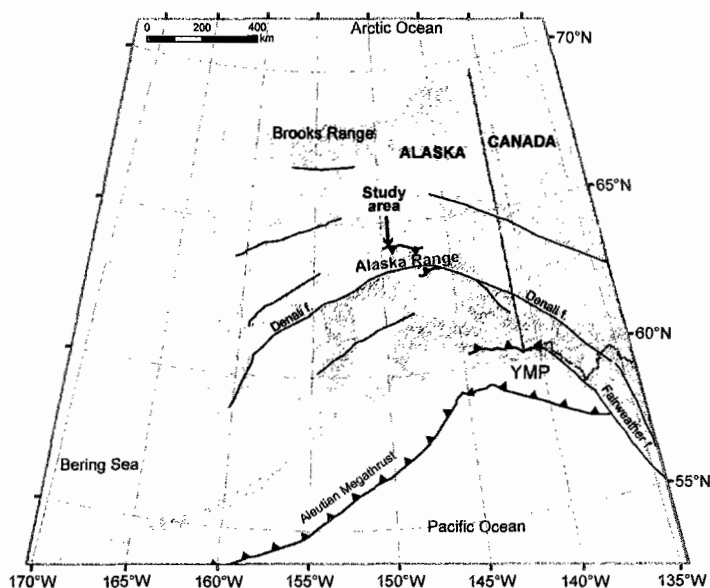
Figure 3.1. Regional DEM of Alaska illustrating the position of the northern foothills fold-thrust belt (NFFTB) relative to the major active tectonic elements and topography. The northern foothills fold-thrust belt is indicated by the thrust fault symbol on the north margin of the Alaska Range, with the study region indicated. The Yakutat microplate, which drives deformation in central Alaska, is labeled as YMP.

3.2   Regional Setting

The Alaska Range is a transpressional mountain belt in south-central Alaska whose modern growth has occurred over the past ~6 Ma (e.g. Haeussler, 2008; Fitzgerald et al., 1995). This deformation is the result of far-field deformation from the subduction and collision of the Yakutat Microplate, approximately 500 km away in southeast Alaska (e.g. Plafker et al., 1994; Haeussler et al., 2008) (Figure 3.1). This collision drives the counterclockwise rotation and northwest migration of south-central Alaska, which is bounded on the north by the Denali – Totschunda fault system. The oblique interaction of south-central Alaska with North America in the region of the Alaska Range is resolved into right-lateral strike-slip on the Denali fault and Denali fault-normal contraction accommodated by east-west striking thrust/reverse faults in the northern Alaska Range (Bemis and Wallace, 2007; Carver et al., 2006; Carver et al., 2008; Chapter IV).

Recent neotectonic studies have recognized numerous active and potentially active faults on the north side of the Alaska Range from Kantishna Hills eastward to Tok (Figure 3.2). In the Alaska Range between the Kantishna Hills and the Wood River,

deformation of Neogene sedimentary rocks, as mapped by Wahrhaftig (1970a; b; c; d; e; f; g; h) led Bemis and Wallace (2007) to define a series of east-west trending faults and folds that they termed the "northern foothills fold-and-thrust belt" (NFFTB). These faults are clearly active in the Pleistocene, with several showing evidence for Holocene deformation. Carver et al. (2006) expanded the understanding of the Donnelly Dome fault (DDF on Figure 3.2) near the Delta River by tracing deformation related to that thrust fault to the west and linking this deformation with the eastern extent of the faults identified and inferred by Bemis and Wallace (2007). Additional active faulting on the north side of the Alaska Range east of the Delta River has been constrained by Carver et al. (2008).
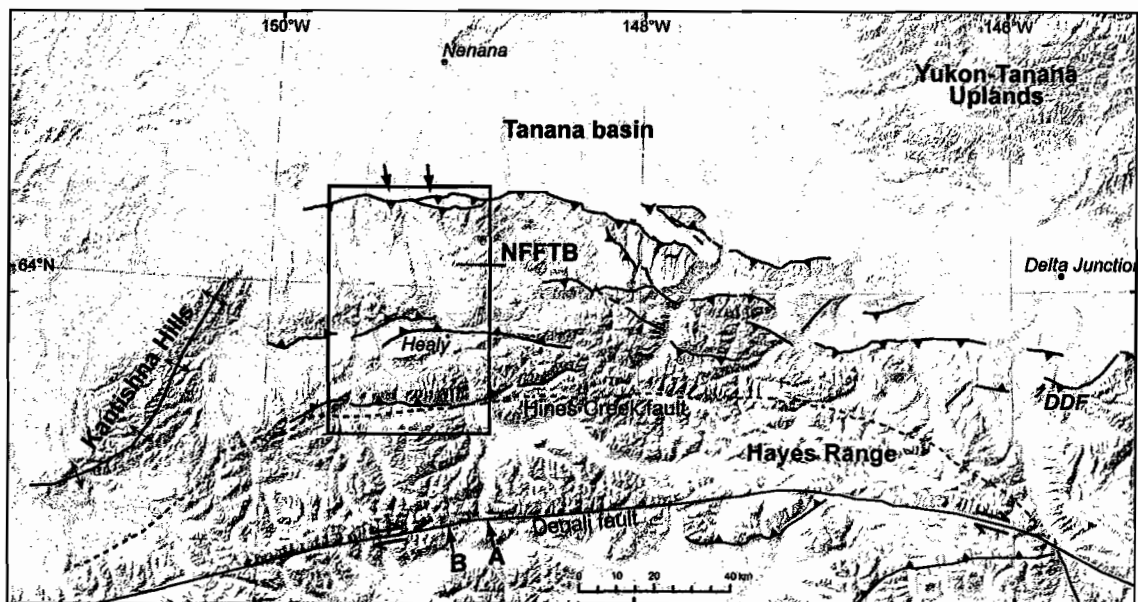
Figure 3.2. Shaded-relief image of interior Alaska, showing the distribution of active faults in the NFFTB in relation to the young topography of the Alaska Range and Tanana basin. The regions of highest topography are highlighted by the extent of modern glaciers, depicted by the white regions. Streams, shown as thin white lines, emanate from the axis and south side of the Alaska Range, flowing across the topographic grain and into the Tanana basin. Labeled geographic features are mentioned in text, except those in italics, which are communities that are shown for geographic reference. The black box outlines the area of Figure 3.3.

NFFTB deformation is only clearly documented for the northern half of the central Alaska Range, the remaining portion between the Denali fault and the NFFTB

exhibits dramatic post-Paleogene deformation, and possibly Quaternary deformation, but individual active structures have not been recognized. While the region close to the Denali fault may be active, we agree with Hauessler (2008) that it is unlikely that individual faults with a slip rate of >2 mm/yr would have been missed in the region between the Hines Creek and Denali faults (Figure 3.2) (except perhaps in the Hayes Range that remains heavily glaciated to this day).

In general, the thrust faults of the NFFTB appear to form a generally north-vergent thrust wedge over a south-dipping basal thrust. The surface trace of this basal thrust primarily occurs at the abrupt range front dividing the Alaska Range from the Tanana basin to the north (Figure 3.2). There are limited geophysical investigations in this region of sufficient resolution to image shallow crustal structures, but Fisher et al. (2004; 2007) identified a nearly horizontal seismic reflector between 5-8 km depth beneath the Alaska Range near the Delta River and is the only geophysically-observed evidence for this basal thrust. However, the widespread uplift of the two regional geomorphic surfaces that span all the individual structures within the NFFTB demonstrate that the uplift of the northern Alaska Range is controlled by a primary thrust fault at depth. Additional and related deformation occurs from faults in the hanging-wall of this basal thrust. The Tanana basin is a modern aggrading basin, with ~2-2.5 km of Neogene sedimentary fill (Hanson et al., 1968), that lies immediately north of the Alaska Range along the entire east-west length, separating it from the Yukon-Tanana Uplands (Figure 3.2).

3.3   Study Area

This study focuses on a transect across the northern foothills of the Alaska Range, north of the Hines Creek fault and covering a swath extending 30 km west from the Nenana River (Figures 3.2 and 3.3). The topography of the region is relatively subdued, except for the abrupt range front at the northern margin and gradually increasing topographic relief to the south. The stratigraphy of the study area can be broadly divided into 3 units – the crystalline basement rocks of the Yukon-Tanana terrane, 1-2 km of Neogene terrestrial sediments, and Quaternary glacial, alluvial, and colluvial deposits.
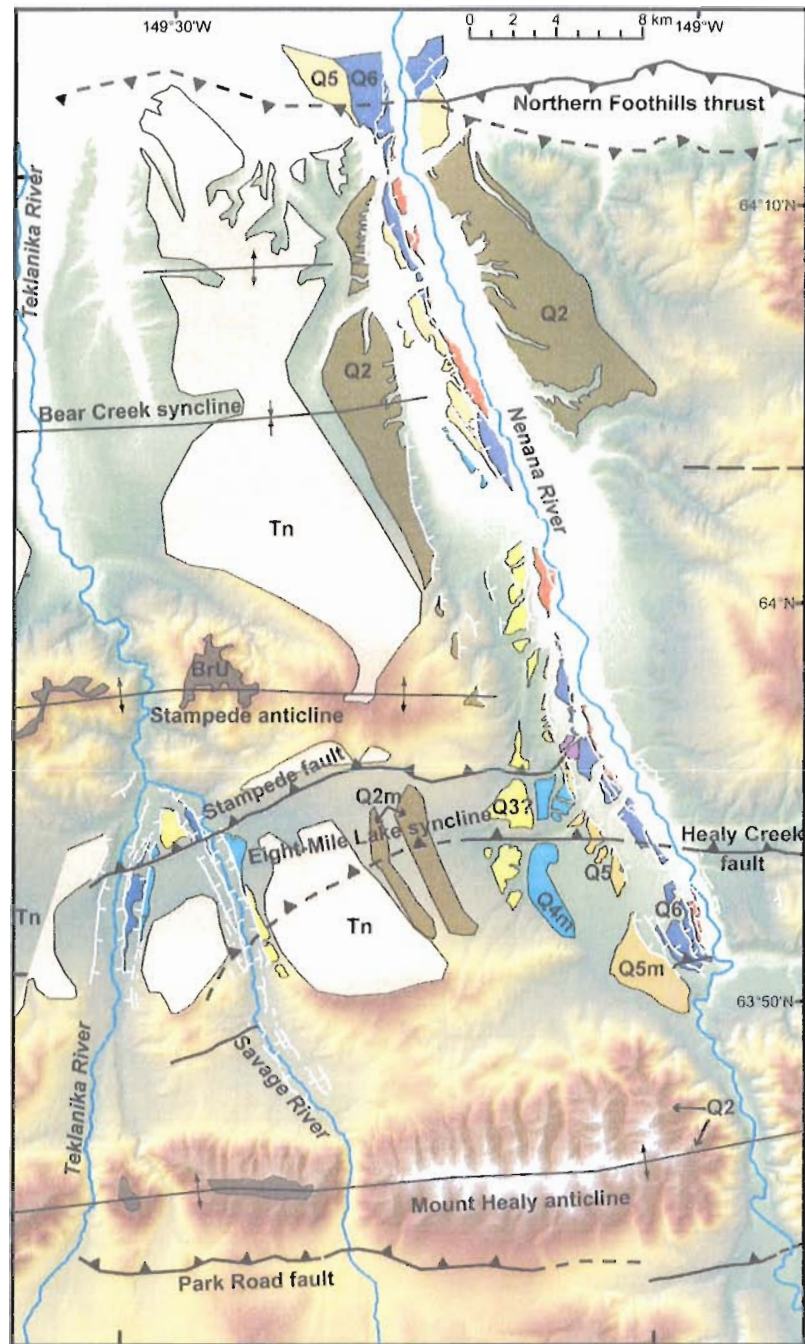
Figure 3.3. Mapped terraces and geomorphic surfaces draped on a DEM of the study area. Quaternary faults are shown with solid lines where well-located and dashed where approximate or uncertain activity since mid-Pleistocene. White lines indicate terrace risers with ticks pointing downhill. Surfaces are labeled, and labels annotated with an 'm' indicate morainal remnants associated with the respective glacial advance. Major south-vergent thrusts lift the east-west trending anticlines that thicken the region between the thrust wedge tip at the range front and the Denali fault to the south. However, the entire region, including synclines, is uplifted as well.

The Nenana River and Teklanika – Savage rivers are two north-flowing systems that have incised courses nearly perpendicular to the modern structures (Figure 3.3), providing a natural cross-section across this fold-thrust belt. These are antecedent streams that have occupied essentially the same course since uplift of the region began. As is common in the lower elevations of interior Alaska, there is poor geologic exposure. However, well-preserved landforms correlated with regional glacial advances spanning the Quaternary occur along these drainage systems (Wahrhaftig, 1958; Ritter, 1982; Thorson, 1986).

3.3.1 *Glacial Sequence and Geomorphic Surfaces*

Glacial advances resulting from global climatic variations throughout the Quaternary are recorded by moraine deposits and fluvial terraces within the northern foothills of the Alaska Range. The timing and regional correlation of many of these events are poorly understood, but Table 3.1 summarizes the current understanding of this sequence and Figure 3.4 shows a schematic east-west cross-section of the relative positions of the landforms associated with the glacial advances. In addition to the fluvial terraces, the Nenana Gravel and an underlying bedrock surface are fundamental datums for understanding the late Cenozoic development of the Alaska Range. The older surface is an exhumed erosional unconformity separating the crystalline basement rocks from the Neogene sediments. This surface is often mantled with scattered fluvial cobbles as a lag following the erosional removal of the poorly consolidated Neogene sediments (Wahrhaftig, 1958) and can often be traced parallel to the structural trend to where these sediments are still present above the unconformity. Due to the time-transgressive nature of this erosion surface (i.e. Wahrhaftig, 1970a; 1970b; 1970d; 1970e) it is not a useful marker for determining slip rates and absolute values for displacement, but it locally provides minimum or maximum constraints on displacement and style of deformation.

The Nenana Gravel is a Pliocene deposit composed of coarse-grained sediments shed from the uplift of the Alaska Range, and whose upper surface represents the former foreland basin surface prior to uplift and deformation in the NFFTB (Wahrhaftig, 1987; Thoms, 2000; Ridgway et al., 2007). This deposit is more widespread (Figure 3.3) and represents a more recent and relatively discrete period of time than the bedrock erosional

unconformity and is a important marker for understanding the rates and styles of deformation. Wahrhaftig (1987) concluded that the end of Nenana Gravel deposition occurred prior to ~2.8 Ma, due to the age of a Jumbo Dome, a small intrusion with map relationships that suggest it post-dates the Nenana Gravel. Recently this intrusion has been redated at ~1 Ma (Athey et al., 2006). However, this constraint on the end of Nenana Gravel deposition is likely only valid for the structural domain that includes the intrusion, and due to probable variations in the propagation of thrust faults (Bemis and Wallace, 2007), the age of this upper surface of the Nenana Gravel may vary significantly.

Table 3.1. Approximate Nenana River valley surface ages.

Surface name	Regional Correlation	Marine Isotope Stage*	Age constraints	References
Modern streams	n/a	1	Modern	
Q7	Carlo	2	~19-22 ka	Dortch (2006); Wahrhaftig (1958; 1970a; 1970b)
Q6, Q6II	Riley Creek	2	~22-28 ka	Dortch (2006); Wahrhaftig (1958; 1970a; 1970b); Ritter (1982)
Q5	Healy	4	~60 ka	Dortch (2006); Beget (2001); Ritter (1982); Wahrhaftig (1958; 1970a; 1970b)
Q4	Lignite Creek	6	~130-191 ka	Thorson (1986); Beget and Keskinen (1991); Beget (2001); Reger et al. (2008)
Q3?	???	n/d	n/d	Could be Bear Creek glacial advance of Thorson (1986)
Q2	Browne	n/a	~1.47-1.60 Ma	Our inferred correlation to a major glacial advance recognized in Yukon Territory, Canada (Westgate et al., 2001)
Tn	Nenana Gravel	n/a	>1 Ma ~2.0 – 2.6 Ma	Age of Jumbo Dome (Athey et al., 2006) Onset of Pleistocene glacial cooling (IUGS) and 2 Ma Dawson Cut Interglaciation near Fairbanks, AK (Péwé et al., 2009)
BrU	Bedrock unconformity	n/a	~6 Ma	Base of Nenana Gravel (Triplehorn et al., 2000)
			Oligocene-Miocene	Base of Usibelli Group – varies regionally

Notes: n/d = no data; n/a = not applicable.
* (Gibbard et al., 2010).

3.4   Progressively Deformed Geomorphic Surfaces

Figure 3.3 shows the distribution of fluvial terraces and geomorphic surfaces in the Nenana River valley, and along the Teklanika River and its major tributary the Savage River. We mapped these using stereo air photo pairs, orthorectified satellite imagery, the USGS National Elevation Dataset digital elevation model, and locally 1:1200-scale topographic maps from Usibelli Coal Mine, Inc. Correlations of deposits and landforms are derived from the mapping of Wahrhaftig (1970e; 1970c; 1970f), Ritter (1982), Thorson (1986), and through analysis of map relations.

3.4.1 Regional Profiles

We compiled longitudinal profiles of the mappable terraces and geomorphic surfaces to examine the contributions of individual structures to the regional deformation. As the faults near the Nenana River valley all strike within a few degrees of east or west (Figure 3.2), we projected the terraces onto a vertical plane simply by plotting elevation against the UTM northing coordinate for each point (Figure 3.4). We sampled the surfaces at a 50 m spacing along a profile line drawn on each surface, tracing the terrace tread where it is unmodified by erosion or deposition. Where we had multiple sources of elevation data, we only show the profile data from the highest resolution source. In addition to the elevation sources listed above, we also include profiles extracted from a proprietary high-resolution photogrammetric DEM (derived from 2 ft contours) that
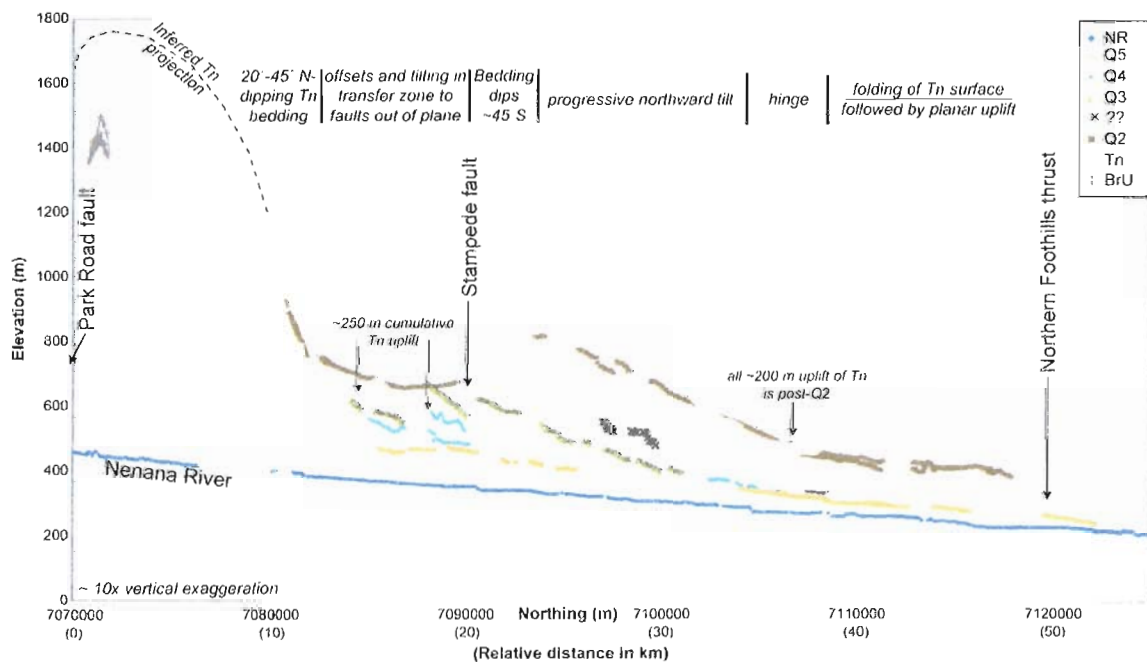
Figure 3.4. Profiles of geomorphic surfaces along the Nenana River valley, projected onto a north-south vertical plane. Zones of uplifted and tilted terraces are separated from zones of simple uplift by narrow hinge zones and faults. The progressive rotation of terraces require a listric thrust fault at depth, yet the regional uplift recorded by stream-parallel sections of the terraces require a relatively planar thrust fault at depth. These faults intersect below the hinge zones. Both absolute position (UTM northing coordinate) and relative distance is given on the x-axis.

covers a narrow strip adjacent to the highway that follows the Nenana River. Several sources of uncertainty impact the elevation of these profile points, including variable thickness of loess deposits on top of the terrace tread, hummocky organic mats which vary in thickness with vegetation patterns, colluvial deposition from nearby hillslopes and erosion of the surface, and the vertical resolution of the source data. For the oldest surfaces, erosion/deposition and source data resolution are the largest sources of uncertainty, but this 1-5 meter scale variability is negligible relative to the >100 meters of uplift and deformation of these landforms.

Figure 3.4 shows the characteristics of the regional uplift and local structures as recorded by the deformed sequence of surfaces along the Nenana River and where measured bedding dips reflect the inclination of the Tn surface. The cumulative deformation of this fold-thrust belt since the end of Nenana Gravel deposition is recorded by the Tn surface, with successively lower terraces recording more recent intervals of time. We sampled multiple segments of the Tn and Q2 surfaces north of the Stampede anticline to identify a representative average profile of these surfaces.

3.4.2   Local Profiles and Fault Activity

We present more detailed local surface profiles from landforms that the Quaternary faults cross within our transect. Of particular interest are the Stampede fault, Park Road fault, and Northern Foothills thrust. The Healy Creek fault projects into the transect from the east, but decreases from >1 km of displacement east of the Nenana River (Bemis and Wallace, 2007) to <100 m to the west between the Nenana and Savage Rivers as it transfers slip north onto the Stampede fault. We collected GPS profiles along the terrace treads because the resolution of the USGS DEM is not adequate for examining fault-related deformation of the middle to late Pleistocene terraces. These surveys were performed with a Trimble GeoXH, with the Terrasync data collection software, and points were collected every 70-100 m with closer spacing in zones of visible deformation. The survey data was post-processed against three widely-spaced continuous GPS stations within ~140 km using Trimble's Pathfinder Office v4.0 to correct for atmospheric and GPS errors. For the Stampede fault, the survey points have been projected parallel to the fault trace onto a vertical plane that is perpendicular to the fault.

Although streams in tectonically active areas typically have a concave-up longitudinal profile on a regional scale (e.g. Pazzaglia et al., 1998), short stretches can be approximated as linear. As such, the abandoned floodplains of the these streams can be similarly approximated as linear. Deviations from this linear projection represent either tectonic deformation, deposition/erosion on the terrace tread, or errors internal to the data source. In our local terrace profiles we fit linear regressions to linear segments of the terrace profiles in order to project the terrace surfaces across the fault and make accurate measures of cumulative offset.

3.4.3 Northern Foothills Thrust

Latest Pleistocene terraces cross the Northern Foothills thrust where the Nenana River emanates from the northern foothills into the Tanana basin (Figure 3.3). North of the range front, the terraces become the proximal portion of the broad, low-gradient alluvial fans formed by the aggradation of glacial outwash on the basin floor. West of the Nenana River, the style of long-term deformation is clearly defined by the Tn and Q2 surfaces. East of the Nenana River there is less preservation of the older geomorphic surfaces, but the fault trace occurs a few kilometers north from the primary topographic range front and has uplifted a surface that was part of the basin floor at the time of fault initiation. Figure 3.5 shows the profiles of the surfaces from the Bear Creek syncline (Figure 3.3) to the north across the Northern Foothills thrust. These profiles show that the Tn surface is broadly folded with a subtle vergence to the north. Lower terraces, such as Q2, are planar and appear to cut across this fold, suggesting a change in fault geometry through time. The folding recorded by the Tn surface (Figure 3.5) requires distributed shear or migration of fold hinges through time, whereas the planar terraces suggest uplift over a planar fault, indicating that the fault tip of the Northern Foothills thrust was propagating towards the surface following abandonment of Tn and had breached the surface by the time Q2 formed. Cumulative offset measurements of Tn and Q2 (Table 3.2) are only minimum values, as the equivalent surfaces on the footwall of the faults is buried beneath younger alluvium. Neither Q3(?) or Q4 is present north of the Bear Creek syncline, and only late Pleistocene terraces are preserved across the fault trace. A small (2-4 m) scarp was observed in the field on Q5 east of the Nenana River, but surveys of

the Q6 and Q7 terraces, which have well-preserved treads across the fault projection west of the river, do not have evidence of fault-related surface displacement. A nearly continuous scarp extends east from the Nenana River on Q5 and older surfaces for >12 km. Preliminary paleoseismic investigations of the Northern Foothills thrust at a site ~8.5 km east of the Nenana River indicate that the most recent surface-rupturing earthquake on this fault occurred prior to ~26 ka (Appendix A). Given the lack of deformation of the Q6 and Q7 terraces across the fault and the large low-gradient fan formed by these deposits out into the basin, we infer that most of the post-Q6 incision is climatically-induced.
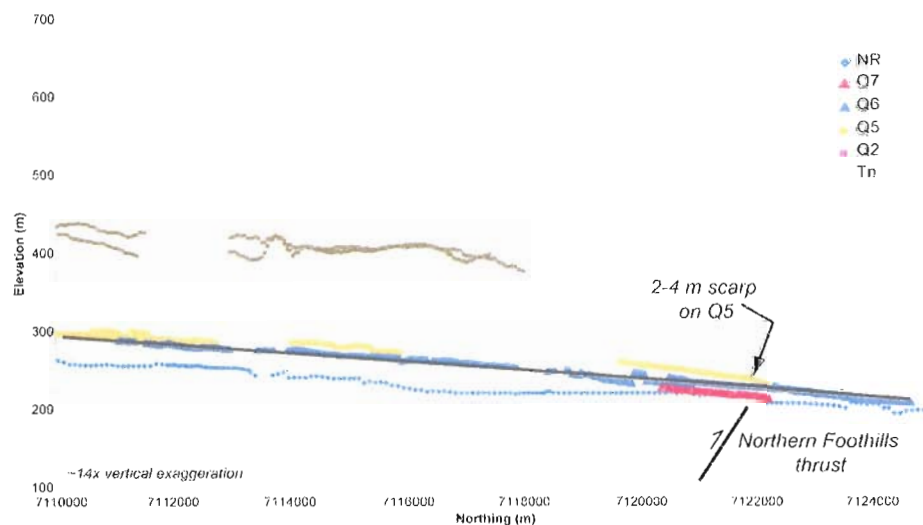
Figure 3.5. Geomorphic surface profiles across the Northern Foothills thrust. Depths of the Tn and Q2 surfaces north of this fault are unknown, so offsets for these surfaces record only a minimum value. These minimum values (Table 3.2) were measured between the surface and the low point immediately north of the fault and between the broad alluvial fans formed where the rivers emanate from the range. The scarp on Q5 was observed in the field on the east side of the Nenana River, but similar scarps do not occur on the Q6 and Q7 terraces immediately west of the river. The irregularity of the points on the high surfaces and the Nenana River are due to the low resolution of the USGS DEM, except a couple segments where closely-spaced points on the Nenana River indicate coverage by the high-resolution DEMs. The NFT is shown schematically in the subsurface.

3.4.4 Stampede Fault

The Savage and Teklanika rivers originate in the higher peaks near the Denali fault and flow northwards across the bedrock ridge formed by the Mount Healy anticline, the Eight-Mile Lake syncline, and then converge before flowing through the bedrock-

cored Stampede anticline (Figure 3.2). Along this course, these streams cross the Park
Road fault/Hines Creek fault and the Stampede fault. Well-defined fluvial terraces
extend downstream from immediately north of the bedrock core of the Mount Healy
anticline and parallel both streams to their confluence. Figure 3.6 shows the compilation
of the profiled terraces along both sides of the Savage River and the east side of the
Teklanika River where these surfaces cross the Stampede fault, illustrating the
progressively larger offsets of the older features. The fault is crossed by multiple terraces
correlated with each of 2 separate glacial advances, and each terrace of a given advance
has different values of cumulative uplift (Table 3.2). These differences are likely the
result of an along-strike change in slip rate/fault geometry or slightly different timing of
terrace formation between the Savage and Teklanika rivers. The northward tilting of the
Q4 terrace relative to the stream gradient mimics a greater degree of tilting shown by
successively older terraces that only appear on the east side of the Savage River.
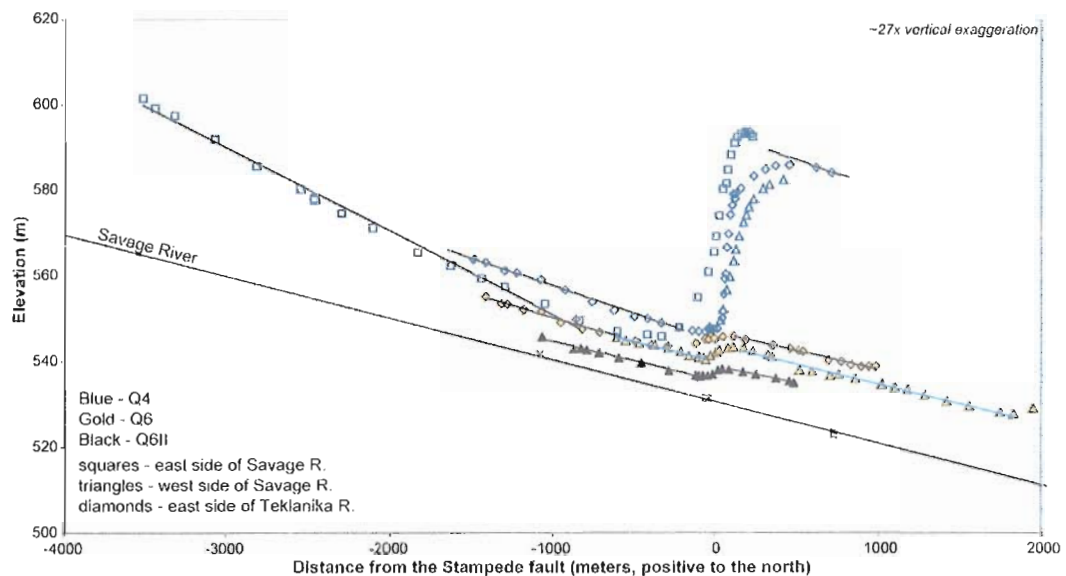
Figure 3.6. Differential GPS profiles across the surface trace of the Stampede fault, illustrating progressive
displacement across the Stampede fault during the mid-late Pleistocene. Hanging-wall and footwall panels
are essentially parallel, although the Q4 offsets only had short segments preserved on the hanging-wall and
were assumed to be parallel to calculate displacements. Black lines are the linear least squares regressions
for sets of points, with blue lines used on a Q6 surface to distinguish it from the adjacent profile. The ages
of these terraces demonstrate that the slip rate is relatively constant over the timespan of these offsets.

3.4.5   Park Road Fault

This fault was interpreted by Bemis and Wallace (2007) from several previously mapped fault segments (Wahrhaftig, 1958; Wegner, 1972; Sherwood and Craddock, 1979) to explain the uplift and deformation of the Mount Healy anticline and folding of the Neogene units on the northern limb of this fold. The fault trace as depicted on Figure 3.3 is modified from Bemis and Wallace (2007) based on new observations of fault scarps in alluvial fans and deformation of the small patch of Nenana Gravel south of Mount Healy anticline. There are no continuous geomorphic surfaces preserved across the fault and fold, but Thorson (1986) describes a cross-valley architecture for the Nenana River canyon through the Mount Healy anticline that suggests a series of perched U-shaped valleys, correlating the highest of these with the Q2 advance (Figure 3.3). A 6 m offset of a late Pleistocene alluvial surface east of the Nenana River (Wahrhaftig et al., 1975) and new observations of fault scarps in late Pleistocene alluvium near the Savage River demonstrate recent fault activity. The folded Tn surface and terraces on the north limb of the Mount Healy anticline indicate a fault bend or intersection at depth.

3.4.6   Healy Creek Fault

The Healy Creek fault is a major, steeply north-dipping reverse fault that is clearly defined on the east side of the Nenana River (Wahrhaftig, 1970e). This fault forms a prominent scarp on the high terrace immediately east of the river and can be traced for more than 10 km eastward. However, the continuation of the fault across the Nenana River is not as clear. Field surveys and topographic profiles of the late Pleistocene terrace surfaces that cross the westward projection of the Healy Creek fault show these terraces are not deformed by the fault. Bemis and Wallace (2007) argue for an offset where the Healy Creek fault projects across the Q5 surface (Figure 3.3), but this could be apparent due to erosion of the terrace surface on the south side of the fault trace. Just west of Q5 (Figure 3.3), offsets become very distinct where the fault trace projects across the Q4 and Q3(?) surfaces and landforms. Despite extensive weathering of the Q4 moraines (Q4m), they are approximately 70 – 80 m higher north of the fault trace, in a similar manner to the larger Q3(?) surface offset (Figure 3.4). The Q3(?) surface offset decreases to the west as the displacement of surfaces across the Stampede fault

immediately north increases along the same distance. Projection of the fault across the Q2 lateral moraines aligns the fault with an ~50 m high offset of the Tn surface. This offset appears to be a fold rather than a discrete scarp, and becomes less pronounced farther west as it begins to curve to the southwest (Figure 3.3).

Table 3.2. Dip-slip offsets of geomorphic surfaces.

Fault	Surface	Offset (m)	Uncertainty (+/-, m)	Comments
Northern Foothills thrust*				
	Tn	880	220	Vertical offset a minimum value
	Q2	530	120	Vertical offset a minimum value
	Q5	9	3	
Stampede fault†				
	Tn	2000	450	Offset measured graphically
	Q2	850	190	Offset measured graphically
	Q4(a)	140	35	East side of the Teklanika River
	Q4(b)	100	26	East side of the Savage River
	Q6(a)	16	4	East side of the Teklanika River
	Q6(b)	8	2	West side of the Savage River
	Q6II	7	2	West side of the Savage River

Note: Uncertainties only account for variation from the range of possible fault dips and does not account for errors due to the projection of surfaces and the projection of survey data onto a vertical plane.

* Offsets calculated for a 20° dip, with the uncertainty representing the range of offsets that would result for fault dip from 15°-25°.

† Offsets calculated for a 28° dip, with the uncertainty representing the range of offsets that would result for fault dip from 21°-35°, except where otherwise noted.

3.5   Regional Cross-section

Limiting our cross-sectional analysis to the deformation described by the upper beds and surface of the Nenana Gravel and younger landforms ensures that we are capturing only the deformation on structures that were active during the Quaternary. The widespread uplift of the entire northern foothills belt, and in particular the uplifted synclinal axes that occur between major anticlines, provides strong evidence for a single south-dipping, relatively planar thrust fault extending the north-south width of the NFFTB. The dip of this basal thrust is unconstrained by independent observations; however, as the folding of the Tn surface occurs over additional hanging-wall structures, the intersection of these hanging-wall faults provide some constraint on the basal thrust at depth. Therefore, given the spacing of the hanging-wall faults and the locations of the Eight-Mile Lake and Bear Creek synclines (Figure 3.5), we define a range for the dip of the basal thrust of between 15°-25° (Figure 3.7). Steeper dips would require steeper hanging-wall faults, and with the documentation by Veenstra et al. (2006) of crustal

thickness between 25-30 km across this portion of the Alaska Range, the basal thrust would project into the ductile zone at dips greater than 25-30°. Shallower dips for the basal thrust would produce a very thin thrust wedge (Figure 3.7) and requiring a weak detachment surface to support the observed wavelength of structures. Because the basement of the northern foothills is composed of crystalline metamorphic rocks, we do not expect it to form a weak detachment surface.

The broad panel of progressively northward tilted terraces north of the Stampede fault (Figure 3.5) illustrate a style of deformation that is difficult to reconcile with typical structural models of fault-related folds. Instead, we argue that the progressive rotation is produced in the hanging-wall of a concave-up, listric thrust fault (e.g. Amos et al., 2007; Seeber and Sorlien, 2000), as shown in Figure 3.7. This style of faulting results in a
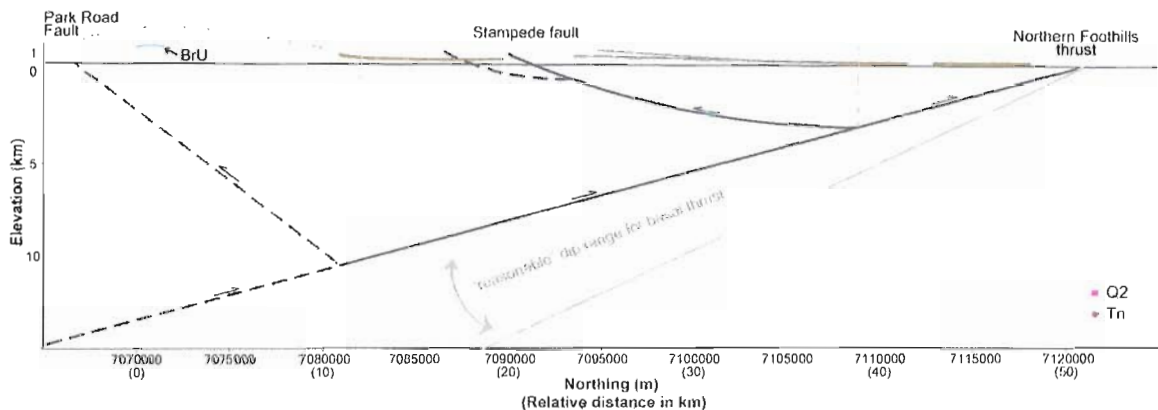
Figure 3.7. North-south cross-section based on constraints from profiles of geomorphic surfaces. The geometry is based primarily upon the deformation recorded by the oldest two surfaces, Tn and Q2, which are the only surfaces shown here for clarity. The younger surfaces provide controls on location of hinges and patterns of continued deformation. The best fit lines for planar segments of the rotated portions of Tn and Q2 that we used to reconstruct the surface rotation are shown over the profile points. The location of the bisector for the Stampede fault intersection with the basal thrust is based on the hinge recorded in the Q5 surface. Because there are a range of fault dip angles allowable for the given constraints, "reasonable" range indicates a range of basal thrust dips to which the Park Road and Stampede fault can be fit by changing the dip or radius of curvature so as to intersect at the appropriate hinge bisector and known surface trace.

relatively simple geometry while minimizing geometric space problems to produce the tilted panels (Figure 3.8). Standard fault-related fold models do not adequately fit this structure. For example, in a typical fault-bend fold (Suppe, 1983), the length of the dipping limb equals the amount of offset on the fault at depth. Furthermore, terraces

formed over a growing fault-bend fold do not fan – subsequent terraces would simply be folded to the same angle as older ones (e.g. Amos et al., 2007; Burgette, 2008). Fault-propagation folding (Suppe and Medwedeff, 1990) and its modification of tri-shear fault-propagation folding (Erslev, 1991) do not produce a wide zone of tilting of progressively emplaced terraces, particularly after the fault has propagated to the surface (Figure 3.8). Detachment folds are a common way to created broad, progressive tilting of a dip panel; however, in the NFFTB, we have no evidence of a likely detachment horizon, the fault tip is at the surface, and it would have to be an extremely asymmetric detachment fold.
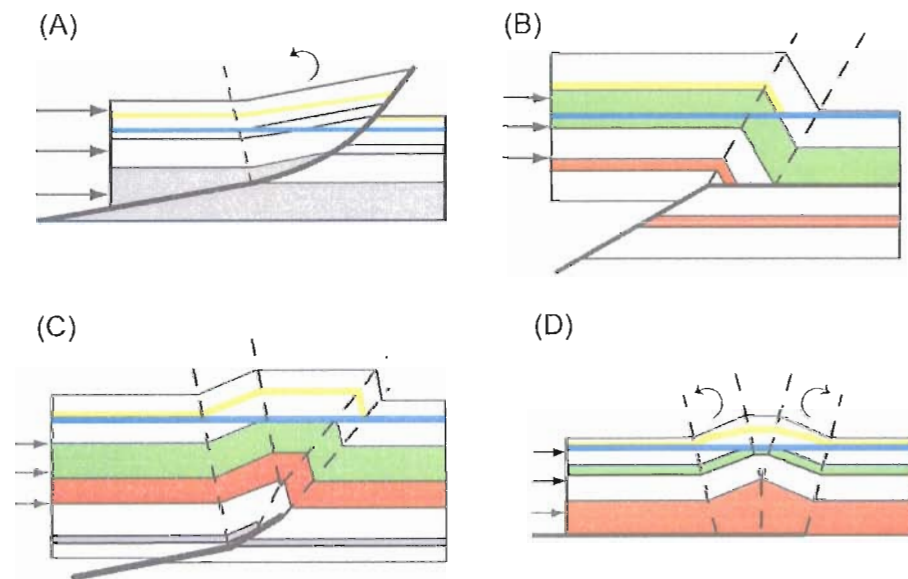
Figure 3.8. Examples of progressive terrace deformation over common idealized styles of fault-related folds. In each example, the thick blue line represents the modern stream profile, the folded thick orange line depicts an older, deformed terrace, and the upper surface represents the former ground surface prior to fault initiation. The rest of the colored bands represent the original subsurface stratigraphy and the thin dashed lines depict fold hinges. A) illustrates the change in the geometry of terrace deformation over a ramp to listric thrust fault transition, with the curved arrow highlighting the panel of progressively rotated terraces over the listric segment (modified from Amos et al. (2007)). B) shows the deformation of terraces above a fault-bend fold, showing the planar uplift above the dipping ramp and parallel tilting of surfaces in the fold forelimb above the flat. Modified from Burgette (2008). C) illustrates an early stage in the growth of a fault-propagation fold, where folding is concentrated above the propagating fault ramp. This style of faulting can produce a long tilted panel above the propagating ramp, but the terraces above this segment will be parallel and progressively shorter. Modified from Burgette (2008). D) Terrace deformation above a detachment fold, and highlighting the two, opposite-facing progressively rotated panels. Modified from Amos et al. (2007).

3.6   Fold-thrust Belt Development and Temporal Variations in Thrust Activity

A critical aspect for the timing of development of this segment of the NFFTB is the occurrence of two points that have experienced little uplift relative to rest of the transect (Figure 3.4). These points delineate zones that overlie only one of the major faults of the thrust wedge at depth (Figure 3.7). The Bear Creek syncline (Figures 3.3 and 3.4) occupies one of these points, south of the range front fold recorded only by the Tn surface. Planar terraces cutting across the folded older surface indicate this fold in the Nenana Gravel formed during the propagation of the fault to the surface, with the end of folding coinciding with the fault tip reaching the surface. Possible evidence for shearing during this early phase of fault-propagation folding occurs as distributed millimeter-scale shear zones in the Nenana Gravel. These shears, where observed, show a locally-consistent dip and sense of vergence. Considering that the Q2 glacial deposits and outwash are incised into all three fault-related anticlines in this transect, it appears that all three faults initiated growth prior to Q2. Lateral moraines assigned to the Q2 advance extend across the Eight-Mile Lake syncline and indicate aggradation of these moraines (Q2m) above the Tn surface (Figure 3.3), providing additional evidence for a lack of pre-Q2 incision at this point.

Following Q2, an extended period of uplift occurred on all three major faults in the wedge, as shown by the significant uplift of the Mount Healy anticline, the progressive rotation of post-Q2 terraces over the Stampede fault, and the regional uplift of the thrust belt accommodated by the basal detachment of the thrust wedge, the Northern Foothills thrust. A long gap in time exists between the Q2 and Q5 glacial advances in which most of the uplift at the range front occurred. However, we argue that the portion of the uplift accommodated by the Northern Foothills thrust across the entire transect has been essentially constant during that time interval because there is only on the order of ~50 m more relief above the Nenana River of the Q2 deposits in the 8-Mile Lake syncline than for the same deposits in the Bear Creek syncline. Where deposits between Q2 and Q5 exist, notably in the hanging-wall of the Stampede fault (Figures 3.4 and 3.8), they are also progressively deformed. Therefore, this thrust system maintained critical wedge taper between Q2 and Q5 by essentially simultaneous displacement on all

the major faults in this segment of the NFFTB.

We combine dip-slip offsets of surfaces (Table 3.2) with the range of possible fault dips constrained by our cross-section (Figure 3.7) to calculate a range of values for cumulative dip-slip offset across each surface. Plotting these values against the known and probable surface age correlations for these surfaces allow us to constrain the range of slip rates for these faults and to compare these rates through time (Figure 3.9). Uncertainties include the variation in offset due to poorly constrained fault dips and the range of ages associated with the glacial advance (Table 3.1). The slip rates indicated by individual surfaces consistently indicate slip rates between 0.25 – 1 mm/yr, except for the youngest surfaces across the NFT.
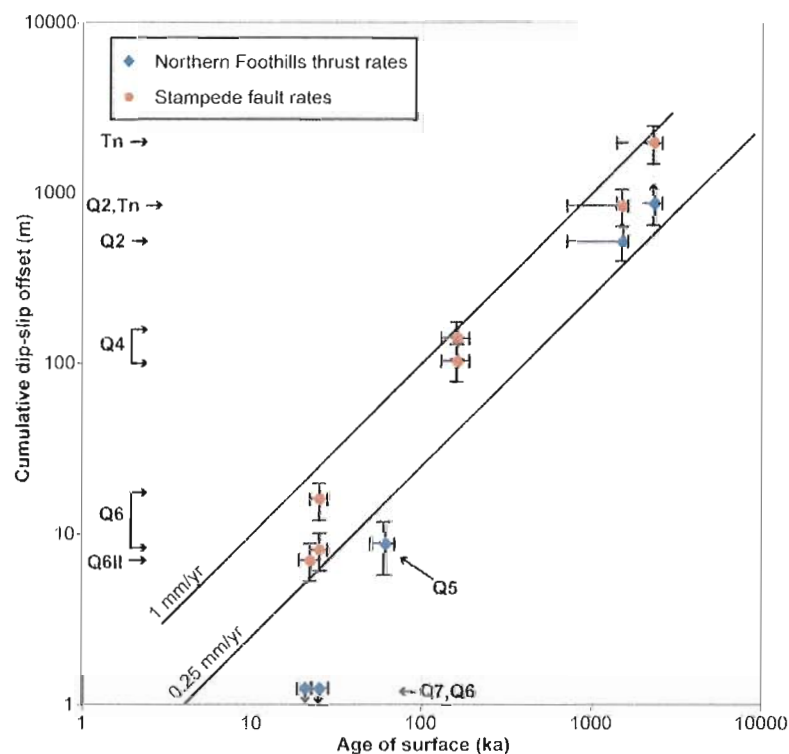
Figure 3.9. Plot illustrating the range of slip rates for the Northern Foothills thrust and Stampede fault based on offset geomorphic surfaces. Plotted on logarithmic axes in order to display the broad range of ages on a single plot. Uncertainties in dip-slip offset based on the range of likely fault dips, and age uncertainties based on range of timing for glacial advances given in Table 3.1. Vertical error bars that use an arrow for the oldest two NFT rates indicate that the dip-slip offsets shown are a minimum. Note that all slip rates except one fall within the the range of 0.25 – 1 mm/yr. The slip rates for the NFT that fall below 0.25 mm/yr illustrates the slowing and cessation of slip on the NFT during the late Pleistocene to present. The extended negative error bars on the Tn and Q2 surfaces indicate the possibility that these could correlate to younger glacial advances, but stratigraphic order establishes the age relative to one another.

3.7   Discussion

The geometry of the NFFTB meets the general requirements for a coulomb wedge with the south-dipping basal detachment and the north-dipping topographic slope, although the cumulative shortening of the wedge is relatively low (e.g. Chapple, 1978; Davis et al., 1983; Dahlen et al., 1984). However, because the backthrusts transport material towards the rear of the wedge, they are able to more efficiently thicken the wedge than foreland-vergent thrusts and require less horizontal displacement to maintain wedge taper. In the NFFTB these backthrusts have progressively thickened the wedge, within the resolution of these terraces, throughout the Pleistocene. Despite a lack of intermediate terraces between Q2 and Q5 at the range front, the small scarp on Q5 and no subsequent deformation indicates that foreland propagation of the thrust wedge has ceased. In terms of critical wedge theory, this wedge is currently in a subcritical state which will persist until critical wedge taper is restored through the ongoing thickening accommodated by the Park Road and Stampede faults.

This switch to a phase of wedge thickening was likely triggered by the loss of glacial ice along the main axis of the Alaska Range during the late Pleistocene. Figure 3.10 shows two profiles across the Alaska Range across our study transect to approximate the range of ice volume that occupied the rear of the thrust wedge. These glaciers filled the large U-shaped valleys during glacial advances (e.g. Manley and Kaufman, 2002; Briner and Kaufman, 2008) and, as recently as Q5 (~60 ka), was thick enough for the ice to advance through the narrow gorge of the Nenana River through the Mount Healy anticline and form a piedmont lobe near the town of Healy (Figure 3.3). The loss of ice lowered the topographic slope, reducing the wedge taper and driving the thrust system to a subcritical state. The widespread preservation of Quaternary landforms suggests that the topographic slope has not otherwise been reduced by a significant erosion event. Furthermore, despite the lower density of ice, the removal of mass through glacial melting occurred much more rapidly than mass removal through erosion.
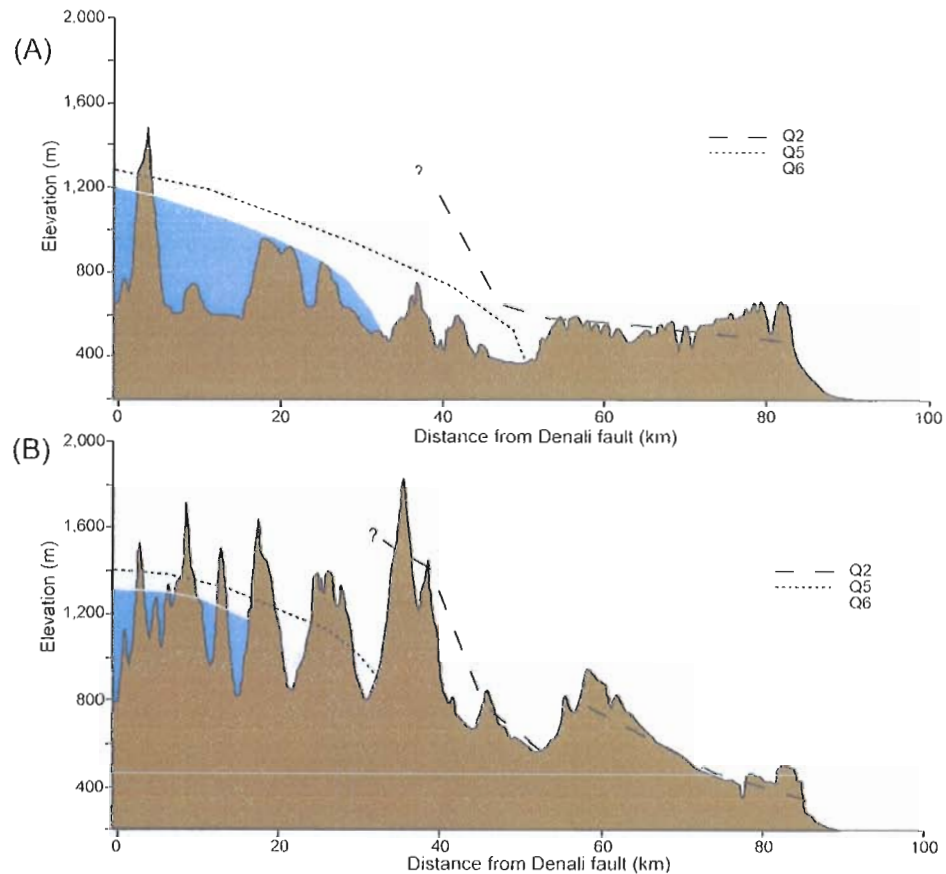
Figure 3.10. Modern topographic profiles across the Alaska Range and estimated glacial surface profiles during Pleistocene advances. Profile lines shown on Figure 3.3. Profile A illustrates the elevation down part of the Nenana River valley across the Alaska Range and Profile B follows the approximate divide between the Nenana and Teklanika rivers. The extent of Q2 is estimated from mapped deposits, and is significantly deformed across the northern foothills. Q6 is derived from the map of late Wisconsin glacial extents by Manley and Kaufman (2002). The Q5 profile is approximated from mapped deposits and glacial landforms occurring higher than the mapped Q6 limits (Wahrhaftig, 1958; 1970e; 1970f). Profile A demonstrates that the topographic slope is reduced across the Alaska Range along the glacial valleys, and profile B shows that a significant amount of ice was present in the higher elevations outside of the large valleys as well.

Looking along the strike of the Alaska Range orogenic wedge, the easily observed parameters of topographic slope and fault activity changes from the characteristics of our Nenana River transect. Figure 3.11 shows the correlation of the average elevation along the main axis of the Alaska Range with the activity of the range-bounding faults (the orogenic wedge tip), demonstrating that post-glacial fault activity has continued where the Alaska Range is the highest. We speculate that the orogenic wedge tip can maintain activity because these portions of the range are already tall, thereby retaining a greater

topographic slope even after the reduction in glacial mass during interglacial times. Furthermore, these highest elevations are the accumulation zones for modern glaciers, whereas the saddle occupied by the Nenana River is occupied by large glacial lobes during the maximum glacial extents, indicating that the axis of the Alaska Range in our study transect experiences the greatest fluctuations in mass due to glacial-interglacial cycles.
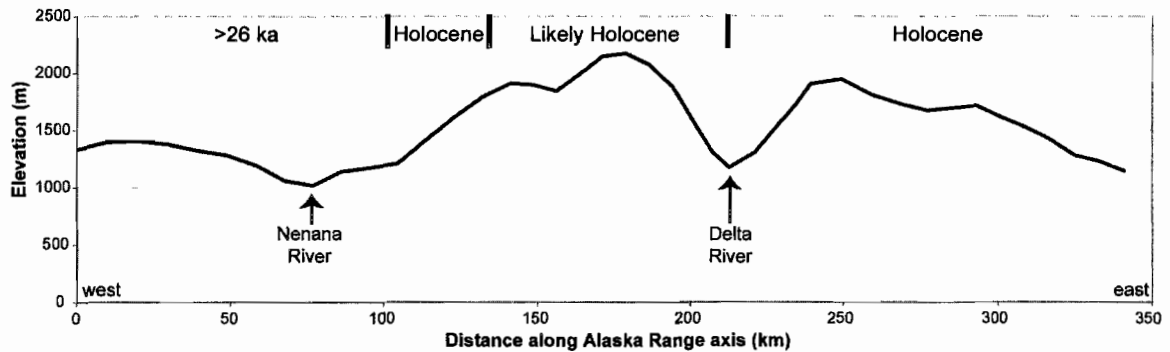
Figure 3.11. Topographic profile along the axis of the Alaska Range illustrating the correlation of higher range elevations with recent activity of range-bounding faults. We resampled the USGS DEM to 10 km resolution for the Alaska Range to approximate an average elevation surface, from which we extracted a topographic profile parallel to, and offset 20 km north of, the Denali fault (Figure 3.2). Because the orogenic wedge of the Alaska Range is accommodating Denali fault-normal shortening, we project the constraints on the timing of the most recent fault rupture of the range-bounding faults back to the corresponding portions of the topographic profile. Holocene fault activity as observed (from west to east) in Chapter II, Carver et al. (2006), Carver et al. (2008), and Carver et al. (in revision). The >26 ka limit on fault activity is described in this chapter and Appendix A. The occurrence of Holocene fault activity corresponding with regions of higher elevation of the Alaska Range suggests these portions of the range have sufficient topographic slope to maintain critical wedge taper throughout the glacial-interglacial cycles despite fluctuations in glacial loading. The lower Alaska Range elevations adjacent to the Nenana River indicate an already low topographic slope relative to other portions of the range, and the occurrence of multiple generations of moraines suggests that the glaciers here largely retreated during interglacial periods, introducing larger mass fluctuations than along-strike portions of the wedge.

This process we propose here differs in two primary ways from the often envisaged feedback of glacially-enhanced erosion and tectonic uplift in an orogenic wedge (e.g. Brozovic et al., 1997; Whipple and Meade, 2006; Tomkin and Roe, 2007; Berger et al., 2008). First, if the mass of the expanded glaciers exceeds the mass removed by erosion, this will drive the wedge toward a critical state and wedge propagation, instead of the glacial advance enhancing erosion and promoting a shift to wedge thickening. Secondly, this interaction occurs at a different time scale than is

typically modeled for the orogenic response to glacially-enhanced erosion (e.g. Whipple and Meade, 2006; Tomkin and Roe, 2007). Glacial loading in the Alaska Range is cyclic corresponding with the major climatic cycles of the Quaternary, whereas studies of steady-state orogens developed under the influence of glaciers indicate response times on the order of millions of years (e.g. Whipple and Meade, 2006; Tomkin and Roe, 2007). The relatively low shortening rate across the Alaska Range may facilitate recognition of this balance because at lower slip rates, it will take longer for the deformation to regain critical taper.

3.8   Conclusions

Widespread preservation of multiple geomorphic surfaces in the sub-arctic environment of the northern Alaska Range combined with fairly slow slip rates create a record of progressive deformation for the entire Quaternary (since ~2.6 Ma). This record of progressive deformation is essential for the development of models of subsurface structure and active faults due to overall poor geologic exposure and a lack of significant geophysical and other subsurface data. Using the progressive deformation, we constrain a model of an orogenic wedge with a south-dipping basal thrust and a north-dipping topographic slope. Internal deformation of the wedge is largely accommodated by two major north-dipping faults that intersect the basal thrust at depth. The slip rates for the Stampede fault and Northern Foothills thrust, shown on Figure 3.9, demonstrate that the faults within this system maintained similar rates through time and thus the thrust wedge maintained critical taper simultaneous with its foreland propagation. The recent shift of deformation to predominantly wedge thickening is speculated to result from the retreat of Pleistocene glaciers from the central Alaska Range, which effectively decreased the topographic slope and upset the force balance within this orogenic wedge.

3.9   Bridge

The previous chapter uses the sequence of fluvial terraces along Nenana River valley as structural markers to constrain the structural geometry and rate of deformation across this portion of the northern Alaska Range fold-thrust belt. Converting the slip rates of these individual faults into a horizontal shortening rate across the system, and allowing for generous uncertainties, suggests that 1-3 mm/yr of shortening is accommodated within the Alaska Range north of the Denali fault.

In Chapter IV, I use the orientation and magnitude of shortening of the Alaska Range relative to the orientation and slip rate of the Denali fault system to demonstrate that the Denali fault is strongly strain-partitioned. The shortening rate estimate derived from Chapter III and slip rates for the Denali fault constrain the rates and relative motions of crustal blocks and these are used to develop a revised tectonic model for the Quaternary deformation of south-central Alaska.

CHAPTER IV

STRAIN-PARTITIONING ON THE DENALI FAULT AND QUATERNARY GROWTH

OF THE ALASKA RANGE: TRANSPRESSIVE DEFORMATION ALONG A

CURVED FAULT

As the lead author, I led the compilation and interpretation of data and wrote the following manuscript. Co-authors Gary Carver and Ray Weldon provided mentoring, insight into the tectonic processes, additional interpretations, and critical review of the manuscript.

4.1   Introduction

The relationships between active faults within an orogen provide insights into the processes that drive growth of mountain belts. For transpressional mountain belts, the degree of strain-partitioning, obliquity of plate motion, erosional surface processes, and crustal rheology work together to control the distribution of active faults within that orogen. However, the relative importance of these factors is largely unknown. We seek a better understanding of the role of strain-partitioning and the factors that control it in the development of transpressional orogens by examining a well-defined active mountain belt associated with a continental transform that is purely strike-slip through 70° of a smoothly varying curve.

The Alaska Range of south-central Alaska is an arcuate mountain belt that extends from near the Alaska/Canada border westward for over 1000 km to where it curves southward and joins the Aleutian volcanic arc (Figure 4.1). The Denali fault system (DFS) is a major intracontinental right-lateral strike-slip system that parallels, and generally lies within, the Alaska Range for much of its length. The main trace of the Denali fault has been active since at least the late Cretaceous (e.g. Ridgway et al., 2002)
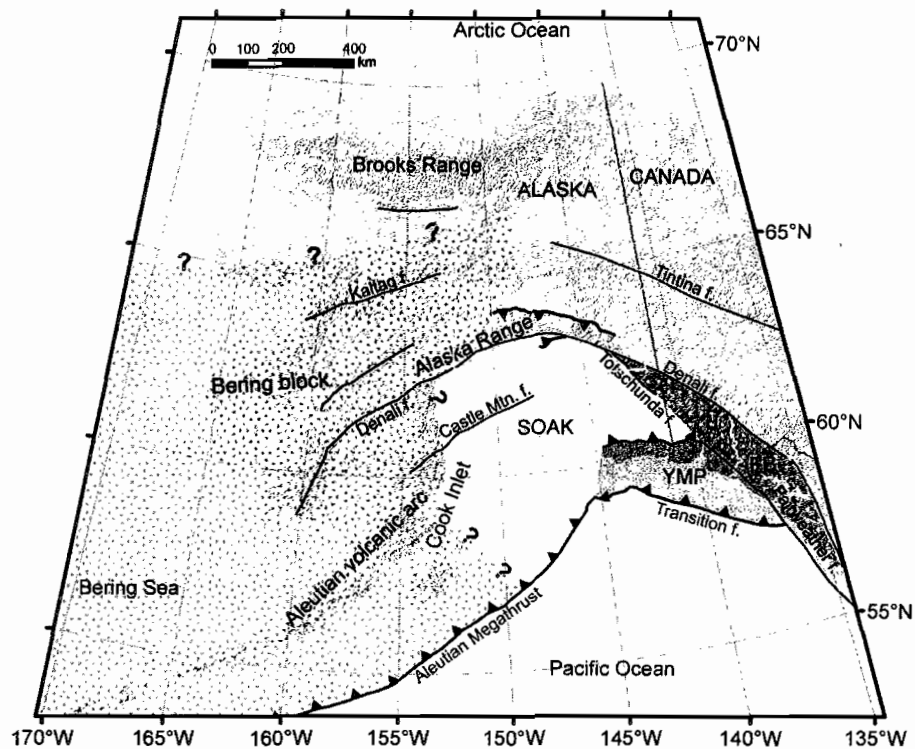
Figure 4.1. Location map showing topography, geographic features and some major Cenozoic tectonic features of Alaska. Black lines are faults are from Plafker et al. (1994). White lines are major rivers. The Yakutat Microplate (YMP), Fairweather Block (FB), and Southern Alaska Block (SOAK) (shown by different shades of gray transparent overlay) and the Bering Block (BB) are translating and rotating crustal blocks in the complex North America – Pacific plate boundary in southern Alaska. The Yakutat Microplate is being thrust under and accreted to southern Alaska, and this collision drives the deformation to the north by pushing the Southern Alaska Block (SOAK) to the north-northwest which imparts a counterclockwise rotation and indentation into North America. The white box indicates the region covered by Figure 4.2.

with a cumulative offset for the portion of the fault in eastern Alaska and Canada on the order of 350-400 km (e.g. Lowey, 1998; Nokleberg et al., 1985). The Totschunda fault is a NW-striking right-lateral strike-slip fault that intersects the Denali fault near Mentasta Pass (Figure 4.2) and is thought to have recently developed as a more direct connection between the Fairweather fault and the Denali fault, bypassing the eastern Denali fault (e.g. Richter and Matson, 1971; Haeussler, 2008; Freymueller et al., 2008). Richter and Matson (1971) suggest that the Totschunda fault developed after ~2 Ma. The activity of the Denali fault system was demonstrated by the 2002 M7.9 Denali fault earthquake sequence (Eberhart-Phillips et al., 2003). This earthquake initiated on a thrust fault near the northern apex of the Denali fault, rupturing 48 km of the previously unknown Susitna

Glacier fault, stepped onto the main trace of the Denali fault and propagated 226 km southwest to Mentasta Pass where it made a 20° bend onto the Totschunda fault and ruptured an additional 66 km of that fault (Haeussler et al., 2004) (Figure 4.2). Post-earthquake studies determined Holocene – late Pleistocene slip rates for this fault system and identified a clear westward decrease in slip rate between the Denali-Totschunda fault junction to a site just east of the Denali Massif (Figure 4.2) (Matmon et al., 2006; Mériaux et al., 2009; Taylor et al., 2008).
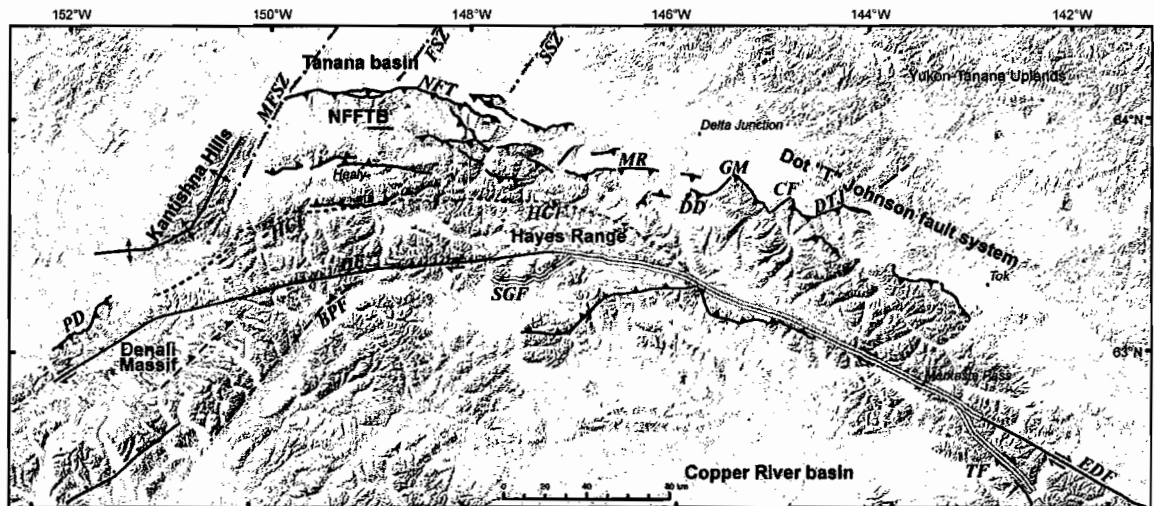
Figure 4.2. Quaternary faults and related structures of the Alaska Range shown on a shaded relief DEM. Black lines are faults, teeth shown on hanging wall of thrust/reverse faults and arrows showing relative motion are only indicated on major strike-slip faults. The thick gray dot-dash lines indicate the locations of the left-lateral Minto Flats (MFSZ), Fairbanks (FSZ) and Salcha (SSZ) seismic zones. The black dashed line is the Hines Creek fault (HCF), a fault of uncertain recent activity. The transparent white line with black outline on the Denali fault indicates the rupture of the fault system during the 2002 Denali fault earthquake sequence. Thin white lines denote streams. Regions of the northern Alaska Range thrust system referred to in text are labeled, as well as the two zones of highest elevations, the Hayes Range and Denali Massif. The irregular white pattern delineates the modern glacial extents in these regions of higher elevation. Note how the thrust faults remain sub-parallel to the Denali fault through 70° of curvature near Mentasta Pass to the Denali Massif. Abbreviations for faults: DF = Denali fault, EDF = Eastern Denali fault, TF = Totschunda fault, PD = Peters Dome fault, NFT = Northern Foothills thrust, MR = Molybdenum Ridge fault, DD = Donnelly Dome fault, GM = Granite Mountain fault, DTJ = Dot "T" Johnson fault, SGF = Susitna Glacier fault, BPF = Broad Pass fault, CF = Canteen fault. Faults summarized from Carver et al. (in revision), Carver et al. (2008), Haeussler (2008), and Bemis and Wallace (2007).

A popular and longstanding method for describing the tectonics of south-central Alaska has been through describing the absolute and relative motions of crustal blocks. The unique small-circle arcs described by the Denali fault proper and the Denali –

Totschunda fault systems inspired inferences of rotating crustal blocks even before plate tectonic theory (St. Amand, 1957). Recent models presented by Haeussler (2008), Freymueller et al. (2008), and Ruppert (2008) use different combinations of geologic, geodetic, and seismologic observations to interpret the boundaries and motions of blocks. These models generally define southern Alaska, south of the DFS, as rotating counterclockwise in response to NW-directed subduction and indentation of the Yakutat microplate. A recent addition to these models is the proposed Bering Block (or Bering Plate), a crustal block first inferred from seismicity patterns (Mackey et al., 1997) and recently supported by geodetic observations (Cross and Freymueller, 2008; Freymueller et al., 2008) that argues for clockwise rotation of much of western Alaska relative to North America.

Numerous authors have implicated thrust faults on the north side of the Alaska Range as part of their tectonic models (e.g. Freymueller et al., 2008; Haeussler et al., 2008; Matmon et al., 2006; Mériaux et al., 2009; Taylor et al., 2008). However, because these studies focus on other aspects of Alaskan neotectonics, they do not explore the constraints on the local tectonics presented by these structures. The rates, style, and orientations of these faults can tell us how strain is partitioned and how the westward decrease in slip rate on the Denali fault is kinematically accommodated. To address these issues, we analyze the distribution and rates of Quaternary faults and the cross-sectional width and volume of the Alaska Range relative to the Denali fault to constrain the patterns of strain accumulation. We present the orientation and style of faulting in the northern Alaska Range thrust system and other young faults in the Alaska Range and define the controls on the topographic growth of the range. Comparing range width, fault orientation, and cross-sectional volume to the orientation and position along the curve of the Denali fault system will illustrate the distribution of cumulative strain and how the strain is accommodated.

4.2   Quaternary Faults of the Alaska Range

4.2.1   Denali Fault System

The Denali fault system forms the northern boundary of the Southern Alaska Block and is the primary structure accommodating rotation (Figure 4.1). Recent slip rate

studies by Matmon et al. (2006) found a late Pleistocene/Holocene slip rate on the Totschunda fault of ~6 mm/yr. The adjacent segment of the eastern Denali fault has a slip rate of ~8.5 mm/yr, and west of the junction between faults, the main trace of the Denali fault has a slip rate of ~13 mm/yr (Mériaux et al., 2009; Matmon et al., 2006) (Figure 4.2). This slip rate is shown to decrease westward along the Denali fault, with a slip rate of ~10 mm/yr near the Susitna Glacier fault (Matmon et al., 2006) and decreasing further to ~7 mm/yr west of the Broad Pass fault (Mériaux et al., 2009) (Figure 4.2). The slip rate of the Denali fault west of the Denali Massif is undocumented, but is inferred to be less than 1-2 mm/yr (Haeussler, 2008; and references therein). To accommodate this decrease in slip rate, strain must be accommodated on the SE-striking thrust faults south of the Denali fault (Haeussler, 2008) or transferred across the Denali fault into the northern foothills fold-thrust belt (Matmon et al., 2006; Mériaux et al., 2009). Mériaux et al. (2009) propose that ~4 mm/yr of fault-normal slip would be transferred across the Denali fault near the junction with the Totschunda fault if there is no deformation or rotation occurring south of the Denali fault. This value would increase to 12 mm/yr across the northern foothills west of the Susitna Glacier fault (Figure 4.2) where the Denali fault slip rate is ~7 mm/yr.

4.2.2 Northern Alaska Range Thrust System

Several recent studies have documented young thrust fault-related deformation in the northern Alaska Range (Bemis, 2004; Bemis and Wallace, 2007; Carver et al., 2006; 2008). The distribution of these faults extends from north of the Denali Massif in the west, to north of the DFS-TF fault junction in the east (Figure 4.2). While there is significant lateral variability in the structures described by these studies, the northern topographic range front is clearly defined by young faults or folds for nearly this entire distance. These structures form the boundary between the active uplift of the Alaska Range and the subsiding Tanana basin. Quaternary activity of these faults is most clearly shown by the deformation of the Nenana Gravel, a distinctive, thick sequence of coarse-grained alluvial and braided river deposits that was laid down by north-flowing streams during the early growth of the Alaska Range (Wahrhaftig, 1987) beginning ~6 Ma (Fitzgerald et al., 1995; Triplehorn et al., 2000). The top of the Nenana Gravel is an

important regional structural marker, as it records the initiation of uplift of the proto-Tanana basin floor to from the northern flank of the Alaska Range (Thoms, 2000; Bemis and Wallace, 2007). The age of this surface is poorly constrained, but is inferred here to be between ~2.6 Ma and 1 Ma (minimum age from Athey et al. (2006); revised from the original interpretation of ~2.8 Ma by Wahrhaftig (1987); maximum age inferred from the local occurrence of glacial deposits in the uppermost section of the deposit (Carter, 1980; Thorson, 1986; Thoms, 2000)). We will briefly describe deformation of this thrust system from west to east across the northern flank of the Alaska Range (Figure 4.2).

The Peters Dome – Kantishna Hills region (Figure 4.2) is the least studied in terms Quaternary deformation despite being the most seismically active. Lesh and Ridgway (2007) identify clear geomorphic evidence of post-glacial folding of the SW end of the Kantishna Hills anticline. Additional evidence for Quaternary folding of the Kantishna Hills is based on the mapped deformation of the Nenana Gravel on the flanks of the anticline (Reed, 1961). From satellite imagery, we also identify a new fault, which we informally call the Peters Dome fault (Figure 4.2), based on uplift and deformation of the Nenana Gravel and an alignment of scarp-like lineaments that offset late Pleistocene glacial landforms.

The northern foothills fold and thrust belt (NFFTB) is separated from the Kantishna Hills by the Minto Flats Seismic Zone, and extends to the east across the northern flank of the Alaska Range to near the Delta River (Figure 4.2). Bemis and Wallace (2007) and Carver et al. (2006) describe the western and eastern portions of the belt respectively. In general, faults and folds in the NFFTB trend approximately east-west, with both north and south-vergent structures. Quaternary deformation of the NFFTB is only clearly documented north of the Hines Creek fault (Figure 4.2), and although the region between the DFS and the Hines Creek fault exhibits dramatic early Tertiary deformation, individual Quaternary-active structures are unknown (Csejtey et al., 1992; Sherwood and Craddock, 1979). We believe this area is inactive, although Haeussler (2008) suggests that faults with a slip rate of <2 mm/yr could be missed.

We estimate a maximum value of ~3 mm/yr horizontal shortening across the NFFTB west of Healy (discussed in Chapter III). Earlier line-length restoration of the

balanced cross-section from Bemis and Wallace (2007) across the NFFTB immediately east of Healy (Figure 4.2) were interpreted to yield a possible maximum horizontal shortening rate of ~8 mm/yr. This rate is likely too high, because subsequent mapping by Athey et al. (2006) did not find active faulting where Bemis and Wallace (2007) inferred a significant fault in their balanced cross-section.

The informally-named Dot "T" Johnson fault system extends east from the Delta River to near Tok (Figure 4.2). Carver et al. (2008) identified several segments of a previously unknown north-vergent thrust fault along the northern margin of the Alaska Range and the south side of the Tanana River. They also expanded constraints on several previously known active faults (Donnelly Dome fault, Granite Mountain fault, Canteen fault; Plafker et al. (1994)) to develop a model of range-bounding thrust faults separated by NNE-trending strike-slip faults. The NNE-trending faults align with older structures in the Yukon-Tanana Uplands (e.g. Foster, 1970), but the recent activity of these faults is mostly restricted to portions within and immediately adjacent to the Alaska Range. This suggests that the older structures have been reactivated as lateral tear faults in the thrust sheet and are not independent active faults. Carter (1980) measured a 1000 m section of tilted Nenana Gravel on the footwall of the Granite Mountain fault, which has uplifted a bedrock unconformity containing relict patches of Nenana Gravel (Holmes and Pewe, 1965) on its hanging-wall about 1 km above the exposure. The greater than 2 km of vertical separation on the upper surface of the Nenana Gravel indicates a horizontal shortening rate on the order of 1.4-3.5 mm/yr (assuming a 30 degree dip for the Granite Mountain fault). The Canteen fault is a NNE-trending left-lateral/oblique slip fault interpreted as a lateral tear connecting the Granite Mountain fault to the Dot "T" Johnson fault and has a slip rate of 1-2 mm/yr based on offsets of glacial moraines (Carver et al., 2008), suggesting a similar rate on the thrusts that it connects kinematically.

4.2.3   Other Quaternary and Inferred Active Alaska Range Faults

Besides the Susitna Glacier fault, very little is known about the Quaternary activity of faults in and adjacent to the Alaska Range on the south side of the DFS. The faults indicated on Figure 4.2 were identified on the basis of bedrock mapping and involve the deformation of Neogene sedimentary rocks (individual fault names noted on

Figure 4.2). Unfortunately, due to the extensive glaciation throughout the Quaternary (Hamilton, 1994) there are essentially no Quaternary markers older than latest Pleistocene with which to identify deformation related to active faults immediately south of the DFS. So, unless the fault has a high slip rate or has had a surface rupture recently in deposits conducive to scarp preservation, Quaternary activity is very difficult to discern. For example, despite being the initiation point of the 2002 Denali fault earthquake sequence, the Susitna Glacier fault was previously unknown because the topographic signature of its pre-existing scarp was too subtle to be observed at the resolution of previous regional investigations (Crone et al., 2004). Thus, we infer that it is likely that additional faults like this exist, but the landscape is too young to have recorded enough cumulative deformation for these to be readily observed at the current resolution of mapping and topographic data.

4.3   Orientation of Alaska Range Deformation Relative to the Denali Fault System

Quaternary faults in and adjacent to the Alaska Range display characteristic trends on their respective sides of the DFS. The thrust faults shown on Figure 4.2 south of the DFS all have a ~NE/SW strike and intersect the Denali fault at oblique angles. As such, these faults are oriented at a high angle to the SOAK block motion. Due to limited data presently available for these faults, we limit our interpretation of these faults to their NE strike and reverse style. However, the region north of the the Denali fault has seen more research related to late Cenozoic deformation, and more landforms and deposits exist by which to assess Quaternary deformation. To investigate possible along-strike changes in shortening across the Alaska Range north of the Denali fault, we divided the Denali fault from 143° W to 153° W (Figure 4.2) into 10 km segments, and measured the volume, width and structure orientations of the Alaska Range for a 10 km wide swath perpendicular to the respective Denali fault segment. Each swath ends at the northern range-bounding fault or fold, and we measured the orientation of the segment of the range-bound structure and any additional active faults lying within that swath. Because range width can be affected by other factors, and the widest portion of the Alaska Range also corresponds with the lowest range crest elevations (Bemis et al., 2006), the volume of swaths across the range is probably the most representative first-order estimate of

along-strike variations in cumulative shortening. These measurements are plotted in Figure 4.3.
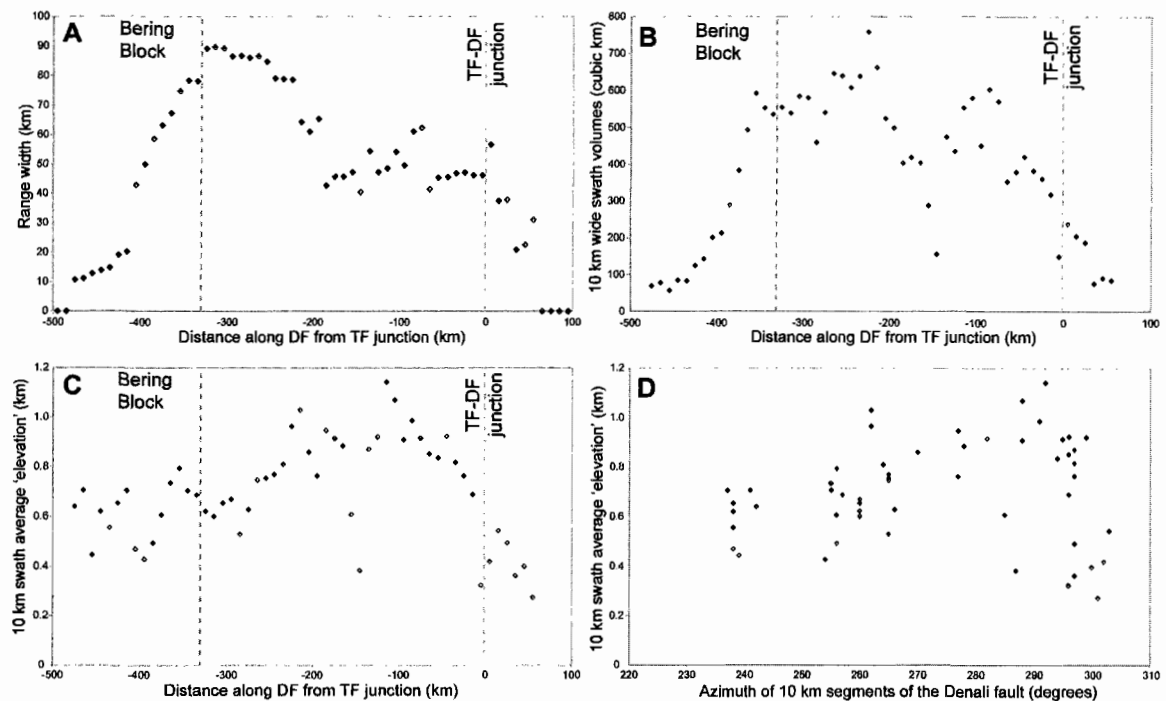
Figure 4.3. Plots comparing the width, volume, and elevation of the Alaska Range north of the DFS relative to along fault distance and the orientation of the DFS. We divided the Denali fault into 10 km long segments and analyzed a perpendicular, 10 km wide swath north from the Denali fault to the range-bounding structure or topographic break. Distances are measured east to west along the fault from the Denali fault – Totschunda fault intersection. Vertical dashed lines denote the Denali fault – Totschunda fault junction and the Minto Flats Seismic Zone, which we infer to be the primary boundary between North America and the Bering Block. A) The width of the Alaska Range (measured as the length of the swath) as it varies along the strike of the Denali fault. Note that the near zero range width values are not plotted on subsequent figures because they have no volume or average elevation. B) The volume of the Alaska Range (measured above the lowest elevation at the north end of the swath) for each 10 km segment along the strike of the Denali fault. C) Average height above local base level for each swath along the strike of the Denali fault. Average height determined by dividing the swath volume by the length and width of the swath. D) Same as C), but plotted as the average height varies with the azimuth of the corresponding 10 km segments of the Denali fault. Comparing the westward increase in range width from approximately -50 to -300 km shown in A) with only a minor increase in range volume over the same distance in B) indicates that range width is not an appropriate proxy for shortening rate.

Figure 4.3a illustrates the east to west increase in the width of the Alaska Range north of the DFS that was used by Meriaux et al. (2009) to infer a westward increase of DFS-parallel shortening to correspond with the westward decrease in slip rate on the DFS. Comparing this view to the along strike swath volumes in Figure 4.3b illustrates

that there is little difference between the uplifted volumes between the NFFTB and Dot "T" Johnson systems. Furthermore, Figure 4.3c shows that there is perhaps a slight inverse trend when the volumes are converted to average relative elevation (volume/swath width/swath length). This same trend occurs when the average relative elevation is plotted against the azimuth of the corresponding DFS segment (Figure 4.3d).

As shown by the map view on Figure 4.2 and the plot of Figure 4.4, the surface traces of active faults north of the DFS are dominantly parallel to subparallel to the strike of the Denali fault, despite an ~70 degree change in the strike of the Denali fault over the 400 km from Mentasta Pass to Denali. Where faults occur with a strike highly oblique to that of the Denali fault, they tend to be near vertical strike-slip or oblique-slip faults and commonly correspond with along-strike changes in architecture of the thrust system (Bemis and Wallace, 2007; Carver et al., 2008) and thus are inferred to be tears in the thrust system. We averaged the orientations for swaths that crossed multiple fault traces, and fit the regression shown on Figure 4.4 to these points. The direct relationship (slope of 1.3) between the orientation of the Denali fault and the Quaternary-active faults indicates that the azimuth of the northern Alaska Range faults rotate along with the Denali fault.

4.4   Discussion

The parallelism of the faults of the northern Alaska Range thrust system to the DFS indicates that the maximum compressive stress has been perpendicular to the DFS during the Quaternary growth of these faults. Characteristically, the mapped traces of thrust faults have some sinuosity related to topography and lithologic/rheologic controls on subsurface fault geometry. Outside of this local variability, major thrust fault segments should be responding to the regional stress field and be oriented perpendicular to the maximum compressive stress. These geologic observations are supported by Ruppert (2008) who used stress tensors derived from regional earthquake focal
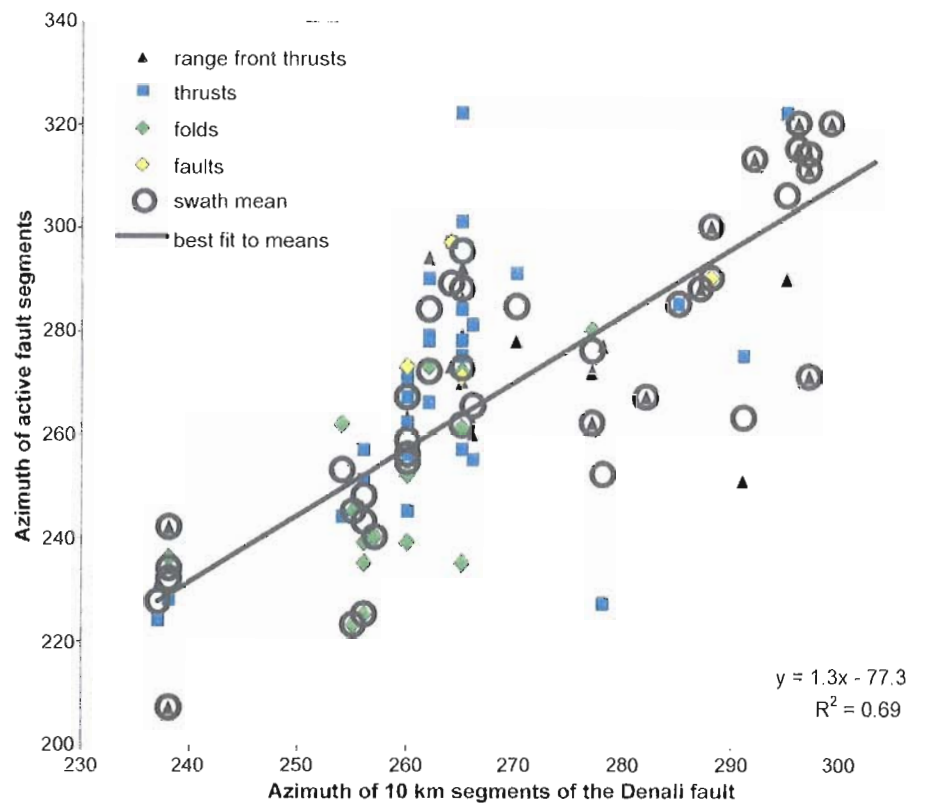
Figure 4.4. Plot of the azimuth of Quaternary faults north of the DFS relative to the azimuth of the Denali fault. The azimuth of each fault within a 10 km swath plotted perpendicular to the Denali fault is plotted with respect to the azimuth of the corresponding 10 km Denali fault segment. We plot the azimuths of all faults, distinguished by general type, and whether they are the range-bounding structure or not. We also show the mean azimuth for each swath (open black circle) with the least squares best fit line for the means representing the trend of increasing active fault azimuth with increasing Denali fault azimuth, demonstrating the parallelism of these fault systems.

mechanisms to show that maximum compressive stresses in the Alaska Range north of the Denali fault are predominantly DFS-normal. Therefore, the prevailing pattern of Denali fault-parallel thrust faults across the northern Alaska Range indicates that these faults, and thus the style of Quaternary Alaska Range growth, is fundamentally due to the strain-partitioning of the NW-directed motion of the Southern Alaska Block into fault-parallel and fault-normal components. Furthermore, the difference in shortening direction north and south of the Denali fault system allows us to build upon previous models of south-central Alaska tectonics to show that the Southern Alaska Block is rotating, shortening internally, and translating to the northwest, driving strike-slip motion on the Denali fault, NW-SE contraction south of the DFS, and north-south contraction

across interior Alaska north of the DFS.

4.4.1 Revised Model of Central Alaska Active Tectonics

Recent tectonic models of south-central Alaska all include a Southern Alaska Block with the Totschunda fault and central Denali fault acting as the northern boundary (Haeussler, 2008; Freymueller et al., 2008; Mériaux et al., 2009). The western boundary is poorly constrained, but is thought to follow the western Alaska Range south towards Cook Inlet (Figure 4.1). The southern boundary of the Southern Alaska Block is essentially the Aleutian Megathrust, with the actively accreting Yakutat Microplate driving counter-clockwise rotation of the Southern Alaska Block. A sliver of crust sandwiched between the Totschunda – Fairweather fault alignment and the eastern Denali fault is referred to by Freymueller et al. (2008) as the Fairweather Block, and by Haeussler (2008) as the St. Elias Block (Figure 4.1). Freymueller (2008) estimate this block to be translating NW at <3 mm/yr relative to North America. Several models for the motion of the Southern Alaska Block describe predominantly rigid counterclockwise rotation of the block. Alternatively, Meriaux et al. (2009) argues that rotation is not required and that the Southern Alaska Block could simply be migrating to the northwest, parallel to the Totschunda fault – Fairweather fault alignment. Haeussler (2008) invokes both the Southern Alaska Block rotation and northwestward translation of the pole of rotation of <7 mm/yr. We argue that northwestward translation of the Southern Alaska Block is necessary for the style of growth in the Alaska Range, but the slip rates required by pure translation are not supported by geologic constraints.

Figure 4.5 presents our diagram of block motions for central Alaska, illustrating a combination of motions relative to a fixed North America shown with the relative motions across major structures and block boundaries. Block boundaries are either major faults or seismicity lineaments and separate portions of the crust that are moving relative to one another or deforming internally. Significant structures that accommodate some of the internal block deformations are shown schematically to illustrate orientations and relative motions.

We argue that the counterclockwise rotation and northwestward translation of the Southern Alaska Block combined with northwestward translation of the Fairweather
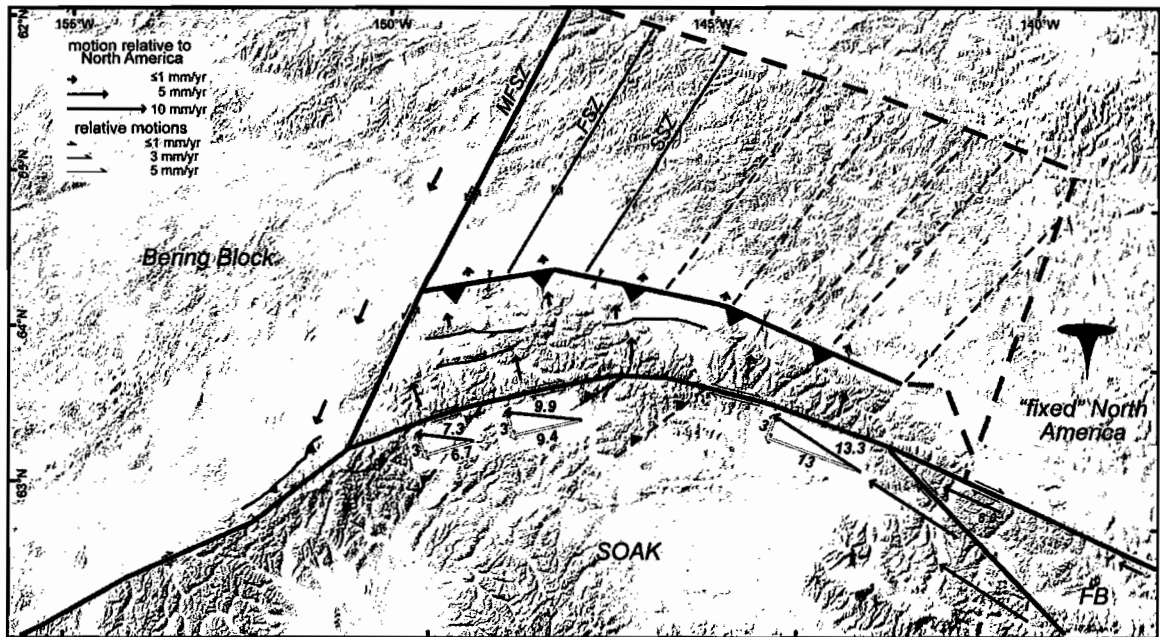
Figure 4.5. Block diagram illustrating the active tectonics of central Alaska with vectors illustrating the motions of blocks relative to North America. Block motions are shown with black vectors with full arrowheads and are scaled to central Denali fault paleoseismic slip rates (white arrows with outline) with a 3 mm/yr fault-normal component to represent the best estimate of paleoseismic slip rates for the Totschunda fault and eastern Denali fault (TF paleoseismic rate = 6 ± 1.2 mm/yr, TF calculated rate = 5.6 mm/yr; EDF paleoseismic rate = 8.4 ± 2.2 mm/yr, EDF calculated rate = 8.0 mm/yr). Thickest black lines are block boundaries, and these are dashed where the style or location of the boundary is uncertain. Immediately north of the Denali fault – Totschunda fault intersection, the eastward change from solid to dashed block boundary illustrates the eastward end of Quaternary faulting and the dashed line depicts the likely formerly active range front before the fault intersection migrated to the present location. Thin black lines show generalized fault traces, with solid lines depicting those with known seismic/late Quaternary activity and dashed lines show faults mapped in bedrock. Thin, one-sided arrows depict relative motion across block boundaries. Motions of <1 mm/yr are poorly constrained and have been rounded up to ~1 mm/yr for visibility. Bering Block vectors are shown schematically from Cross and Freymueller (2008). The northwestward motion of the Southern Alaska Block south of the Totschunda and Denali faults yields the rotation, internal deformation, and indentation of the Southern Alaska Block into North America, producing fault-normal shortening that lifts the northern Alaska Range and drives the rotation of crustal blocks to the north.

Block drives oblique motion across the central Denali fault. Therefore, the direction and magnitude of this oblique motion across the central Denali fault is the sum of eastern Denali and Totschunda fault slip rates and orientations. Because the central Denali fault strongly partitions this oblique strain, we use the paleoseismic slip rates for the central Denali, eastern Denali and Totschunda faults (Matmon et al., 2006; Mériaux et al., 2009) to determine the range of Denali fault-normal horizontal strain that is transferred across the fault. We determine these values by back-calculating the slip rates for the eastern

Denali and Totschunda fault using the fault orientations, the paleoseismic slip rate for the central Denali fault nearest the fault intersection, and assuming a range of Denali fault-normal shortening rates and comparing the calculated rates to the measured slip rates Matmon et al. (2006). Figure 4.5 illustrates the best fit model, where a Denali fault-normal shortening rate of 3 mm/yr accommodates eastern Denali and Totschunda fault slip rates that closely match the paleoseismic rates. Values of Denali fault-normal shortening lower than 3 mm/yr requires more slip on the eastern Denali fault than is supported by geologic observations. A Denali fault-normal shortening rate of 5 mm/yr results in ~11 mm/yr slip on the Totschunda fault and ~3 mm/yr on the eastern Denali fault, which may be more representative of slip rates farther from the Denali – Totschunda fault intersection as shown by estimates of 1-4 mm/yr of slip across the eastern Denali fault in the Yukon Territory, Canada (Haeussler, 2008; Seitz et al., 2008). Therefore, ~3-5 mm/yr of Denali fault-normal strain is transferred across the central Denali fault.

The paleoseismic rates for the central Denali fault decrease to the west, but there is no evidence for a corresponding increase in the DFS-normal shortening across the Alaska Range. Therefore, assuming 3 mm/yr as the constant DFS-normal horizontal shortening rate across the northern Alaska Range thrust system, we calculate the orientation and magnitude of the the Southern Alaska Block motion in the vicinity of each of the paleoseismic sites. Approximately 27° of counterclockwise rotation of the Southern Alaska Block motion vector is shown (Figure 4.5) between the Dot "T" Johnson system and the middle of the NFFTB, and the decrease in rate indicates several mm/yr of shortening within the Southern Alaska Block. Between the westernmost paleoseismic sites, there is no counterclockwise rotation, probably because the Southern Alaska Block motion vector here is more ideally oriented for shortening on thrusts near the Denali Massif, likely contributing to its dramatic growth.

4.4.2. NNE-trending Seismic Zones North of the Alaska Range

Widespread shallow crustal seismicity in interior Alaska is dominated by three, NNE-trending left-lateral seismic zones (Figure 4.2). There are currently two models that attempt to explain this pattern of deformation. Page et al. (1995) propose that these

NNE-trending seismic zones are the boundaries of crustal blocks undergoing counterclockwise vertical-axis rotation within a broad dextral shear zone between the Denali fault and the sub-parallel Tintina fault to the north. Alternatively, Freymueller et al. (2008) suggest that these NNE-trending seismic zones could be the diffuse eastern margin of the Bering Block because they are aligned with the modeled local Bering Block motion with the appropriate sense of displacement.

Due to the agreement of the seismologically-determined (Ruppert, 2008) and our geologically-derived directions of a Denali fault-normal maximum compressive stress north of the Denali fault, we propose instead that the left-lateral displacement across the Fairbanks and Salcha seismic zones (Figure 4.5) is driven by the same DFS-normal compressive stress that drives the active thrust faults of the northern Alaska Range (Figure 4.5). Because the Minto Flats seismic zone has a different orientation for its maximum compressive stress than that of the Fairbanks and Salcha seismic zones, and its greater along-strike extent (Figure 4.5), we argue that it is the primary structure accommodating relative motion of the Bering Block. To the east of the seismic zones, as the fault-normal compressive stress rotates clockwise due to the curvature of the DFS, the style of interaction of the fault-normal stress with the NNE-trending fault zones changes as well. North of the Dot "T" Johnson thrust system (Figure 4.2), the DFS-normal stress is sub-parallel to the pre-existing NNE-trending bedrock fault zones (Figure 4.5) and does not allow significant relative displacement across these structures north of the Alaska Range. In the west, the north-south compressive stress is more favorably aligned to drive left-lateral slip on steeply dipping, NNE-trending structures. A possible consequence is that the greatest range width occurs where the foreland is actively deforming (Figure 4.2 and 4.5). This foreland deformation may prevent the corresponding portion of the Alaska Range from increasing significantly in elevation.

The strong strain-partitioning exhibited by the Denali fault precludes the Page et al. (1995) model of a broad dextral shear zone between the Denali and Tintina faults driving the NNE-trending seismic zones. While we agree with Freymueller et al. (2008) that the Minto Flats seismic zone is a boundary for the Bering Block, their added inference that the southwestward translation of the crustal blocks between the seismic

zones could be driving the thrust faults in the Alaska Range is not supported by the eastward continuity of active thrust faulting in the Alaska Range beyond the active seismic zones.

4.4.3   *The Totschunda Fault and the Initiation of the Quaternary Thrust System*

Correspondence of the intersection of the Totschunda fault with the Denali fault and the eastern extent of the active northern Alaska Range thrust system is not likely to be a coincidence. Three significant events in the Alaska Range occurred between ~1-2 Ma that appear to constrain a fundamental tectonic adjustment to lead to the modern configuration of the Alaska Range. Thermochronometry studies in the Hayes Range indicate rapid exhumation of these mountains began ~1.5 Ma, whereas this region contains no indication of the 6 Ma event that is seen at the Denali Massif (Haeussler, 2008; Fitzgerald et al., 1995). In the NFFTB, the age of the upper surface of the Nenana Gravel is constrained as between ~2.6 and >1 Ma (Athey et al., 2006; Wahrhaftig, 1987). This cessation of deposition would have resulted from the initiation of uplift of the northern foothills. The other event to occur in this time frame is the formation of the Totschunda fault sometime after 2 Ma. Therefore, loosely constrained between 1-2 Ma, we argue that the formation of the Totschunda fault cut off much of the strain from the eastern Denali fault as a more direct connection between the Fairweather fault in southeast Alaska to the Denali fault. This trajectory generated a more oblique and narrower indentor into central Alaska and initiated the Quaternary propagation of thrust faults north of the Denali fault to accommodate a greater magnitude of fault-normal compressive stress.

4.5   Conclusions

The recognition of the northern Alaska Range thrust system, it's extent from near Mentasta Pass to near the Denali Massif (Figure 4.2), and the relationship of this thrust system with the Denali fault system is a significant step forward in our understanding of the tectonics of central Alaska and the behavior of a major intracontinental strike-slip fault. We use the distribution of Quaternary faults in the Alaska Range to determine the regional stress field, illustrating the parallel relationship of thrust faults north of the DFS with the DFS, and the characteristically SW-striking oblique traces of the thrust faults

south of the DFS. The decoupled patterns of strain accommodation across the Denali fault indicate that essentially no DFS-parallel shear is transmitted north of the Alaska Range, indicating that it is the north-south compression that is driving shallow seismicity, and the rotating crustal blocks of Page et al. (1995). This distribution of faults demonstrates that the Denali fault system is strongly strain-partitioned, in that the oblique indentation of the Southern Alaska Block is partitioned into a fault-parallel component to drive strike-slip on the Denali fault, and a fault-normal component driving thrust faulting and foreland deformation to the north of the fault. Paleoseismic estimates of slip rates across the Alaska Range north of the Denali fault require both counterclockwise rotation and northwestward translation of the Southern Alaska Block to drive the deformation in central Alaska.

CHAPTER V

CONCLUDING SUMMARY

5.1   Introduction

This dissertation investigates the mechanisms of strain accommodation within the broad region of continental deformation in the convergent plate boundary of southern Alaska. This region exhibits the rotation of crustal blocks, diffuse zones of deformation, and the growth of a major mountain belt, the Alaska Range, adjacent to an intracontinental transform fault. The faults between and within these zones interact at different spatial and temporal scales and reflect the principle stresses that drive deformation. I utilize the deformation recorded in Quaternary deposits and landforms to explore the temporal interactions of faults within a fold-thrust belt and to constrain the regional patterns of crustal deformation.

5.2   Constraints on Contractional Deformation From Quaternary Landforms

Chapter II presents a 1:25,000 scale map of the Quaternary geology and active faulting on the northern margin of the Alaska Range. It is positioned approximately halfway between the better-studied Nenana and Delta river corridors through the Alaska Range, and closer to the main population center and infrastructure hub of Fairbanks. This mapping identified two major thrust faults and a right-lateral fault that trends oblique to the thrust faults. The topography of the region has developed through the progressive uplift on these structures, which, combined with Quaternary glacial cycles, produced a sequence of fluvial terraces that record the uplift. I used the geometry of progressive deformation to define the subsurface geometry of the faults. This study demonstrated both the activity of this portion of the northern margin of the Alaska Range, and the utility of using landforms for geologic studies in tectonically-active regions of poor geologic exposure.

Chapter III examines a transect across the fold-thrust belt of the Alaska Range

north of the Denali fault where 3 major thrust faults comprise an active, north-vergent orogenic wedge. The goal of this study was to understand how the faults in this system balance thickening and foreland propagation through time to maintain critical taper of the wedge. Using a sequence of geomorphic surfaces preserved across the fold-thrust belt I show that critical taper is maintained by simultaneous activity on all the major faults of the system. This balance was recently upset, perhaps by the loss of Pleistocene ice that had contributed to the topographic slope of the orogenic wedge, such that the foreland propagation has ceased while slip continues on the wedge-thickening faults.

Comparing these two studies, it is clear that the dynamics of an orogenic wedge can vary significantly along strike. Whereas the transect in Chapter III demonstrates that the western portion of the fold-thrust belt is in a sub-critical state, the recent activity of the range-bounding faults in the Japan Hills study area (Chapter II) indicates this portion of the fold-thrust belt is near critical taper. This change occurs over ~60 km, and corresponds with a significant increase in the average elevation of the axis of the Alaska Range. A less obvious point is the importance of the relatively low shortening rates across this system for studying the long-term fault interactions of this orogenic wedge. These low rates in concert with good preservation of Quaternary landforms in this region enable the analysis of fault interactions on the scale of 10^4 to 10^6 years. However, it is unknown whether the balance of orogenic wedge thickening and propagation observed here is unique to relatively low slip rate, basement-involved fold-thrust belts or if higher slip rate and/or thin-skinned orogenic wedges maintain critical taper in the same manner.

5.3   Partitioning of Styles of Strain Accommodation

Chapter IV integrates the insights into the geometry of Quaternary thrust faulting from Chapters II and III with other recent studies I have contributed to (Carver et al., 2008; in review) of active faulting in the Alaska Range. These results show that the Denali fault partitions the NW-directed strain imposed from the far-field collision of the Yakutat microplate into Denali fault-parallel strike-slip and fault-normal compressional components. This strong partitioning of transpressional strain exerts the primary control on the distribution of crustal deformation and mountain growth in central Alaska. I use the nature of strain-partitioning with the paleoseismic slip rates for the Denali fault and

constraints on shortening rate across the Alaska Range north of the Denali fault to refine regional tectonic models. Similar shortening rates across the northern Alaska Range thrust system from east to west require that the Southern Alaska Block rotates counterclockwise, shortens internally, and migrates to the NW. Because the Denali fault accommodates the fault-parallel component of strain, the vertical-axis rotations of crustal blocks inferred from seismicity patterns north of the Alaska Range (Page et al., 1995) cannot be driven by a large dextral shear zone between the right-lateral, sub-parallel Denali and Tintina faults (Figure 4.5). Instead, the same Denali fault-normal maximum compressive stress that drives the northern Alaska Range thrust system drives shortening between the Denali and Tintina faults. This shortening is accommodated by left-lateral slip on the NNE-trending Fairbanks and Salcha seismic zones. Similar NNE-trending structures observed in the bedrock geology east of these seismic zones do not accommodate active deformation, because they are unfavorably oriented to the Denali fault-normal maximum compressional stress as the Denali fault curves to the SE.

5.4   Implications for Seismic Hazard in Central Alaska

The recognition of active faults in the Alaska Range through this and related studies over the past several years has significantly advanced our understanding of the earthquake potential for central Alaska. This improved knowledge of the distribution of active faults and the modifications to the Quaternary tectonic framework will contribute greatly to future revisions of seismic hazard assessments and help to guide future research efforts to characterize active faults in Alaska.

APPENDIX A

PRELIMINARY PALEOSEISMIC RESULTS FROM THE NENANA RIVER VALLEY,

CENTRAL ALASKA RANGE, ALASKA

A.1   Introduction

This appendix presents the preliminary results from 6 paleoseismic trenches excavated across 3 thrust/reverse faults that display surficial evidence of late Pleistocene or Holocene surface-rupturing earthquakes. These faults are part of the northern foothills fold-thrust belt (NFFTB) near the Nenana River valley (Table A.1 and Figure A.1), and were previously uncharacterized for their contribution to the seismic hazard of this important infrastructure corridor.

An early goal of these paleoseismic investigations was to establish slip rates and paleoearthquake chronologies to examine the possible temporal relationships of faults within a fold-thrust belt on timescales of $10^2 - 10^4$ yrs. Our observations preclude interpretations on that time scale, but contribute details on the timing of activity and style of faulting that will be useful for characterization of these faults as seismogenic sources and interpretations of regional tectonics. Being the first paleoseismic studies on these faults, and among the first in Alaska north of the Denali fault, I anticipate these preliminary results will be useful to future neotectonic investigations in this region and other high-latitude regions.

All radiocarbon dates reported here are calibrated ages (cal BP) unless otherwise noted. Details on pretreatment procedures, AMS results, and calibration methods are provided in Appendix B.
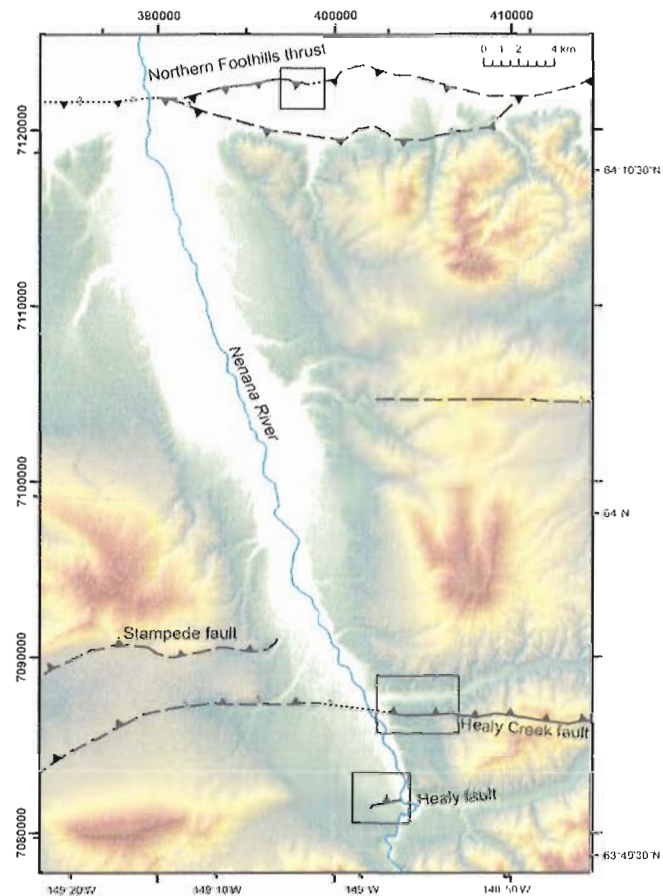
Figure A.1. Location map for paleoseismic investigations along the Nenana River valley. Base image is a shaded-relief DEM, colored by elevation. The black boxes show the locations of the more detailed locations maps for investigations at each site.

Table A.1. Summary of paleoseismic trenches in the Nenana River valley.

Trench Name	Coordinates*	Fault Type	Length / Width (m)⁺	Depth Range (m)	Paleoseismic Results[§]
Healy fault T1	402,348 E, 7,081,533 N	Reverse, 45° N dip	5 / 1	0.8 - 2	2 discrete fault offsets, 1 event (MRE) well-constrained, secondary extensional faults
Healy fault T2	402,345 E, 7,081,536 N	Reverse, 45° N dip	24.5 / 1	1.2 - 2.5	4 discrete fault offsets, 1 event (MRE) well-constrained
Healy fault T3	402,355 E, 7,081,532 N	Reverse, 45° N dip	6 / (1.5 – 3)	2 - 2.4	5 discrete fault offsets
Healy Creek fault T1	403,898 E, 7,086,783 N	Reverse, 60° N to near vertical dip	45 / (8 - 16)	3 - 4.5	Numerous minor shear zones and minor offsets, 1 complex deformation zone, deformation focused at crest and base of scarp
Healy Creek fault ST	403,678 E, 7,086,777 N	Reverse, 60° N to near vertical dip	6 / 1	0.6 – 1.2	Fault not exposed, scarp not tectonic
Northern Foothills thrust WC2	398,221 E, 7,122,594 N	Thrust, ~30° S dip	5 / 1	0.7 – 1.3	Small, probably secondary offsets, 1 probable event (MRE)

* UTM zone 6, WGS 84, measured with differential GPS, horizontal precision <1 m, surveyed location is the NW corner of the trench over the northernmost vertical grid line.
⁺ Width in parentheses indicates width between lower and upper bench walls, respectively.
[§] Age constraints and additional evidence discussed in text.

A.2 Healy fault

A.2.1 Site Description

The Healy fault is a north-dipping thrust fault that forms a prominent linear scarp as it crosses several terraces correlated with the Riley Creek glacial advance (~22-28 ka) (Wahrhaftig, 1970; Thorson, 1979; Bemis and Wallace, 2007; Dortch, 2006) south of the town of Healy (Figure A.2). This fault can be traced from the west bank of the Nenana
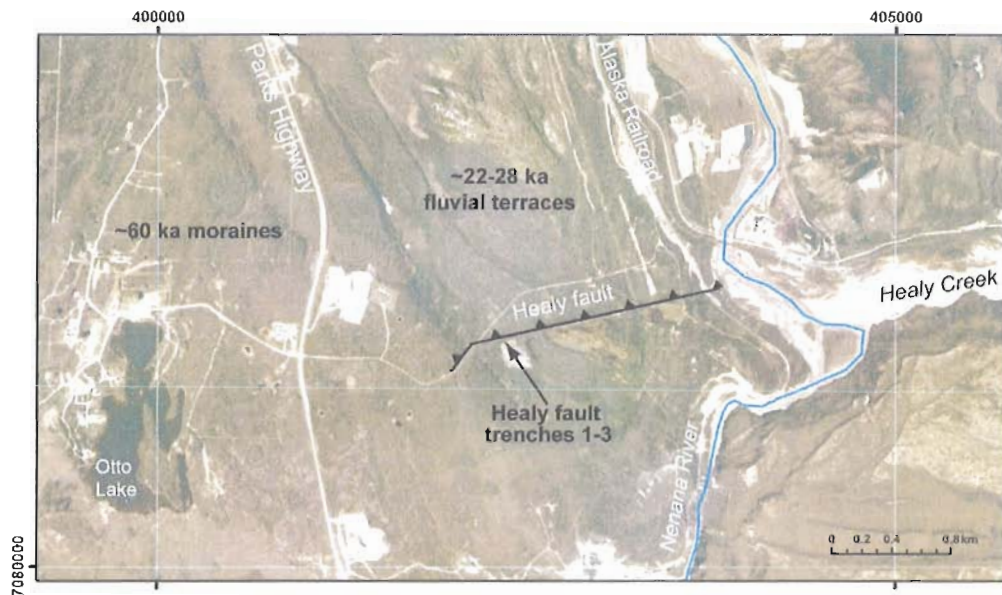
Figure A.2. Satellite orthoimage of the Healy fault area. Area of image shown on Figure A.1. The fault scarp only appears west of the Nenana River and can be traced westward to the edge of the ~60 ka moraines where there is an apparent offset of the moraine surface, but this offset cannot be traced further west across the hummocky topography. East of the Nenana River, the scarp has been eroded by Healy Creek.

River westward to moraine deposits correlated with the Healy glacial advance (~60 ka, Dortch, 2006). Because the fault produced a south-facing scarp on terraces that slope gently north, it blocks local drainage that beavers have utilized to construct networks of dams on each of the terrace surfaces that further prevent surface drainage and facilitates the accumulation of fine-grained sediments (Figure A.3). The dam on the highest terrace level was abandoned sometime within the past 20 years, draining the pond and making this portion of the scarp the target for paleoseismic trenching. Detailed locations and dimensions of individual trenches provided in Table A.1.

← *North*
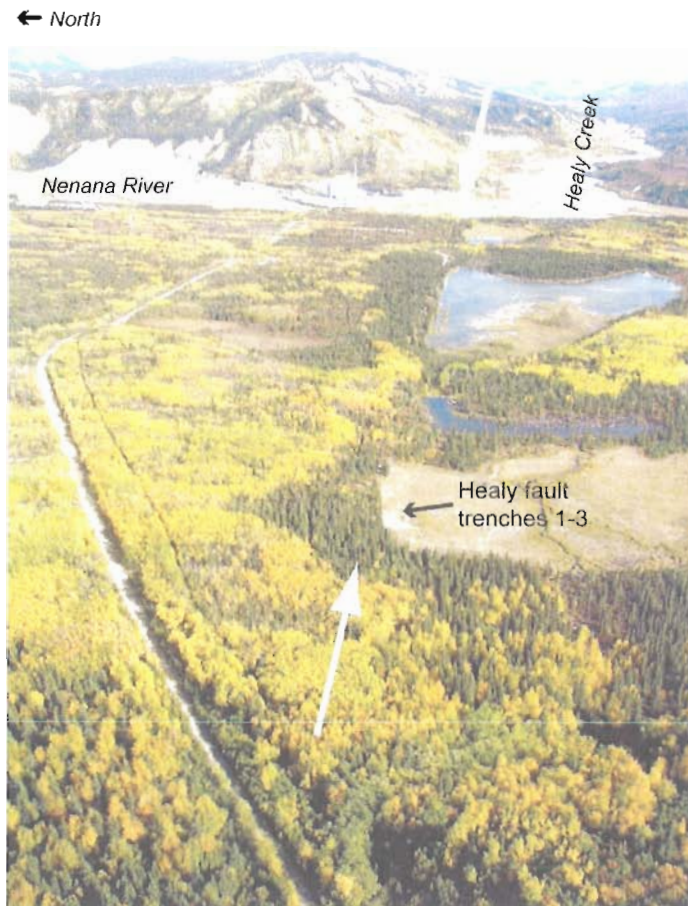
Figure A.3. Oblique photo of the Healy fault scarp. The white arrows highlight the trace of the scarp and the eastward projection of the fault. The ponds on the south side of the fault scarp are the result of beavers exploiting the scarp as part of their dam complexes, and each pond occurs on a separate terrace level. The Healy fault trenches were all excavated on the highest, recently-drained beaver pond at the location shown. The large white building adjacent to the Nenana River is a coal-fired power plant complex on the hanging-wall of this fault.

A.2.2 Synopsis of Stratigraphy

Descriptions of lithostratigraphic units are provided in Table A.2. The stratigraphy in all three trenches are broadly similar and consist largely of fine-grained sediments deposited on top of the fluvial gravels of the original terrace tread. The base of the fine-grained sediment package is characterized on the footwall by a continuous 2-10 cm thick well-sorted fine sand unit. The suite of fine-grained deposits is up to 2.2 m

Table A.2. Unit descriptions for the Healy fault trenches.

Unit Label	Descriptive Name	Dominant Grain Size (size class or cm)	Clast Size Max./Mean (cm)	Matrix/Clast Supported	Comments	Event Relevance	Unit Age*
O1	Modern organic mat	Silt	n/a	n/a	Dark, fibrous, abundant roots, thins up scarp	n/d	< ~700 yr
L1	Recent loess	Silt	n/a	n/a	Reworked on scarp face and below, local pebbles	MRE min age	Holocene
L3	Clayey loess	Silt	n/a	n/a	Clayey matrix, blocky texture	n/d	Pleistocene(?)
O2	Buried organic mat	Silt	n/a	n/a	Dark, fibrous, silty, grades into L2 below	MRE max age	~1500 yr
L2	Buried recent loess	Silt	n/a	n/a	Grayish color, scattered charcoal fragments, Irregular and gradational basal contact	n/d	>1500 yr
L	Recent loesses combined	Silt	n/a	n/a	Grayish-Orange loess below L2, no obvious charcoal fragments, irregular/discontinuous, locally difficult to distinguish from Mpfs	n/d	Late Holocene
Mpfs	Massive pebbly fine sand	Fine sand	2 / 1	n/a	Predominantly v. fine to fine sand, scattered v.c. sand and granules, deformed	n/d	Early – Mid Holocene?
BOS	Bedded organics and sand	Sand	n/a	n/a	Numerous thin, discontinuous dark organic beds and stringers, significant MnO_2 staining, interbedded with thin beds of fine, medium, and (less common) coarse sand, scattered MnO_2 nodules	n/d	Early Holocene – latest Pleistocene
CW	Gravel	Gravel	8 / 2-3	Matrix	Silty and sandy, poorly sorted gravel	n/d	Early – Mid Holocene
Mfs	Massive fine sand	Fine sand	n/a	n/a	Well-sorted fine to medium sand	n/d	Late Pleistocene
clst	Clayey silt	Silt	n/a	n/a	Pods and lenses of uncorrelated clayey silt	n/d	
ps	Pebbly sand	sand	3 / 1	Matrix	Pods and lenses of poorly sorted pebbly sand, uncorrelated	n/d	
St2	Lower pond silts	Silt	n/a	Matrix	Clay-rich silts above basal sand (bs), nutty or sticky texture depending on water content, contains a ~1 cm thick gray horizon – possible ash?, common to locally abundant, 1-2 mm MnO_2 nodules	Min. age for slip rate	Late Pleistocene
Bfs	Basal fine sand	Fine sand	n/a	n/a	Well-sorted, minor, probably secondary silt	n/d	Between ~23 ka and ~17 ka
Vcs	Very coarse sand	Very coarse sand	5 / 2	Matrix	Well-sorted, weak bedding, irregular contacts, some MnO_2 staining, occurs within unit Tg	n/d	> ~23 ka
Tg	Terrace gravel	Cobbles	30 / 4	Clast	Interstitial silt in top 20-30 cm, grades into fresh-appearing loose gravels	Max. age for slip rate	> ~23 ka

Note: n/a = not applicable, n/d = no data
* Ages generalized from radiocarbon results in Appendix B, Table B.1

thick and consist predominantly of irregular packages of silt and fine sand with local lenses of pebbly gravel. Deeper in the section, the silt units contain a distinct clay fraction, producing a blocky texture in units with lower water content and a sticky texture with higher water content. Manganese oxide nodules are common in the deeper parts of the section, as are abundant manganese oxide coatings associated with many of the buried organic horizons. Fine-grained deposits above the fluvial gravels on the hanging-wall of the scarp are predominantly loess, and an abrupt unconformity separating a loose, clean loess from a blocky, clayey silt below indicates erosion of the pre-existing loess cover (Plate A.1, Figures A.4 and A.5).

A.2.3   Paleoseismic Interpretation

Each trench exposed 2-3 discrete ruptures of the basal fluvial gravel – basal fine sand contact. An additional rupture breached higher in the scarp and is well-defined in trenches T1 and T2 (Figures A.4 and A.5, Plate A.1). The cumulative brittle offset of these faults is less than ~1.5 m, indicating that much of the deformation recorded by the offset of the terrace tread is manifest as folding that produced the northward tilts of units along the base of the scarp. I argue that the dramatic folding within the fine-grained sediments, best illustrated in T3 (Figures A.6 and A.7), is the result of horizontal compression imposed by the folding of the fault scarp and/or the strong-shaking from a rupture on this or an adjacent fault. Because seasonal freezing would progress slowly from the ground surface downwards, it is unlikely that deformation of this magnitude was produced by cryoturbation. Many of the smaller-scale folds, such as those occurring in the upper meter on the south ends of T1 and T2, have a consistent vergence to the south, indicating that these are either tectonically-induced or formed by a top-to-the-south shear, likely imposed by gravity, during the cryoturbation process.

Only one fault rupture is uniquely bracketed in the trench stratigraphy. Due to its position at the base of the modern scarp and the relative youth of the offset stratigraphy, this records the most recent event (MRE) on the Healy fault (shown best in Figures A.4 and A.5). Using the procedure described in Appendix B for determining the timing of this event from the stratigraphic sequence of radiocarbon ages, the MRE on the Healy fault occurred sometime during the years 1,528-1,176 cal BP (at 2σ confidence).
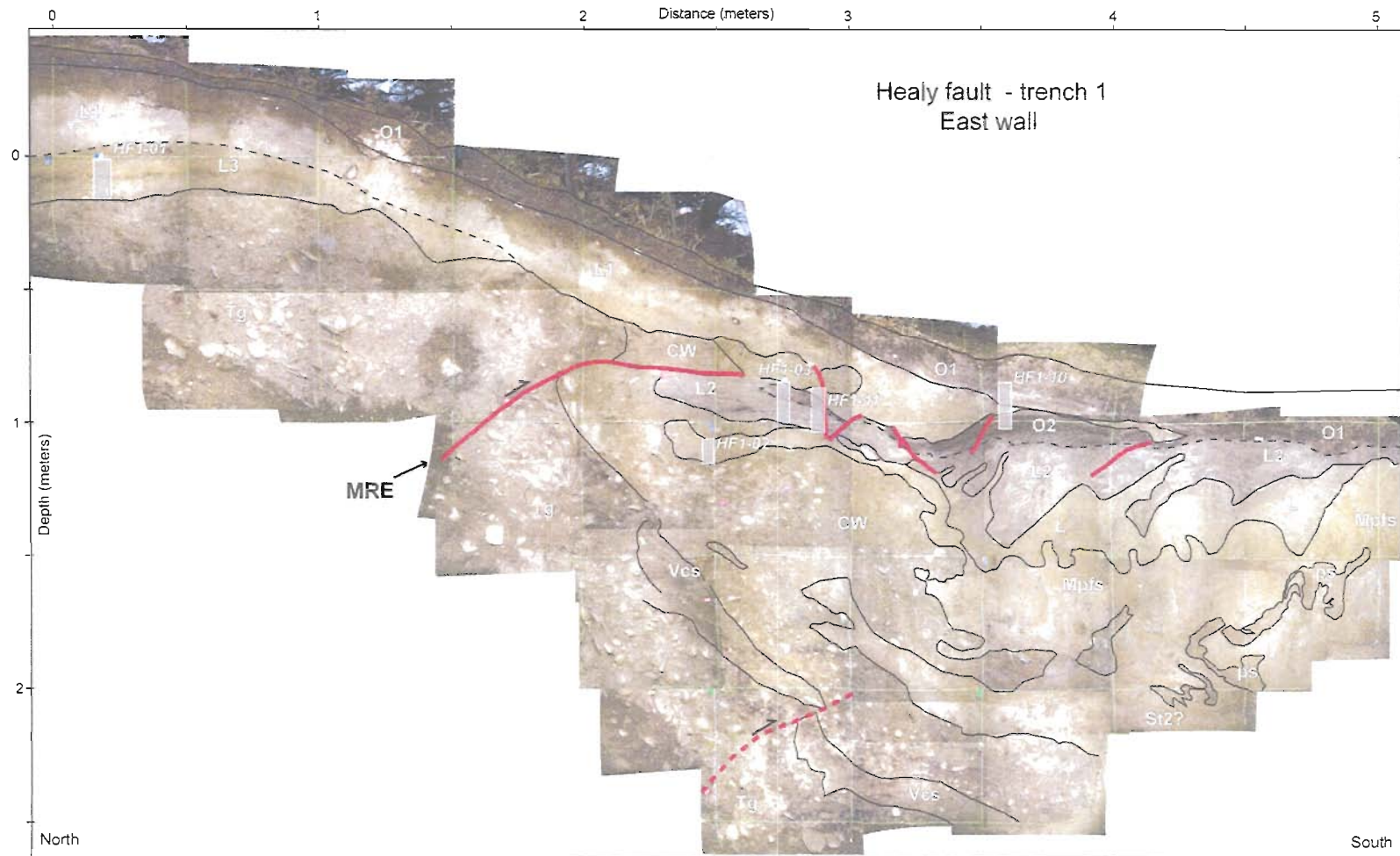
Figure A.4. Photomosaic and trench log of the Healy fault, trench 1, east wall. Thin black lines are contacts, thick red lines are fault traces. Dashed lines on faults depict zones where a single fault plane cannot be traced but fault related deformation is evident. Dashed contacts were not mapped in the field but subsequently mapped on the photomosaics to develop a consistent stratigraphy between this and subsequent trenches. The fault labeled 'MRE' is the trace of the most recent fault rupture on the Healy fault. Excavated and logged August – September 2005.
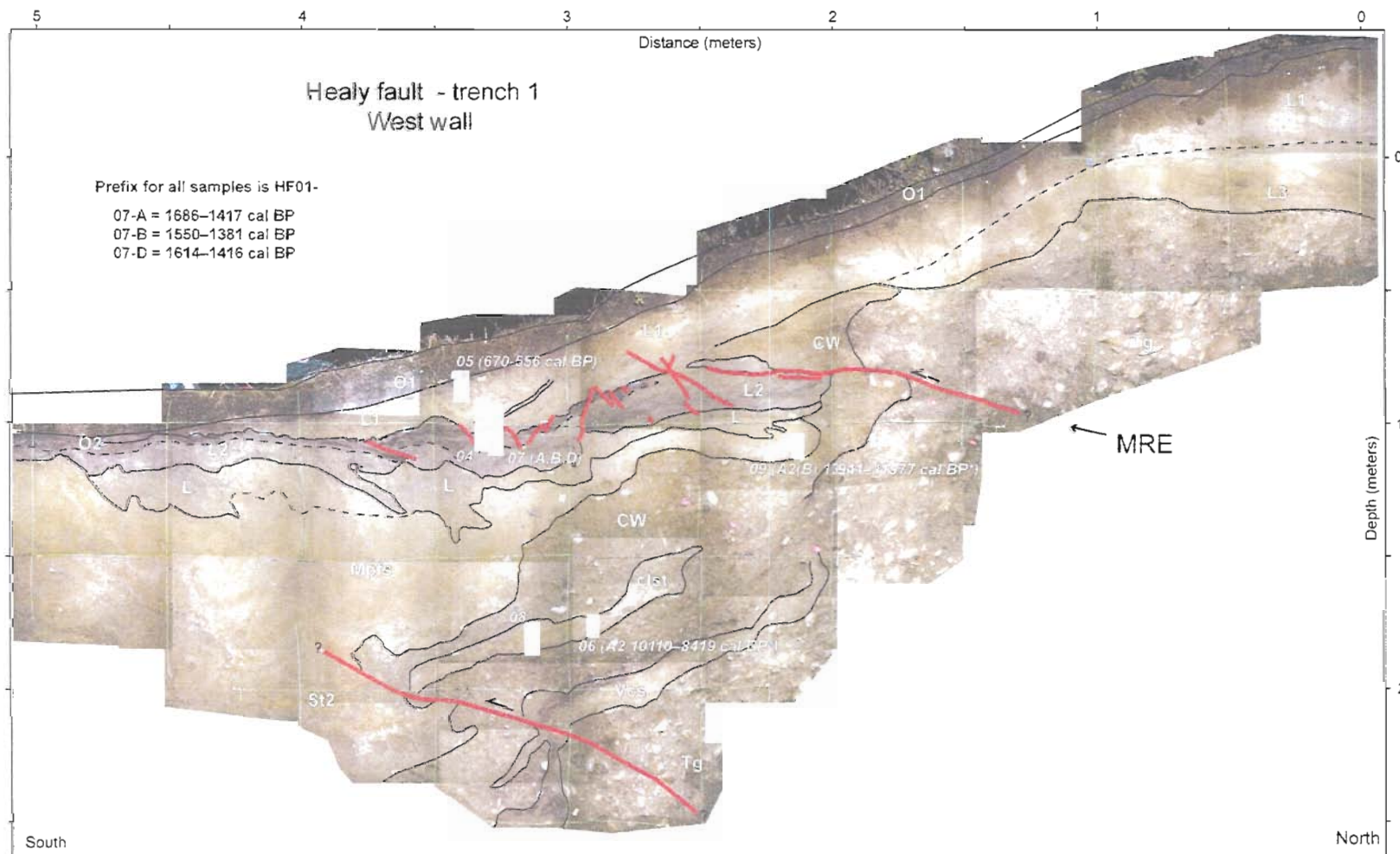
Figure A.5. Photomosaic and trench log of the Healy fault, trench 1, west wall. Thin black lines are contacts, thick red lines are fault traces. Dashed lines on faults depict zones where a single fault plane cannot be traced but fault related deformation is evident. Dashed contacts were not mapped in the field but subsequently mapped on the photomosaics to develop a consistent stratigraphy between this and subsequent trenches. The fault labeled 'MRE' is the trace of the most recent fault rupture on the Healy fault. Excavated and logged August – September 2005.
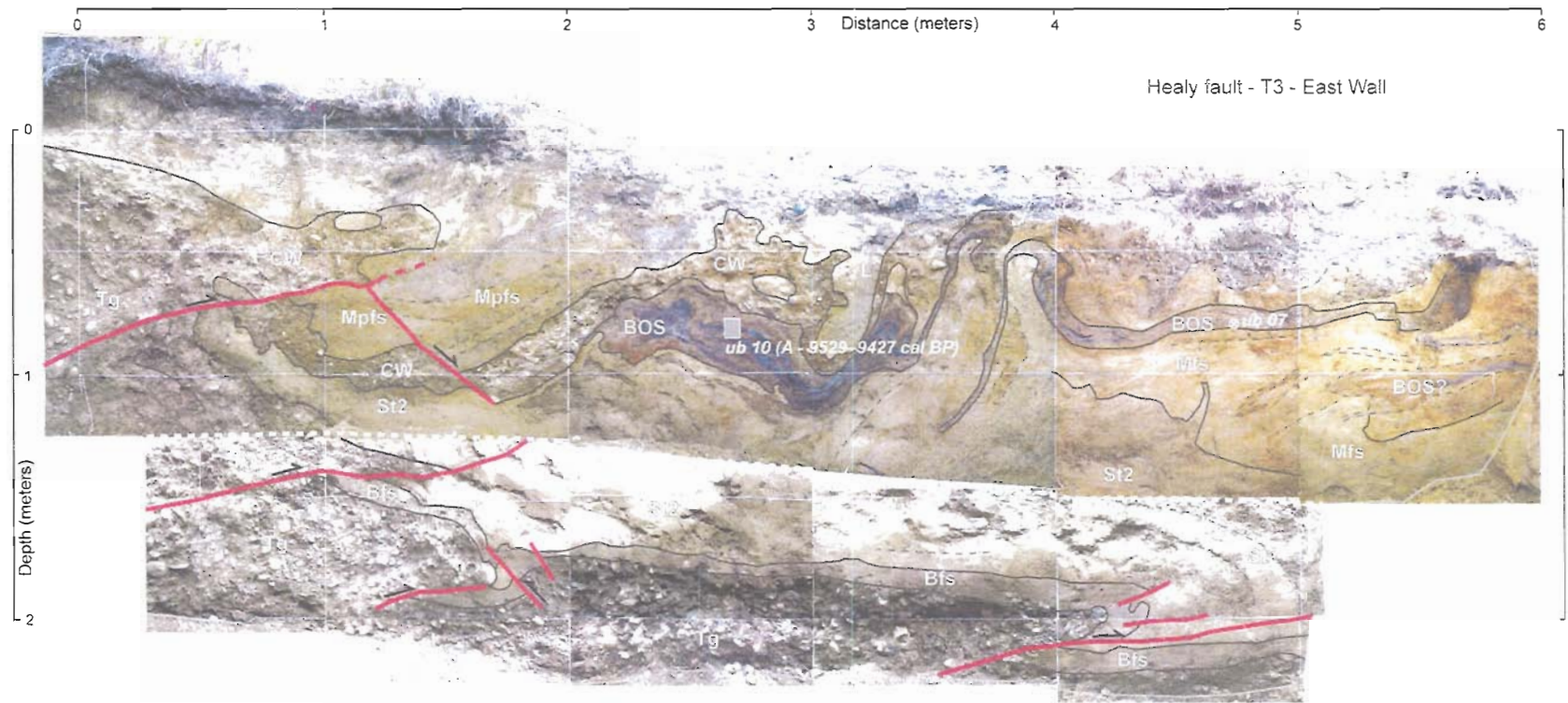
Figure A.6. Photomosaic and trench log of the Healy fault, trench 3, east wall. This trench was excavated as a benched exposure to provide better exposure of deeper stratigraphy. Because trenches 1 and 2 provide good exposure of the uppermost stratigraphy (Figures A.4, A.5 and Plate A.1), I did not map the upper stratigraphy in detail in this trench. Thin black lines are contacts, thick red lines are fault traces. Dashed lines on faults depict zones where a single fault plane cannot be traced but fault related deformation is evident. Thick dashed contacts were not mapped in the field but subsequently mapped on the photomosaics to develop a consistent stratigraphy between this and subsequent trenches. Thin dashed lines highlight discontinuous bedding within units. Excavated and logged August – September 2007.

Figure A.7. Photomosaic and trench log of the Healy fault, trench 3, west wall. This trench was excavated as a benched exposure to provide better exposure of deeper stratigraphy. Because trenches 1 and 2 provide good exposure of the uppermost stratigraphy (Figures A.4, A.5 and Plate A.1), I did not map the upper stratigraphy in detail in this trench. Thin black lines are contacts, thick red lines are fault traces. Dashed lines on faults depict zones where a single fault plane cannot be traced but fault related deformation is evident. Thick dashed contacts were not mapped in the field but subsequently mapped on the photomosaics to develop a consistent stratigraphy between this and subsequent trenches. Thin dashed lines highlight discontinuous bedding within units. Excavated and logged August – September 2007.

A.3 Healy Creek fault

A.3.1 Site Description

The Healy Creek fault is a near-vertical to steeply north-dipping reverse fault with over 1 km of cumulative offset (Wahrhaftig, 1970; Bemis and Wallace, 2007). The surface trace of the fault is expressed by an east-west trending scarp that begins east of the Nenana River on a fluvial terrace and can be traced for about 16 km east (Figure A.8). General trench details are provided in Table A.1.

Figure A.8. Location map of the Healy Creek fault trenches. Shaded-relief base from digitized 1:2400 scale (5 foot contours) topographic maps of the pre-mining topography obtained from Usibelli Coal Mine. The vertically-lined region was mined during the 1980's and 90's as mapped from satellite orthoimagery. The east-west scarp of the Healy Creek fault is clearly visible across the fluvial terrace and as it crosses into rugged topography to the east. White double-ended arrows illustrate the presence of two channels that are incised across the scarp. Between these arrows there is also an irregular north-facing scarp could not be inspected due to removal during mining, but due to the morphology and similar scarp height to the channels, it likely formed during the same erosive event that carved the channels across the scarp.

The first trench on this fault (HCF-T1) was excavated by the Usibelli Coal Mine for us across the main scarp on the high fluvial terrace (Figures A.8 and A.9). To achieve greater depth without shores, a benched trench was dug with a 1.5-2.5 m tall upper wall

and a 1-1.5 m tall lower wall separated by an ~2 m wide step. The total exposure was ~40 m long, and the lower walls separated by ~8-10 m. A second trench (HCF-ST) was excavated by hand across a small step in a channel incised across the scarp (Figures A.8 and A.9). This trench encountered frozen ground below ~0.5 m, but a low water content enabled excavation of up to ~1.2 m depth and 6 m long.
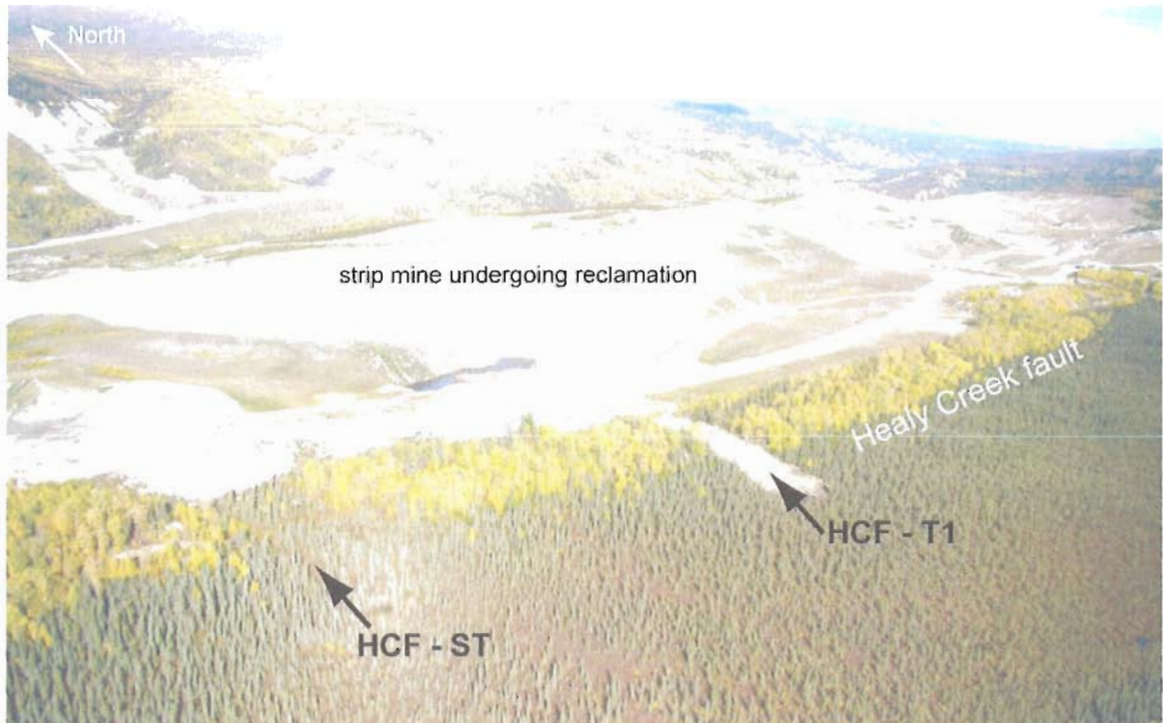
Figure A.9. Oblique photo of the Healy Creek fault scarp showing the locations of the HCF-T1 and HCF-ST trenches. The scarp is clearly highlighted by the vegetation contrast resulting from the deciduous trees preferring the well-drained scarp and the spruce trees on the permafrost dominated terrace surface. The swath of dirt at HCF-T1 is the back-filled trench.

A.3.2 Synopsis of Stratigraphy

Details of mapped lithostratigraphic units are provided in Table A.3. In general, the sediments in HCF-T1 are overwhelmingly fluvial gravels and very coarse sand (Plate A.2). Bedding within the gravels is common and typically defined by grain size variations and degree of matrix vs. clast support. Large-scale packages of gravel can be traced across the scarp face to where they are disturbed at both the crest and base of the scarp (Plate A.2). A thin (10-20 cm) deposit of loess blankets the entire exposure

Table A.3. Unit descriptions for Healy Creek fault paleoseismic trenches.

Unit Label	Descriptive Name	Matrix/ Clast Supported	Clast Shape	Sorting	Clast Size Max. / Mean (size class or cm)	Comments	Unit Age*
T1							
O	Modern organic mat	n/a	n/a	Well	Silt	Dark, organic-rich, fibrous, rooty	<1500
L1	Uppermost loess	n/a	n/a	Well	Silt	Thin, intermixes with base of unit O	Late Holocene
Rss1	Reworked sand & silt	Matrix	Rounded	Poor	15 / 3-4	A couple boulders present that cross unit boundaries	Latest Pleistocene – Early Holocene?
Ug1	Unsorted gravels	Clast	Rounded	Unsorted	25 / 5-10	Silt coatings on clasts, randomly oriented clasts	Late Pleistocene(?)
Ccs1	Massive cobbly v. coarse sand	Matrix	Rounded – sub-angular	Well/poor	50 / 10-15	Massive well-sorted v. coarse sand with cobbles and boulders, no fines, fresh-appearance, flood deposit?	Late Pleistocene(?)
Gp1	Granule & pebble matrix conglomerate	Clast	Rounded – Sub-angular	Unsorted	50 / 10-15	No internal bedding/imbrication	Late Pleistocene(?)
Rcs1	Reworked cobbly sand/silt	Matrix	Rounded – Sub-angular	Unsorted	20 / 5-8	Randomly oriented clasts	Late Pleistocene(?)
L2	Older loess	n/a	n/a	Well	Silt	Thin organic horizons, faint bedding, local cobbles – possibly frost-jacked	Holocene
L3	Tilted loess	n/a	n/a	Well	Silt	Occasional, small (<1 mm) MnO_2 nodules	Latest Pleistocene
Fsg1	Fluvial sand and gravel	Matrix	Rounded – Sub-angular	Mod.	30 / 4-5	Unweathered, weakly bedded, scattered cobbles and pebbles, Coarsens upwards	Late Pleistocene(?)
Scg2	Silty cobble gravel 2	Matrix	Rounded	Poor	10 / 2-3	Uncertain if silt is primary deposit or translocated	Late Pleistocene(?)
Scg1	Silty cobble gravel 1	Matrix	Rounded	Poor	30 / 5-10	Uncertain if silt is primary deposit or translocated	Late Pleistocene(?)
Spg1	Silty pebble gravel 1	Matrix	Rounded	Poor	12 / 2-3	Local weak bedding, uncertain if silt is depositional or translocated	Late Pleistocene(?)
Peb1	Pebble 1	Clast	Rounded	well	10 / 2-3	Clasts have silt coatings	Late Pleistocene(?)
Cob1	Cobbles w/ sandy matrix	Clast	Rounded	Mod.	20 / 5-7	Fresh-appearing gravel, no fines	Late Pleistocene(?)
Fs1	Fluvial sand	Clast	Rounded	Mod-well	7 / 2	Fresh-appearing, bedded coarse sand, no fines	Late Pleistocene(?)
ST†							
Gray-black horizons – peats and organic-rich silts with local wood fragments, grasses and other preserved macrofossils							Holocene
Buff-colored horizons – silty fine-medium sands, clear quartz grains and abundant micas							Holocene
Gray lenses and horizons – loess-like silt							Holocene

Note: n/a = not applicable, n/d = no data.

* Ages generalized from radiocarbon results in Appendix B, Table B.1, Late Pleistocene(?) ages reflect uncertainty in terrace correlation and age.

† Units not mapped in detail due to pervasive shearing and fine-scale bedding - only general trends describe for this trench

immediately below the modern organic mat except above the crest of the scarp (between ~29-35 m), where there is a thick, wedge-shaped block of reworked silt and gravel below ~1 m of loess.

The shallow exposure of HCF-ST encountered a sequence of loess and peat that is very strongly sheared (Figure A.10). The least deformed beds are generally 1-4 cm thick and blanket the topography. Intact macrofossils are abundant within the frozen deposits and consist of wood, grasses, and mosses.

A.3.3   Paleoseismic Interpretation

Numerous steeply-dipping shear zones cut the gravel stratigraphy, but the only dateable offset stratigraphy is the wedge-shaped block of loess. An angular unconformity within the loess deposit that corresponds with a thin colluvial deposit indicates a possible surface rupture. Radiocarbon dates on a charcoal above this unconformity of 11,719-12,640 cal BP and on a suite of manganese oxide nodules from below the unconformity of 14,085-18,484 cal BP constrains a possible earthquake near the end of the Pleistocene. Discussion of the radiocarbon dates on manganese oxide nodules is included in Appendix B.

The shearing within HCF-ST is clearly non-tectonic. The age of 6,546-6,830 cal BP from a plant macrofossil near the base of the trench indicates that this channel is at least 7,000 years old, possibly much older because the base of the fine-grained section is not exposed. The origin of the channel is unclear, but the lack of a tectonic scarp within the channel suggests that this portion of the fault has not experienced a surface rupture for at least 7,000 years.

A.4   Northern Foothills thrust

A.4.1   Site Description

The Northern Foothills thrust represents the basal thrust of the NFFTB near the Nenana River, and is a gently south-dipping, relatively planar thrust fault (Chapter III). I have identified a semi-continuous fault scarp on the ground and with air photos from adjacent to the Nenana River eastward to Windy Creek (Figure A.11). The terrace adjacent to the Nenana River is correlated with the Healy glacial advance (~60 ka, Dortch, 2006) and is offset between 2-4 m (Chapter III). In the east, near Windy Creek,
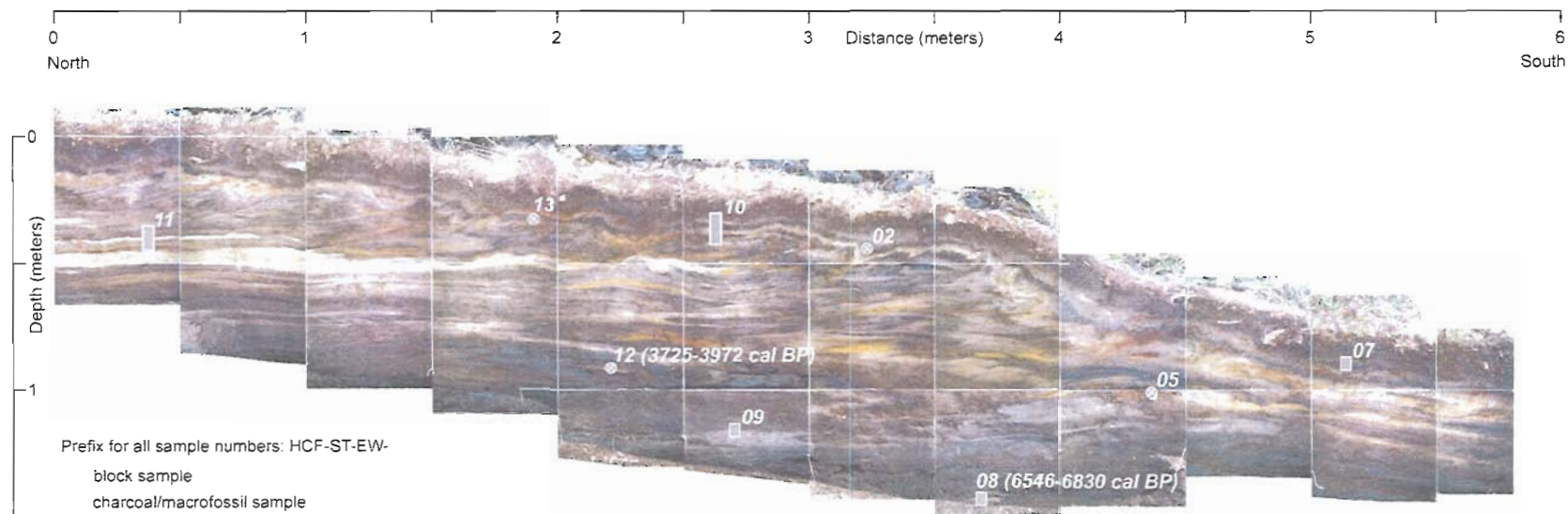
Figure A.10. Photomosaic of the Healy Creek fault ST trench east wall. Trench excavated across small surficial, encountered frozen ground below ~0.5 m, and permanently frozen ground below ~1 m. Alternating light and dark beds of peat and silt define a pervasively-deformed stratigraphy. The scarp results from the stacking of isoclinal folds in the seasonally frozen near surface sediments. Radiocarbon dates show that these sediments accumulated over the past ~6700 yrs. Most of the deformation occurred before the deposition of the uppermost 3 thin beds. Excavated and logged August – September 2007.

this fault offsets an alluvial surface of unknown age, resulting in a large complex north-facing scarp (Figure A.12). We hand-excavated two small trenches across the prominent break-in-slope at the base of the scarp. We abandoned the first trench due to a lack of coherent stratigraphy below a thin mantle of loess and modern organic mat. The second trench was ~5 m long and exposed ~1.3 m of section at the deepest point (Figures A.13 and A.14). Additional details of this trench site are summarized in Table A.1.
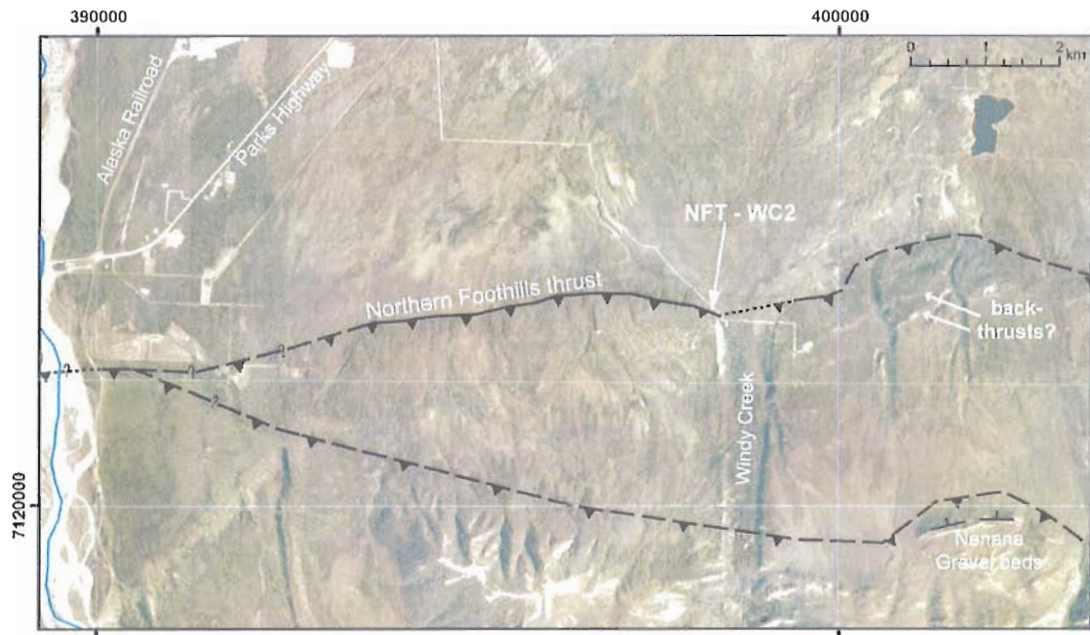
Figure A.11. Satellite image of the location of the NFT-WC2 trench on the Northern Foothills thrust. East of the Nenana River, there has been two traces of the Northern Foothills thrust active during the Quaternary. The southern strand has accommodated most of the cumulative uplift across the range front, but my field and air photo investigations did not find any evidence of late Pleistocene activity. The northern strand is the younger strand, as shown by the scarps in mid-late Pleistocene alluvium. The site of our trench is labeled, as well as two uphill-facing scarps on the uplifted alluvial surface that may be south-vergent backthrusts off the main north-vergent thrust.

A.4.2 Synopsis of Stratigraphy

Details of mapped lithostratigraphic units within the trench exposure are provided in Table A.4. A thin, modern organic mat (O) covers a <15 cm thick, discontinuous loess deposit (L1) that appears to blanket the underlying topography. At the south end of the trench, above the break in slope, this loess is in contact with pebbly gravel unit PG, and below the break in slope overlies a silty, poorly sorted colluvial gravel unit CW1. CW1
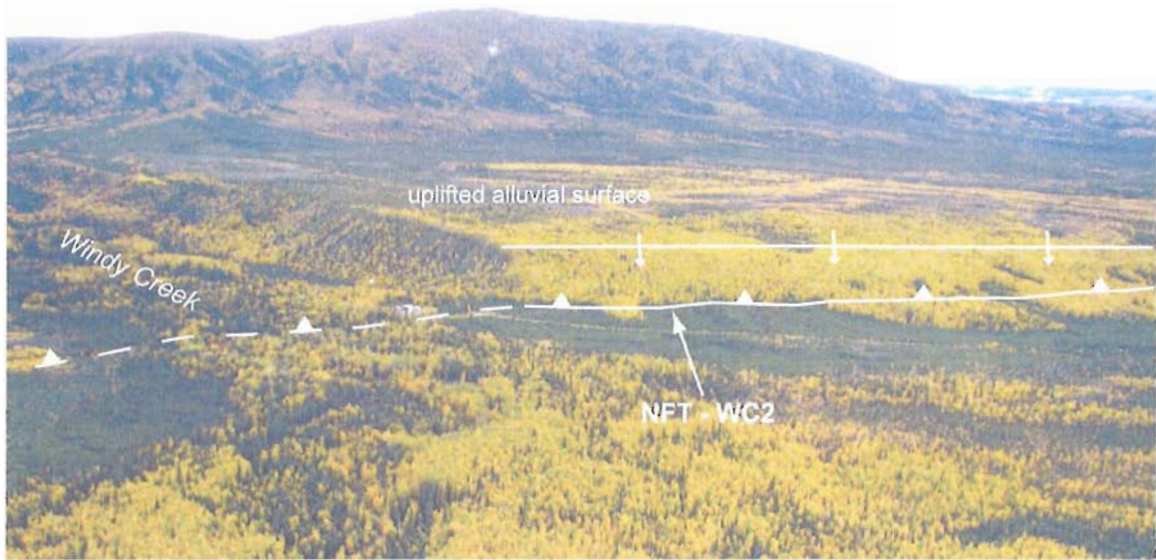
Figure A.12. Oblique photo of the Northern Foothills thrust and the range front of the Alaska Range near Windy Creek. View to the southwest. Recent propagation of the thrust fault into the foreland basin caused uplift of the broad alluvial surface and incision of Windy Creek.

thickens downslope in the trench, but pinches out within about 5 m north of the trench, as determined with a frost probe. Unit CW1 overlies a down-slope thickening sequence of loess, with a line of pebbles separating the upper loess, L2, from the lower loess, L3. The base of L3 was measured with a frost probe and is shown on Figure A.14. All three loess units contain abundant charcoal fragments and less common degraded pieces of wood. Silty gravel unit StG underlies loesses L2 and L3, and appears to be a fluvial gravel with a distinct fraction of translocated silt and clays. The base of this unit is gradational into a silt-free, sandy gravel unit SG.

A.4.3 Paleoseismic Interpretation

We identified two apparent fault offsets within the gravel units, but these were difficult to trace and were not primary surface ruptures. However, the south-dipping fault that places unit StG over L2 truncates against the overlying CW1 (Figure A.13), bracketing the deformational event that likely produced the colluvial wedge (CW1). Samples for radiocarbon dating were only obtained from the loess deposits, and we dated two samples within L1 for a minimum age and 5 samples from within L2 and L3 for a maximum age. The lowest sample in L1 provides a minimum age of 26,591–25,751 cal

Table A.4. Unit descriptions from the paleoseismic trench on the Northern Foothills thrust.

Unit name	Clast Size Max./Mean (general or cm)	Matix/Clast Supported	Clast Shape	Sorting	Bedding thickness (cm)	Comments	Event Relevance	Unit Age*	Genesis
O	Silt	n/a	n/a	Well	10	Dark, organic-rich, fibrous, rooty	n/d	<18 ka	Modern organic mat
L1	Silt	n/a	n/a	Well	15	Discontinuous, rare granules, weak blocky texture	Min. event age	<18 ka – 26 ka	Loess
CW1	20 / 3-4	Matrix	Well-rounded	Poor	30	Thins onto base of scarp	Post-event	>26 ka	Colluvial wedge
PG	15 / 3-5	Clast	Well-rounded	Poor	50	Minor coarse sand fraction, predominantly pebbles and cobbles, deformed?	n/d	>26 ka	Fluvial gravels
L2	Silt	n/a	n/a	Well	25	Faint bedding, common charcoal, rare wood	Max. event age	>50 ka	Loess
L3	Silt	n/a	n/a	Well	50	Faint bedding, common charcoal, rare wood	n/d	>50 ka	Loess
StG	20 / 3-5	Matrix	Well-rounded	Poor	50	Partial cementation by translocated silts, gradational contact into unit SG below	n/d	>50 ka	Fluvial gravel w/ translocated silt
SG	15 / 3-5	Clast	Well-rounded	Poor	>50		n/d	>50 ka	Fluvial gravels

Note: n/a = not applicable, n/d = no data

* Ages generalized from radiocarbon results in Appendix B, Table B.1
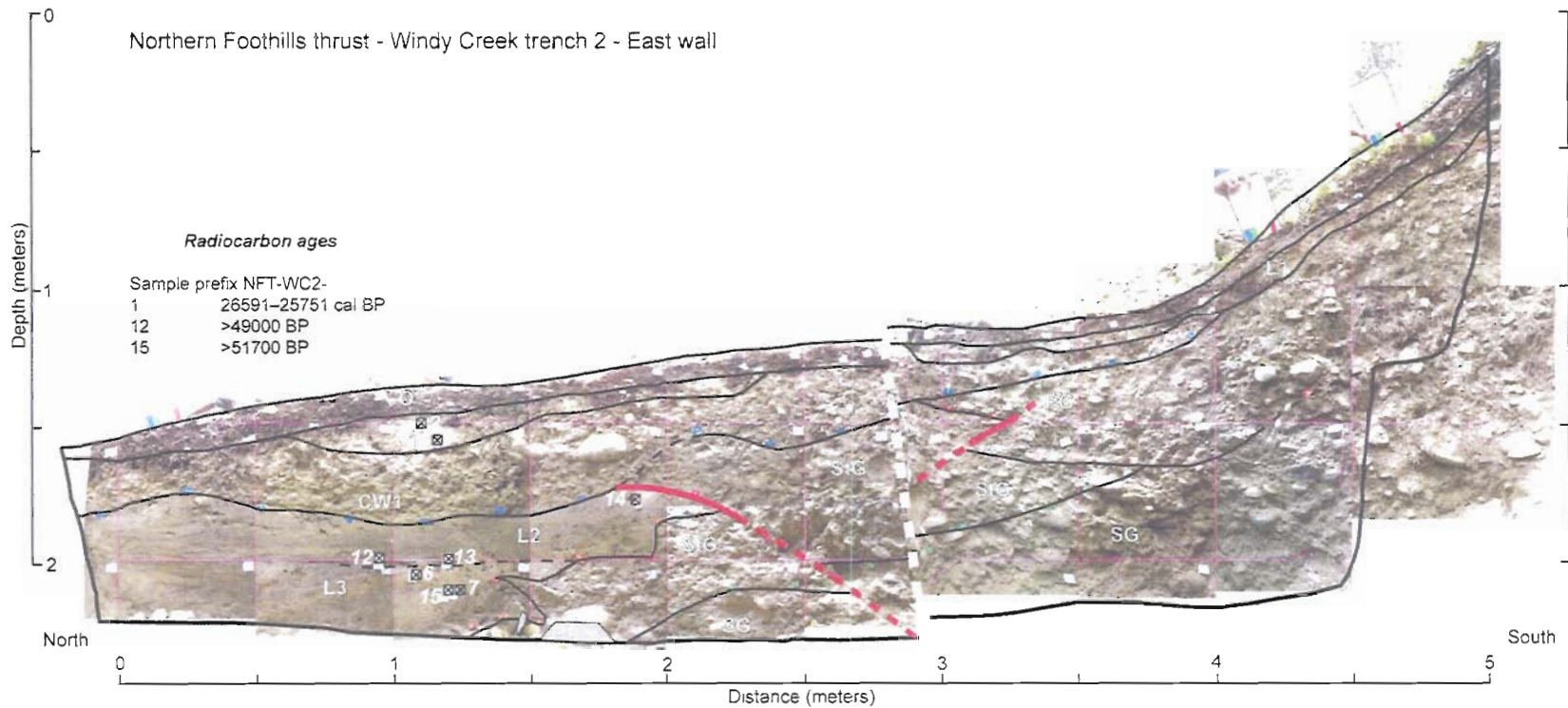
Figure A.13. Photomosaic and trench log of the Northern Foothills thrust, trench WC2, east wall. Black lines are contacts, thick red lines are fault traces. Dashed lines on faults depict zones where a single fault plane cannot be traced but fault related deformation is evident. No primary ruptures are evident, but the faults mapped are likely secondary deformation related to folding/faulting higher in the scarp than we were able to excavate. The colluvial wedge is the result of this deformational event, and is constrained by the ages of the overlying and underlying loess sequences. Excavated and logged September 2008.
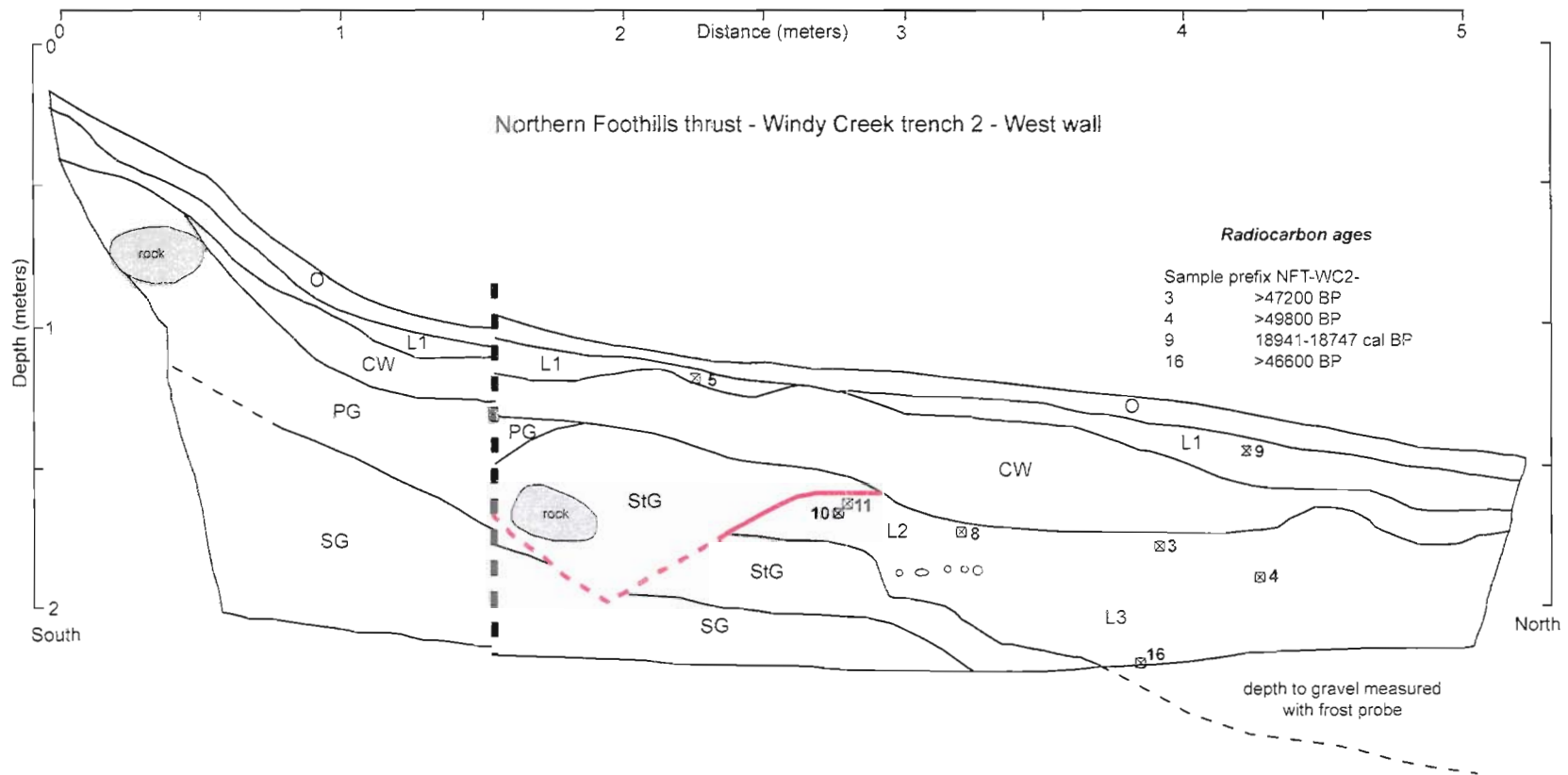
Figure A.14. Trench log of the Northern Foothills thrust, trench WC2, west wall. Black lines are contacts, thick red lines are fault traces. Dashed lines on faults depict zones where a single fault plane cannot be traced but fault related deformation is evident. No primary ruptures are evident, but the faults mapped are likely secondary deformation related to folding/faulting higher in the scarp than we were able to excavate. The colluvial wedge is the result of this deformational event, and is constrained by the ages of the overlying and underlying loess sequences. Poor trench site selection required a lateral jog in the trench to avoid a tree on the footwall, with the location of this jog shown by the thick, near vertical dashed lines on the logs. Excavated and logged September 2008.

BP for this inferred earthquake. All 5 samples from below the colluvial wedge are of infinite age in radiocarbon years. These samples included one sample of wood to verify that the old ages were not simply a result of recycling charcoals from an older deposit.

Field observations from this area did not recognize any additional candidate young fault scarps, which corroborates the lack of offset recorded by the <28 ka terraces west of the Nenana River. Therefore, this portion of the Northern Foothills thrust west of Windy Creek has either a >26 ka recurrence interval, more recent earthquakes occur as distributed deformation and are undetected, or the fault is now inactive.

APPENDIX B

AGE CONTROL ON LANDFORMS AND PALEOEARTHQUAKES IN THE

NORTHERN FOOTHILLS OF THE ALASKA RANGE

B.1   Radiocarbon Dating

I collected samples of organic material and block samples across key stratigraphic horizons from each of our paleoseismic trenches to provide stratigraphic age control on the timing of deformation. Additional samples were collected from the loess cover overlying sections of terrace gravels for in-situ terrestrial cosmogenic nuclide surface exposure (TCN) analysis. Only a portion of the samples collected were analyzed because multiple samples at each site were collected to provide backup and additional options for possible dating strategies. All of the collected samples are labeled on the trench logs in Appendix A, but only those samples analyzed are described here. For clarity, only the analyzed samples are shown on the TCN sections.

B.1.1   Sample Preparation

I pretreated the first suite of samples at the Center for Accelerator Mass Spectrometry (CAMS) at the Lawrence Livermore National Laboratory. These samples are noted on Table B.1. I pretreated the rest of the samples in the Archaeometry Facility in the Department of Anthropology, University of Oregon. Samples and standards (process and background) were pretreated using standard acid-alkali-acid (AAA) procedures, sealed in quartz tubes under vacuum, and combusted to CO_2 gas. The samples were then submitted to CAMS for graphitization and AMS analysis.

B.1.2   Results

Table B.1 summarizes the ^{14}C ages, the respective calibrated ages, and the locations and purpose of each sample. I calibrated the ^{14}C ages through OxCal v4.0.5 (Bronk Ramsey, 1995; 2001) using the IntCal04 calibration curve (Reimer et al., 2004).

Table B.1. Radiocarbon analysis results.

Sample Name*	CAMS Lab Number[†]	14C Age (BP)[§]	Calibrated age interval (cal BP)[#]	Sample material**	Sampled Unit	Significance	Notes
HF01-05-A	128367	650 ± 30	670 - 556	Charcoal (a)	Base of O1	Min. limiting age	LLNL
HF01-07-A	128368	1645 ± 30	1686 – 1417	Charcoal (a)	Top of O2	Max. limiting age	LLNL
HF01-07-B	128369	1580 ± 40	1550 – 1381	Charcoal (b)	Top of O2	Max. limiting age	LLNL
HF01-07-D	128370	1640 ± 30	1614 – 1416	Charcoal (b)	Top of O2	Max. limiting age	LLNL
HF01-10-A	128371	1075 ± 30	1056 – 931	Peat	Top of O2	Disregard – unclear what was dated	LLNL
HF01-10-A	128372	795 ± 30	765 – 672	Humics	Top of O2	Disregard - unclear what was dated	LLNL
HF01-06-A2	144863	8230 ± 300	10110 – 8419	Mn-oxide nodules	clst	Below a colluvial wedge	
HF01-09-A2(B)	144874	11090 ± 410	13941 – 11977	Mn-oxide nodules	Mpfs	Above a colluvial wedge	
HF-T2-WW-08	136504	635 ± 35	666 – 552	Charcoal (b)	BOS	Mixed up sample/contaminated?	
HF-T2-WW-12	144870	1210 ± 30	1256 – 1059	Charcoal (b)	Reworked L1	Min. limiting age	
HF-T3-WW-1b-06	140777	23560 ± 370	24338 – 22850	Mn-oxide nodules	Tg	Max age terrace tread	
HF-T3-WW-ub-03	140779	8020 ± 35	9015 – 8767	Charcoal (b)	BOS	Age of prominent contact in mid-section	
HF-T3-EW-ub-10A	140780	8445 ± 35	9529 – 9427	Charcoal (b)	BOS	Age of prominent contact in mid-section	
HF-T3-WW-ub-05	144875	21890 ± 2380	30307 – 17871	Mn-oxide nodules	St2	Min. age terrace tread	
HCF ST EW-12	136501	3565 ± 35	3972 – 3725	Wood	Undivided		
HCF T1 WW 11a	136502	1720 ± 35	1709 – 1546	Charcoal (b)	O	Age of fine-grained deposits on base of scarp	
HCF T1 WW R8a	136503	10320 ± 110	12640 – 11719	Charcoal (b)	L2/L3 contact	Max age of L2 – possible min. age for deformational event	
HCF-T1-R5(A)	144872	13490 ± 750	18484 – 14085	Mn-oxide nodules	L3	Possible max age for deformational event	
HCF-ST-08B	144873	5870 ± 50	6830 – 6546	Macrofossil	Undivided	~Max. age of exposed deposits	
NFT-WC2-03	140772	>47200	Infinite	Charcoal (a)	L2	Max. limiting age	
NFT-WC2-15	140773	>51700	Infinite	Charcoal (a)	L3	Max. limiting age	
NFT-WC2-16	140775	>46600	Infinite	Charcoal (b)	L3	Max. limiting age	
NFT-WC2-12	140776	>49000	Infinite	Charcoal (a)	L2	Max. limiting age	
NFT-WC2-01	140778	26160 ± 210	26591 – 25751	Charcoal (b)	L1	Min. limiting age	
NFT-WC2-09	144866	15565 ± 45	18941 - 18747	Charcoal (a)	L1	Suggests slow loess accumulation during past ~26 ka	
NFT-WC2-04	144867	>49800	Infinite	Wood	L2	Max. limiting age	
BB-01	140774	3285 ± 35	3613 - 3410	Charcoal (b)	Loess	Shielding constraint	
SavW1-05-30	140771	4635 ± 35	5467 – 5303	Charcoal (b)	Loess	Shielding constraint	
SavW1-03-9A	144864	5480 ± 30	6385 – 6209	Charcoal (b)	Loess	Shielding constraint	
06SB17-AOR	144865	370 ± 35	504 – 317	Charcoal (a)	Loess	Shielding constraint	Outer rings of twig
06SB17-B	144871	3600 ± 35	4065 – 3830	Charcoal (b)	Loess	Shielding constraint	
Fish-01-58	144868	6870 ± 30	7788 – 7625	Charcoal (a)	Loess	Shielding constraint	
Fish-06-10	144869	245 ± 35	430 – (-4)	Charcoal (a)	Loess	Shielding constraint	

Note: All pretreatment performed by Bemis in the UO Archaeometry prep lab except those marked with (LLNL) in the notes column whose pretreatment was performed by Bemis at LLNL CAMS.

* Site name codes: HF = Healy fault (01 = trench 1, T2 = trench 2, T3 = trench 3); HCF = Healy Creek fault (T1 = large trench, ST = small trench); NFT-WC2 = Northern Foothill Thrust, Windy Creek trench 2; BB = Bear Bait TCN profile; SavW1 = Savage W1 TCN profile; 06SB = Pott's Bluff TCN profile; Fish = Fish Creek TCN profile.

† AMS analysis at the Center for Accelerator Mass Spectrometry (CAMS) at Lawrence Livermore National Laboratories.

§ The quoted age is in radiocarbon years using the Libby half life of 5568 years and following the conventions of Stuiver and Polach (1977). Sample preparation backgrounds have been subtracted, based on measurements of radiocarbon-dead standards pretreated in parallel with samples.

Ages calibrated with Oxcal v4.0.5 (Bronk Ramsey, 2001) using the IntCal04 calibration curve (Reimer et al., 2004), with ages quoted at 2σ errors.

** (a) fresh-appearing, angular edges, woody texture preserved/growth rings visible – likely burned in-situ or very little transport, (b) rounded edges, some woody texture present – possibly reworked, transported prior to deposition, or minor in-situ weathering, (c) well-rounded, no woody texture visible – strongly weathered.

B.1.3   Manganese Oxide Nodules

Trenches on the Healy fault and Healy Creek fault (Appendix A) both exposed pre-Holocene fine-grained sediment that contained common to locally abundant, <2 mm nodules of iron-manganese oxides (referred to here as Mn-oxides). No chemical analyses were performed on these nodules, but the nodules were identified both in the lab and in the field by immersion in 3% H_2O_2 solution and comparison with stratigraphically adjacent sediment and organic material that were immersed in H_2O_2 separately. Invariably the H_2O_2 exposed to the nodules effervesced vigorously and the H_2O_2 exposed to the other sediment and organics did not.

In the Healy fault trenches (Appendix A), the stratigraphy below unit BOS (Figures A.4-A.7 and Plate A.1) contain no readily-identifiable organic material suitable for radiocarbon dating, but Mn-oxides are abundant. Unit BOS itself is partially characterized by the abundant Mn-oxide staining of the interbedded silts and thin organic-rich silts. Several charcoal specimens from within unit BOS were examined under a binocular microscope. These specimens showed well-preserved wood grain that was partially coated with a black rind. A subsample of this rind passed my test for Mn-oxides. From this observation, I hypothesized that the Mn-oxide nodules often precipitated onto small organic fragments in the sediment and may have preserved traces of this original organic material within the core of the nodule.

In an attempt to date the pre-Holocene stratigraphy of the Healy fault and Healy Creek fault trenches that is devoid of original organic material, I made collections of Mn-oxide nodules from several horizons below unit BOS in the Healy fault trenches and unit L3 from T1 on the Healy Creek fault. Each collection was composed of 3-10 Mn-oxide nodules harvested from a narrow (<1 cm) horizontal zone. One exception to this is sample HF-T3-WW-lb-06 which was a Mn-oxide-rich, dark gray blocky mass within fluvial gravels. Of eight total Mn-oxide samples submitted, five resulted in radiocarbon ages, and these are shown on Table B.1 as those with Mn-oxide listed for the sample material. Because of the greater density of manganese oxide and that the dateable carbon fraction was likely only a small portion of this, I submitted larger samples than the typical target sample mass for charcoal of ~2.5 mg. The masses of samples that yielded

radiocarbon ages were all >10 mg, and four of the five were >25 mg. A couple sample splits were attempted, but the duplicates had smaller sample sizes and apparently did not yield enough CO_2 for AMS analysis. The large errors on the successful samples suggests that even the >25 mg samples contained only very small quantities of carbon.

Most of these samples are stratigraphically consistent with either adjacent ages from radiocarbon samples or independent determinations of the feature that is dated, and except for HF01-06-A2 and HF01-09-A2(B), all are internally consistent (within their respective error limits). I have submitted a charcoal sample to determine which of the inconsistent samples are out of stratigraphic order. While caution is necessary in the use of these ages, due to the uncertainty in exactly what is being dated, the observed stratigraphic consistencies are unlikely to occur purely by chance.

B.1.4 Healy Fault Stratigraphic Model

I used the stratigraphic modeling capabilities of OxCal v4.0.5 (Bronk Ramsey, 2008) to determine the age of the most recent event (MRE) on the Healy fault (Appendix A) because it is bracketed by multiple radiocarbon dates in stratigraphic order. This MRE is defined by the truncation of O2 and its burial by unit L1 (Figures A.4 and A.5). With three radiocarbon ages from the top of O2, one from within L1, and one at the base of O1 (Table B.1), I used a "Sequence" model (Bronk Ramsey, 2008) that established the relative position of these units (phases) but assumed no ordering of the samples within each phase (Figure B.1). When processed through OxCal, this model calibrates the individual radiocarbon ages, creating a probability distribution function (PDF) for each. Using a Bayesian statistical approach, stratigraphic context of the individual sample PDFs are used to reduce the variance of individual samples and constrain the time intervals between dated phases (Bronk Ramsey, 2008). Figure B.1 shows the sequence of samples, the respective PDFs, and the calculated PDF for the most recent event on the Healy fault.

B.2 ^{10}Be Cosmogenic Surface Exposure Dating

Of ten total depth profiles collected for dating surfaces with the in-situ accumulation of cosmogenic nuclides, I selected four profiles for processing and analysis. I chose to analyzed only these four profiles in order to get preliminary ages for key sites

and to test how well this method worked before investing time and money into more profiles. Three profiles are from a sequence of fluvial terraces on the hanging wall of the Stampede fault, adjacent to the Savage River (Chapter III). The fourth profile is from the highest extensive fluvial terrace near Gold King Creek (Q3, Chapter II) to provide a maximum age constraint on the sequence of younger fluvial terraces. Site-specific details for each profile location is provided in Table B.2.
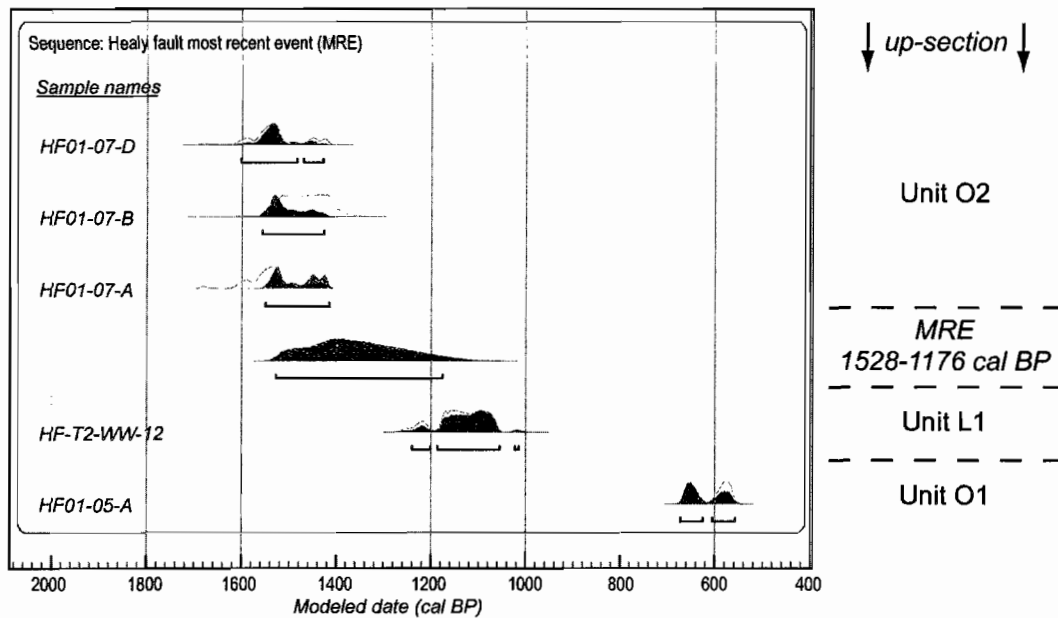
Figure B.1. Stratigraphic sequence model defining the age of the most recent event (MRE) on the Healy fault. Sample names are listed on the far left with the corresponding probability distribution function (PDF) for the individual calibrated ages shown as the light gray shaded curve, and the modeled PDF in dark gray. Brackets beneath modeled PDFs indicate the 95% confidence intervals for the age ranges. Basic stratigraphic context of samples illustrated to the right of the plot (note that uppermost strata is at the bottom of the plot). The modeled age interval for the the earthquake (labeled MRE) is 1528-1176 cal BP. Model analysis performed in OxCal 4.0.5 (e.g. Bronk Ramsey, 2001) with the IntCal04 atmospheric calibration curve (Reimer et al., 2004) and using the unconstrained sequence model as described by Bronk Ramsay (2008). Unmodeled radiocarbon ages for samples used in this model are provided in Table B.1.

The riser face was cleared in a nearly vertical profile 2-3.5 m tall to expose the unmodified terrace surface down through at least 2 m of undisturbed fluvial gravels. For the analyzed depth profiles reported here, we targeted locations on terrace risers that had experience recent erosion of the riser face without erosion of the terrace surface to

Table B.2. Site specific information for TCN depth profiles.

Profile Name	Location* (Latitude/Longitude)	Altitude (m) [†]	Sample Depths (cm) [§]	Thickness (cm)	Topographic shielding [#]	Sediment Density (g/cm^3)**	Modern Cover Thickness (cm) [††]	Comments
Pott's Bluff	64.19190/-147.94895	503 ± 5	100, 150, 200, 250	10	0.9999	1.9	33	Radiocarbon samples in loess cover indicate a depositional hiatus and/or phase of loess stripping
Savage W1	63.89789/-149.44306	523.2 ± 0.2	78, 122, 170, 223, 270	10	0.9998	2.1	45	Inversion of radiocarbon sample ages indicate mixing of cover sediment, contact of loess with blocky clayey silt indicates complex deposition/erosion history
Savage W2	63.89720/-149.44074	520.9 ± 0.1	62, 112, 162, 212, 255	10	0.9998	2.1	15	Thin loess beneath the modern turf suggests either this surface is younger than the deposition of the loess at Savage W1, or that the loess was preferentially stripped from this location
Fish Creek 1	63.89817/-149.42518	578.6 ± 0.2	120, 156, 190, 269, 319	10	0.9999	2.1	75	Loess cover depicts complex Holocene history, unknown pre-Holocene loess cover

Note: These surfaces receive snow cover for much of the winter, but due to the low density of snow relative to loess, the uncertainty that snow cover introduces is minor relative to the uncertain loess cover history.

* Datum is WGS 84.

[†] Relative to mean sea level, positions with submeter precision measured with differential GPS, Pott's Bluff site measured with handheld GPS and verified with nearby differential GPS elevations.

[§] Depth measured to center of sampled interval.

[#] Topographic shielding calculated with the online geometric shielding calculator v1.1 at the CRONUS – Earth website.

** Densities were not measured in the field or on the analyzed samples, but an estimate was calculated for these profiles from similarly-aged terrace deposits collected from the same fluvial systems.

[††] Estimated density of 1.5 g/cm^3 for loess.

minimize this excavation and minimize the duration of exposure to cosmic rays through the riser face. The exposed stratigraphy was described and logged, noting the thickness of loess cover, depth of cryoturbation and the internal stratigraphy of the terrace deposits. Figure B.2 shows these profiles, the basic stratigraphy, and the sample locations from each profile.

B.2.1   Sample Preparation

I performed the sample preparation and pretreatment in the TCN labs at the University of Cincinnati under the supervision of Dr. Lewis Owen. For 19 total samples, the gravel was sieved to obtain the 250-500 μm size fraction. Several samples did not provide enough material in that size fraction, so I crushed a portion of the 500-1000 μm size fraction and sieved an additional quantity to the 250-500 μm size fraction to supplement these samples. Each sample was leached in aqua regia for >24 h, two 5% HF/HNO$_3$ leaches for ~24 h each, and three 1% HF/HNO$_3$ leaches for ~24 h each. More acid leaches than typical was required for these samples due the presence of numerous dark grains in the sample (probably grains of chert). A heavy liquid separation (using lithium heteropolytungstate at density 2.7 g/cm^3) removed acid-resistant and mafic minerals. I added a low-background ^{9}Be carrier to each ~30 g sample of pure quartz, which was then dissolved in concentrated HF and fumed with perchloric acid. Samples were passed through cation and anion exchange columns to separate the Be fraction. Ammonium hydroxide was added to this fraction to precipitate a beryllium hydroxide gel, which was then oxidized at 750° C for 5 min. This beryllium oxide was then mixed with Nb powder, loaded into targets, and submitted for AMS measurement of ^{10}Be/^{9}Be ratios at the Purdue Rare Isotope Measurement Laboratory at Purdue University.

B.2.2   Results

The AMS results for these samples and details of basic data conversions are provided in Table B.3. To determine surface exposure ages from my depth concentration profile, I follow the same general procedure used by Burgette (2008). However, these calculations are considered preliminary because I intend to employ an online ^{10}Be depth-
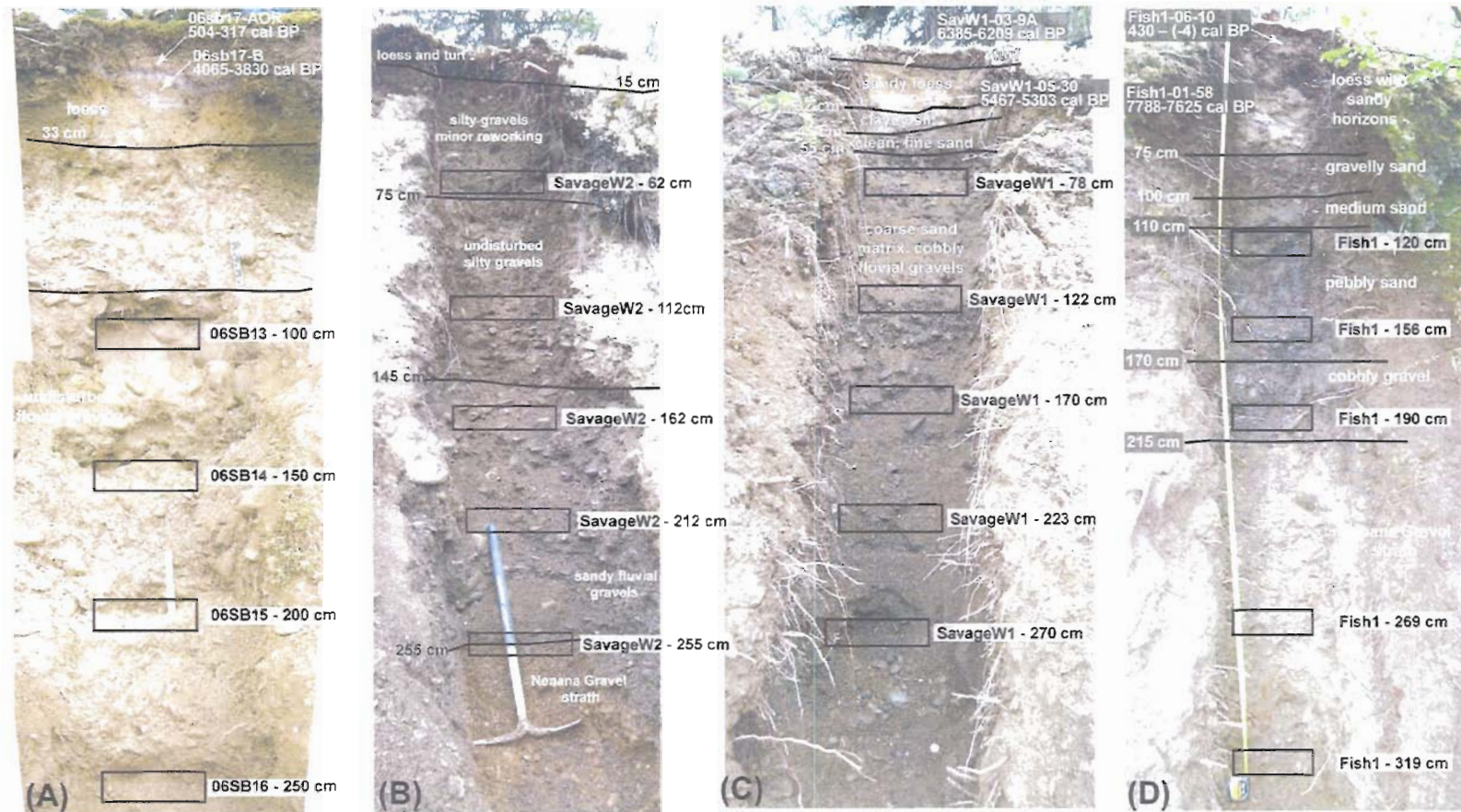
Figure B.2. Photographs of the exposures sampled for TCN dating. Locations and depths of stratigraphic contacts labeled. Stratigraphic units labeled with a generalized descriptive name. Approximate sample intervals shown with rectangles with corresponding sample names and depths. (A) Pott's Bluff profile from the Japan Hills-Gold King Creek map area (Chapter II). (B) Savage W2 profile. (C) Savage W1 profile. (D) Fish Creek 1 (Fish1) profile. Profiles shown in B-D are on terraces adjacent to the Savage River near the Stampede fault (Chapter III). The Nenana Gravel unit exposed in profiles B and D beneath the terrace gravel is an extensive Pliocene alluvial deposit that is grossly similar to the recent fluvial gravels except for the interstitial clays that provides a weak cementation for this unit. (C) was photographed after sampling, so spoils from collecting the higher samples obscures much of the gravel stratigraphy. Profile depths are not scaled relative to one another.

concentration profile calculator that is nearing completion (Marrero et al., 2009; S. Marrero, personal communication, 2009) in order to ensure a standardized procedure and to easily test different shielding scenarios.

A robust minimum surface exposure age for each depth profile can be calculated by assuming that the present cover of fine-grained sediment was deposited the day before sample collection, thus providing no appreciable shielding during the life of the terrace. To calculate this minimum, I use the linear regressions for each depth profile from Figure B.3 and calculate the ^{10}Be concentration at the top of the terrace gravels for each profile. This concentration and appropriate attributes for the profile, including location, density, topographic shielding, etc. are input into the CRONUS online calculator (standard model input and parameters, v2.2; Balco et al., 2008). The resulting no-shielding model ages with respective 1σ uncertainties are given in Table B.3. The three profiles at the Savage River, Savage West 1, Savage West 2, and Fish Creek 1, have 1σ uncertainties larger than the exposure ages. Because of the scatter of the profile points (Figure B.3) and resulting large uncertainties, I do not extend modeling for these profiles at this time. A pseudo-maximum age for the terrace surface can be modeled by assuming that the present loess cover has been present since immediately after terrace formation. This pseudo-maximum age for the Pott's Bluff profile is ~112 ka (Table B.2). I call this a "pseudo-maximum" age because the presence of Holocene radiocarbon ages within the modern loess cap show that the assumption of constant loess cover is not valid. Also shown by the radiocarbon ages and loess stratigraphy is that gaps of time are missing within the loess sequence, and significant surficial loess stripping has occurred during the history of these terraces (Thorson and Bender, 1985). It is very likely that thicker sequences of loess has existed on these terrace surfaces in the past (Thorson and Bender, 1985), so the actual age can be even older than the pseudo-maximum.

Sample	Mass of Quartz (g)	Be Carrier (g)*	$^{10}Be/^9Be$ (10^{-12})[†]	Measured ^{10}Be $(10^5$ atoms/g quartz)[‡]	^{10}Be No-Shielding Model Age (ka)[§]	^{10}Be Modern Cover Since Formation Model Age - (ka)
Pott's Bluff profile					82.0 ± 7.3	112
06SB13 - 100 cm	30.192	0.4139	3.124 ± 0.1216	3.26442 ± 0.13357		
06SB14 - 150 cm	29.997	0.3929	1.934 ± 0.0742	1.91388 ± 0.07878		
06SB15 - 200 cm	30.0561	0.3981	1.045 ± 0.0465	1.02715 ± 0.05069		
06SB16 - 250 cm	30.6036	0.4045	0.7565 ± 0.0698	0.73134 ± 0.07292		
Savage West 1 profile					$5.2 \pm 1.4 \times 10^4$	
SavageW1 - 78 cm	29.5945	0.4105	0.4000 ± 0.0372	0.38647 ± 0.04248		
SavageW1 - 122 cm	30.9134	0.401	0.3737 ± 0.0222	0.33416 ± 0.02635		
SavageW1 - 170 cm	29.9389	0.4095	0.2813 ± 0.0185	0.25568 ± 0.02422		
SavageW1 - 223 cm	29.9586	0.4009	0.2703 ± 0.0212	0.23792 ± 0.02618		
SavageW1 - 270 cm	23.9162	0.3829	0.2125 ± 0.0266	0.21091 ± 0.03741		
Savage West 2 profile					$5.7 \pm 2.3 \times 10^{12}$	
SavageW2 - 62 cm	24.6849	0.427	0.2517 ± 0.0206	0.28598 ± 0.03252		
SavageW2 - 112 cm	31.3605	0.4035	0.3656 ± 0.0206	0.32365 ± 0.02475		
SavageW2 - 162 cm	24.064	0.3935	0.2104 ± 0.0233	0.21419 ± 0.03435		
SavageW2 - 212 cm	29.7715	0.3833	0.2442 ± 0.0219	0.20115 ± 0.02609		
SavageW2 - 255 cm	25.268	0.4006	0.1458 ± 0.0147	0.12950 ± 0.02457		
Fish Creek 1 profile					$37.4 \pm 3.1 \times 10^5$	
Fish1 - 120 cm	30.3538	0.4505	1.561 ± 0.0595	1.74737 ± 0.07179		
Fish1 - 156 cm	30.1143	0.3981	1.706 ± 0.0852	1.69958 ± 0.08977		
Fish1 - 190 cm	27.5137	0.4105	0.8612 ± 0.0368	0.94677 ± 0.04618		
Fish1 - 269 cm	26.2675	0.3794	0.3711 ± 0.0255	0.36665 ± 0.03288		
Fish1 - 319 cm	25.5134	0.4035	0.3126 ± 0.0246	0.33313 ± 0.03445		

* Carrier concentration = 1155 ppm ^9Be.

[†] AMS measurements from Purdue Rare Isotope Measurement Laboratory (PRIME lab), using the ^{10}Be standard, 07KNSTD.

[‡] Ratio to concentration conversion and error propagation following routine outlined by G. Balco (http://hess.ess.washington.edu/math/docs/common/ams_data_reduction/). Mean background determined from 3 sample blanks = 1.24 ± 0.42 $(\times 10^5)$ (atoms/g quartz) and subtracted from measured values.

[§] Exposure ages determined with the CRONUS calculator v2.2, using the standard configuration and calibration datasets.

Figure B.3. TCN depth profile results for the Pott's Bluff and Savage West 1 sites. All plots shown with depth on the y-axis for an intuitive representation of the profile points. Depths are shifted by subtracting the amount of fine-grained cover sediment, such that 0 cm depth shown in these plots represents the top of the terrace gravels. (a) Pott's Bluff results as the natural log of concentration vs. depth. (b) Savage West 1 results as the natural log of concentration vs. depth. (c) Pott's Bluff results shown as concentration vs. depth. (d) Savage West 1 shown as concentration vs. depth. Plots (a) and (b) are fit with a least squares regression with the corresponding linear equation and R^2 value shown. Plots (c) and (d) are fit by a logarithmic least squares regression with the corresponding fit equation and R^2 value shown. Regressions shown on (c) and (d) are projected beyond the data to illustrate the shape of the curve.
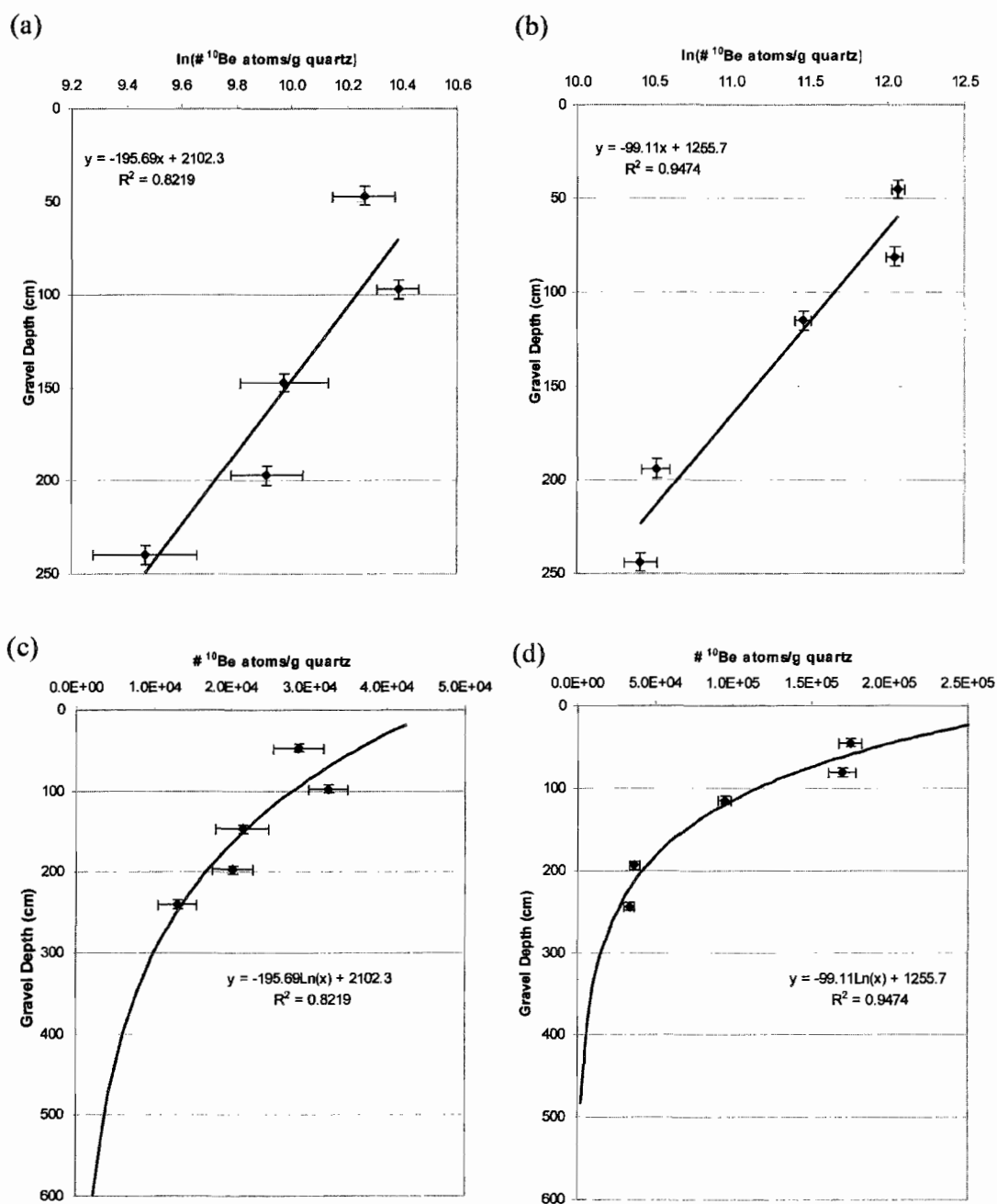
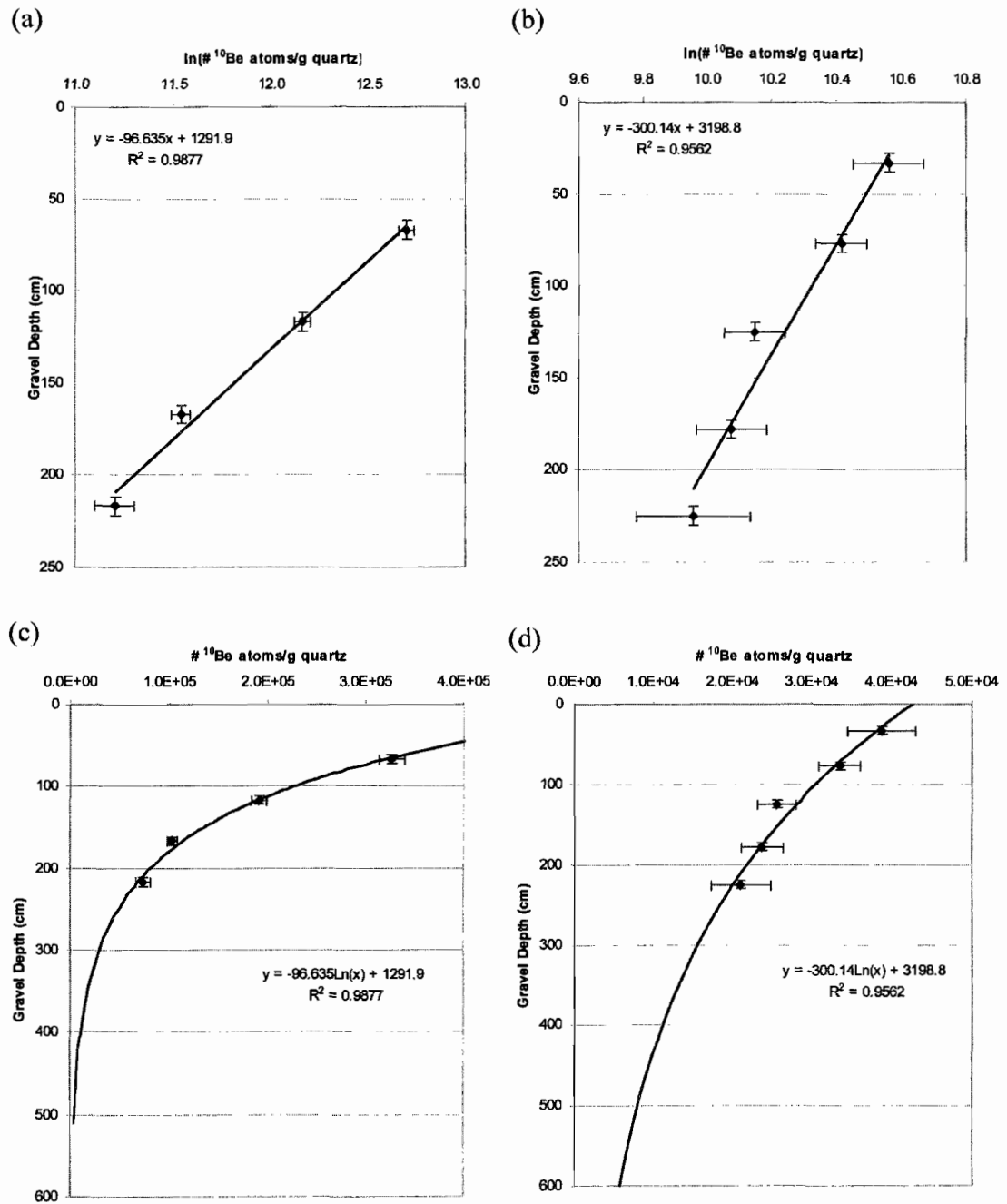Figure B.3 (continued). TCN depth profile results for the Savage West 2 and Fish Creek 1 sites. All plots shown with depth on the y-axis for an intuitive representation of the profile points. Depths are shifted by subtracting the amount of fine-grained cover sediment, such that 0 cm depth shown in these plots represents the top of the terrace gravels. (a) Savage West 2 results as the natural log of concentration vs. depth. (b) Fish Creek 1 results as the natural log of concentration vs. depth. (c) Savage West 2 results shown as concentration vs. depth. (d) Fish Creek 1 shown as concentration vs. depth. Plots (a) and (b) are fit with a least squares regression with the corresponding linear equation and R^2 value shown. Plots (c) and (d) are fit by a logarithmic least squares regression with the corresponding fit equation and R^2 value shown. Regressions shown on (c) and (d) are projected beyond the data to illustrate the shape of the curve.

REFERENCES

Chapter II

Athey, J., Newberry, R., Werdon, M., Freeman, L., Smith, R., and Szumigala, D., 2006, Bedrock geologic map of the Liberty Bell area, Fairbanks A-4 Quadrangle, Bonnifield mining district, Alaska: Alaska Division of Geological & Geophysical Surveys Report of Investigation 2006-2 v. 1.0.1, 98 p., 1 sheet, scale 1:50,000.

Bemis, S.P., 2004, Neotectonic framework of the north-central Alaska Range foothills [M.S. Thesis]: University of Alaska Fairbanks, 142 p.

Bemis, S.P., and Wallace, W.K., 2007, Neotectonic framework of the north-central Alaska Range foothills, *in* Ridgway, K., Trop, J., Glen, J., and Fisher, M. eds., Tectonic Growth of a Collisional Continental Margin: Crustal Evolution of Southern Alaska, Geological Society of America Special Paper 431, p. 549-572.

Capps, S.R., 1912, The Bonnifield region, Alaska: U.S. Geological Survey Bulletin 501, 64 p.

Carver, G., Plafker, G., Metz, M., Cluff, L., Bemis, S.P., Roddick, J., Redington, J., and Sorenson, S., 2006, Late Quaternary growth of thrust faults and associated folds in the eastern part of the Northern Foothills Fold and Thrust Belt, central Alaska Range, Alaska, *in* AGU Chapman Conference on Active Tectonics and Seismic Potential of Alaska, Girdwood, Alaska.

Carver, G.A., Bemis, S.P., Solie, D.N., and Obermiller, K.E., 2008, Active and potentially active faults in or near the Alaska Highway corridor, Delta Junction to Dot Lake, Alaska: Alaska Division of Geological & Geophysical Surveys Preliminary Interpretive Report 2008-3D, 32 p.

Dortch, J.M., 2006, Defining the timing of glaciation in the central Alaska Range using terrestrial cosmogenic nuclide and optically stimulated luminescence dating of moraines and terraces [M.S. thesis]: University of Cincinnati, 77 p.

Dusel-Bacon, C., Wooden, J.L., and Hopkins, M.J., 2004, U-Pb zircon and geochemical evidence for bimodal mid-Paleozoic magmatism and syngenetic base-metal mineralization in the Yukon-Tanana terrane, Alaska: Geological Society of America Bulletin, v. 116, no. 7-8, p. 989-1015.

Fletcher, and Christensen, 1996, A determination of source properties of large intraplate earthquakes in Alaska: Pure and Applied Geophysics, v. 146, no. 1, p. 21-41.

Freymueller, J.T., Woodard, H., Cohen, S.C., Cross, R., Elliott, J., Larsen, C.F., Hreinsdóttir, S., and Zweck, C., 2008, Active Deformation Processes in Alaska, Based on 15 Years of GPS Measurements, *in* Freymueller, J.T., Haeussler, P.J., Wesson, R., and Ekström, G. eds., Active Tectonics and Seismic Potential of Alaska, American Geophysical Union Geophysical Monograph Series 179, p. 1-42.

Gibbard, P.L., Head, M.J., Walker, M.J.C., and Stratigraphy, T.S.O.Q., 2010, Formal ratification of the Quaternary System/Period and the Pleistocene Series/Epoch with a base at 2.58 Ma: Journal of Quaternary Science, v. 25, no. 2, p. 96-102.

Haeussler, P.J., 2008, An overview of the neotectonics of interior Alaska: Far-field deformation from the Yakutat Microplate collision, *in* Freymueller, J.T., Haeussler, P.J., Wesson, R.L., and Ekstrom, G. eds., Active Tectonics and Seismic Potential of Alaska, American Geophysical Union Geophysical Monograph Series 179, p. 83-109.

Reger, R., Stevens, D., and Solie, D., 2008, Surficial-geologic map, Delta Junction to Dot Lake, Alaska Highway Corridor: Alaska Division of Geological and Geophysical Surveys Preliminary Interpretive Report 2008-3A, 48 p.

Ridgway, K.D., Thoms, E.E., Layer, P.W., Lesh, M.E., White, J.M., and Smith, S.V., 2007, Neogene transpressional foreland basin development on the north side of the central Alaska Range, Usibelli Group and Nenana Gravel, Tanana basin, *in* Ridgway, K.D., Trop, J., Glen, J.M., and Fisher, M.J. eds., Tectonic Growth of a Collisional Continental Margin: Crustal Evolution of Southern Alaska, Geological Society of America Special Paper, p. 507-547.

Ridgway, K.D., Trop, J.M., and Jones, D.E., 1999, Petrology and provenance of the Neogene Usibelli Group and Nenana Gravel; implications for the denudation history of the central Alaska Range: Journal of Sedimentary Research, v. 69, no. 6, p. 1262-1275.

Ruppert, N.A., Ridgway, K.D., Freymueller, J.T., Cross, R.S., and Hansen, R.A., 2008, Active Tectonics of Interior Alaska: Seismicity, GPS Geodesy, and Local Geomorphology, *in* Freymueller, J.T., Haeussler, P.J., Wesson, R., and Ekström, G. eds., Active Tectonics and Seismic Potential of Alaska, Geophysical Monograph Series 179, American Geophysical Union, p. 109-133.

Suppe, J., 1983, Geometry and kinematics of fault-bend folding: American Journal of Sciences, v. 283, no. 7, p. 684-721.

Thoms, E.E., 2000, Late Cenozoic unroofing sequence and foreland basin development of the central Alaska Range: Implications from the Nenana Gravel [M.S. Thesis]: University of Alaska Fairbanks, 221 p.

Thorson, R.M., 1986, Late Cenozoic glaciation of the northern Nenana River valley, *in* Hamilton, T., Reed, K., and Berg, H. eds., Glaciation in Alaska—The Geologic Record, Alaska Geological Society, Fairbanks, Alaska, p. 99-122.

Wahrhaftig, C., 1970a, Geologic map of the Fairbanks A-2 quadrangle, Alaska: U.S. Geological Survey Geologic Quadrangle Map GQ-808, 1 sheet, scale 1:63,360.

Wahrhaftig, C., 1970b, Geologic map of the Fairbanks A-3 quadrangle, Alaska: U.S. Geological Survey Geologic Quadrangle Map GQ-809, 1 sheet, scale 1:63,360.

Wahrhaftig, C., 1970c, Geologic map of the Fairbanks A-4 quadrangle, Alaska: U.S. Geological Survey Geologic Quadrangle Map GQ-810, 1 sheet, scale 1:63,360.

Wahrhaftig, C., 1970d, Geologic map of the Fairbanks A-5 quadrangle, Alaska: U.S. Geological Survey Geologic Quadrangle Map GQ-811, 1 sheet, scale 1:63,360.

Wahrhaftig, C., 1970e, Geologic map of the Healy D-2 quadrangle, Alaska: U.S. Geological Survey Geologic Quadrangle Map GQ-804, 1 sheet, scale 1:63,360.

Wahrhaftig, C., 1970f, Geologic map of the Healy D-3 quadrangle, Alaska: U.S. Geological Survey Geologic Quadrangle Map GQ-805, 1 sheet, scale 1:63,360.

Wahrhaftig, C., 1970g, Geologic map of the Healy D-4 quadrangle, Alaska: U.S. Geological Survey Geologic Quadrangle Map GQ-806, 1 sheet, scale 1:63,360.

Wahrhaftig, C., 1970h, Geologic map of the Healy D-5 quadrangle, Alaska: U.S. Geological Survey Geologic Quadrangle Map GQ-807, 1 sheet, scale 1:63,360.

Wahrhaftig, C., 1958, Quaternary geology of the Nenana River valley and adjacent part of the Alaska Range, *in* Wahrhaftig, C. and Black, R.F. eds., Quaternary and Engineering geology in the Central Part of the Alaska Range, U.S. Geological Survey Professional Paper 293, Washington D.C., p. 1-73.

Wahrhaftig, C., 1968, Schists of the central Alaska Range: U.S. Geological Survey Bulletin 1254-E, 22 p.

Wahrhaftig, C., 1987, The Cenozoic section at Suntrana, Alaska: Centennial Field Guide Volume 1: Cordilleran Section of the Geological Society of America, v. 1, p. 445-450.

Wahrhaftig, C., Wolfe, J.A., Leopold, E.B., and Lanphere, M., 1969, The coal-bearing group in the Nenana Coal Field: U.S. Geological Survey Bulletin 1274-D.

Chapter III

Amos, C.B., Burbank, D.W., Nobes, D.C., and Read, S.A.L., 2007, Geomorphic constraints on listric thrust faulting: Implications for active deformation in the Mackenzie Basin, South Island, New Zealand: Journal of Geophysical Research (Solid Earth), v. 112, p. B03S11.

Athey, J., Newberry, R., Werdon, M., Freeman, L., Smith, R., and Szumigala, D., 2006, Bedrock geologic map of the Liberty Bell area, Fairbanks A-4 Quadrangle, Bonnifield mining district, Alaska: Alaska Division of Geological & Geophysical Surveys Report of Investigation 2006-2 v. 1.0.1, 98 p., 1 sheet, scale 1:50,000.

Beget, J.E., 2001, Continuous Late Quaternary proxy climate records from loess in Beringia: Quaternary Science Reviews, v. 20, no. 1-3, p. 499-507.

Begét, J.E., and Keskinen, M., 1991, The Stampede tephra: a middle Pleistocene marker bed in glacial and eolian deposits of central Alaska: Canadian Journal of Earth Sciences, v. 28, no. 7, p. 991-1002.

Bemis, S.P., 2004, Neotectonic framework of the north-central Alaska Range foothills [M.S. Thesis]: University of Alaska Fairbanks, 142 p.

Bemis, S.P., and Wallace, W.K., 2007, Neotectonic framework of the north-central Alaska Range foothills, *in* Ridgway, K., Trop, J., Glen, J., and Fisher, M. eds., Tectonic Growth of a Collisional Continental Margin: Crustal Evolution of Southern Alaska, Geological Society of America Special Paper 431,, p. 549-572.

Berger, A.L., Gulick, S.P.S., Spotila, J.A., Upton, P., Jaeger, J.M., Chapman, J.B., Worthington, L.A., Pavlis, T.L., Ridgway, K.D., Willems, B.A., and McAleer, R.J., 2008, Quaternary tectonic response to intensified glacial erosion in an orogenic wedge: Nature Geosci, v. 1, no. 11, p. 793-799.

Briner, J.P., and Kaufman, D.S., 2008, Late Pleistocene mountain glaciation in Alaska: key chronologies: Journal of Quaternary Science, v. 23, no. 6-7, p. 659-670.

Brozovic, N., Burbank, D.W., and Meigs, A.J., 1997, Climatic Limits on Landscape Development in the Northwestern Himalaya: Science, v. 276, no. 5312, p. 571-574.

Burgette, R.J., 2008, Uplift in response to tectonic convergence: The Kyrgyz Tien Shan and Cascadia subduction zone [Ph.D. dissertation]: University of Oregon.

Carrapa, B., 2009, Tracing exhumation and orogenic wedge dynamics in the European Alps with detrital thermochronology: Geology, v. 37, no. 12, p. 1127-1130.

Carver, G., Plafker, G., Metz, M., Cluff, L., Bemis, S.P., Roddick, J., Redington, J., and Sorenson, S., 2006, Late Quaternary growth of thrust faults and associated folds in the eastern part of the Northern Foothills Fold and Thrust Belt, central Alaska Range, Alaska, *in* AGU Chapman Conference on Active Tectonics and Seismic Potential of Alaska, Girdwood, Alaska.

Carver, G.A., Bemis, S.P., Solie, D.N., and Obermiller, K.E., 2008, Active and potentially active faults in or near the Alaska Highway corridor, Delta Junction to Dot Lake, Alaska: Alaska Division of Geological & Geophysical Surveys Preliminary Interpretive Report 2008-3D, 32 p.

Chapple, W.M., 1978, Mechanics of thin-skinned fold-and-thrust belts: Geological Society of America Bulletin, v. 89, no. 8, p. 1189-1198.

Dahlen, F.A., Suppe, J., and Davis, D., 1984, Mechanics of fold-and-thrust belts and accretionary wedges: cohesive coulomb theory: Journal of Geophysical Research, v. 89, no. B12, p. 10,087–10,101.

Davis, D., Suppe, J., and Dahlen, F.A., 1983, Mechanics of fold-and-thrust belts and accretionary wedges: Journal of Geophysical Research, v. 88, no. B2, p. 1153-1172.

Dixon, J.M., and Liu, S., 1992, Centrifuge modelling of the propagation of thrust faults, *in* McClay, K.R. ed., Thrust Tectonics, Chapman & Hall, London, p. 53-69.

Dortch, J.M., 2006, Defining the timing of glaciation in the central Alaska Range using terrestrial cosmogenic nuclide and optically stimulated luminescence dating of moraines and terraces [M.S. thesis]: University of Cincinnati, 77 p.

Erslev, E.A., 1991, Trishear fault-propagation folding: Geology, v. 19, no. 6, p. 617-620.

Fisher, D., Mosher, D., Austin, J.A., Gulick, S.P., Masterlark, T., and Moran, K., 2007, Active deformation across the Sumatran forearc over the December 2004 Mw9.2 rupture: Geology, v. 35, no. 2, p. 99-102.

Fisher, M.A., Pellerin, L., Nokleberg, W.J., Ratchkovski, N.A., and Glen, J.M., 2007, Crustal structure of the Alaska Range orogen and Denali fault along the Richardson Highway: Special Paper 431: Tectonic Growth of a Collisional Continental Margin: Crustal Evolution of Southern Alaska, v. 431, p. 43-53.

Fisher, M.A., Ratchkovski, N.A., Nokleberg, W.J., Pellerin, L., and Glen, J.M.G., 2004, Geophysical Data Reveal the Crustal Structure of the Alaska Range Orogen within the Aftershock Zone of the Mw 7.9 Denali Fault Earthquake: Bulletin of the Seismological Society of America, v. 94, no. 6B, p. S107-131.

Fitzgerald, P.G., Sorkhabi, R.B., Redfield, T.F., and Stump, E., 1995, Uplift and denudation of the central Alaska Range: A case study in the use of apatite fission track thermochronology to determine absolute uplift parameters: Journal of Geophysical Research (Solid Earth), v. 100, no. B10, p. 20,175-20,191.

Gibbard, P.L., Head, M.J., Walker, M.J.C., and Stratigraphy, T.S.O.Q., 2010, Formal ratification of the Quaternary System/Period and the Pleistocene Series/Epoch with a base at 2.58 Ma: Journal of Quaternary Science, v. 25, no. 2, p. 96-102.

Haeussler, P.J., 2008, An overview of the neotectonics of interior Alaska: Far-field deformation from the Yakutat Microplate collision, in Freymueller, J.T., Haeussler, P.J., Wesson, R.L., and Ekstrom, G. eds., Active Tectonics and Seismic Potential of Alaska, American Geophysical Union Geophysical Monograph Series 179, p. 83-109.

Haeussler, P.J., Saltus, R.W., Ruppert, N.A., and Karl, S.M., 2008, Evidence for Pliocene to present thrust faulting on the south side of the Alaska Range in the vicinity of the Peters Hills piggyback basin: EOS Transactions, AGU Fall Meeting Abstracts, v. 44, p. 08.

Hanson, K., Berg, E., and Gedney, L., 1968, A seismic refraction profile and crustal structure in central interior Alaska: Bulletin of the Seismological Society of America, v. 58, no. 5, p. 1657-1665.

Henstock, T.J., McNeill, L.C., and Tappin, D.R., 2006, Seafloor morphology of the Sumatran subduction zone: Surface rupture during megathrust earthquakes?: Geology, v. 34, no. 6, p. 485-488.

Manley, W.F., and Kaufman, D.S., 2002, Alaska PaleoGlacier Atlas: http://instaar.colorado.edu/qgisl/ak_paleoglacier_atlas,

Molnar, P., Brown, E.T., Burchfiel, B.C., Deng, Q., Feng, X., Li, J., Raisbeck, G.M., Shi, J., Wu, Z., Yiou, F., and You, H., 1994, Quaternary climate change and the formation of river terraces across growing anticlines on the north flank of the Tien Shan, China: The Journal of Geology, v. 102, no. 5, p. 583-602.

Naylor, M., and Sinclair, H., 2007, Punctuated thrust deformation in the context of doubly vergent thrust wedges: Implications for the localization of uplift and exhumation: Geology, v. 35, no. 6, p. 559-562.

Pazzaglia, F.J., Gardner, T., and Merritts, D., 1998, Bedrock fluvial incision and longitudinal profile development over geologic time scales determined by fluvial terraces, *in* Rivers over rock: Fluvial process in bedrock channels, AGU Geophysical Monograph, Washington D.C., p. 207-236.

Péwé, T., Westgate, J.A., Preece, S., Brown, P., and Leavitt, S., 2009, Late Pliocene Dawson Cut Forest Bed and new tephrochronological findings in the Gold Hill Loess, east-central Alaska: Geological Society of America Bulletin, v. 121, no. 1-2, p. 294-320.

Plafker, G., Gilpin, L., and Lahr, J., 1994, Neotectonic Map of Alaska, *in* Plafker, G. and Berg, H. eds., The Geology of Alaska, Boulder, Colorado, Geological Society of America, Geology of North America, v. G-1, plate 12, 1:2,500,000.

Price, R.A., 2001, An evaluation of models for the kinematic evolution of thrust and fold belts: structural analysis of a transverse fault zone in the Front Ranges of the Canadian Rockies north of Banff, Alberta: Journal of Structural Geology, v. 23, no. 6-7, p. 1079-1088.

Reger, R., Stevens, D., and Solie, D., 2008, Surficial-geologic map, Delta Junction to Dot Lake, Alaska Highway Corridor: Alaska Division of Geological and Geophysical Surveys Preliminary Interpretive Report 2008-3A, 48 p.

Ridgway, K.D., Thoms, E.E., Layer, P.W., Lesh, M.E., White, J.M., and Smith, S.V., 2007, Neogene transpressional foreland basin development on the north side of the central Alaska Range, Usibelli Group and Nenana Gravel, Tanana basin, *in* Ridgway, K.D., Trop, J., Glen, J.M., and Fisher, M.J. eds., Tectonic Growth of a Collisional Continental Margin: Crustal Evolution of Southern Alaska, Geological Society of America Special Paper,, p. 507-547.

Ritter, D.F., 1982, Complex river terrace development in the Nenana Valley near Healy, Alaska: Geological Society of America Bulletin, v. 93, no. 4, p. 346-356.

Seeber, L., and Sorlien, C.C., 2000, Listric thrusts in the western Transverse Ranges, California: Geological Society of America Bulletin, v. 112, no. 7, p. 1067-1079.

Sherwood, K.W., and Craddock, C., 1979, General geology of the central Alaska Range between the Nenana River and Mount Deborah: Alaska Division of Geological and Geophysical Surveys Open-File Report 116, 24 p., 3 sheets, scale 1:63,360,

Suppe, J., 1983, Geometry and kinematics of fault-bend folding: American Journal of Sciences, v. 283, no. 7, p. 684-721.

Suppe, J., and Medwedeff, D., 1990, Geometry and kinematics of fault-propagation folding: Eclogae Geologicae Helvetiae, v. 83, no. 3, p. 409-454.

Thoms, E.E., 2000, Late Cenozoic unroofing sequence and foreland basin development of the central Alaska Range: Implications from the Nenana Gravel [M.S. Thesis]: University of Alaska Fairbanks, 221 p.

Thorson, R.M., 1986, Late Cenozoic glaciation of the northern Nenana River valley, *in* Hamilton, T., Reed, K., and Berg, H. eds., Glaciation in Alaska—The Geologic Record, Alaska Geological Society, Fairbanks, Alaska, p. 99-122.

Tomkin, J.H., and Roe, G.H., 2007, Climate and tectonic controls on glaciated critical-taper orogens: Earth and Planetary Science Letters, v. 262, no. 3-4, p. 385-397.

Triplehorn, D.M., Drake, J., and Layer, P.W., 2000, Preliminary 40Ar/39Ar ages from two units in the Usibelli Group, Healy, Alaska: New light on some old problems: Alaska Division of Geological and Geophysical Surveys, Short Notes on Alaskan Geology, Professional Report 119, p. 117-127.

Uba, C.E., Kley, J., Strecker, M.R., and Schmitt, A.K., 2009, Unsteady evolution of the Bolivian Subandean thrust belt: The role of enhanced erosion and clastic wedge progradation: Earth and Planetary Science Letters, v. 281, no. 3-4, p. 134-146.

Veenstra, E., Christensen, D.H., Abers, G.A., and Ferris, A., 2006, Crustal thickness variation in south-central Alaska: Geology, v. 34, no. 9, p. 781-784.

Wahrhaftig, C., 1970a, Geologic map of the Fairbanks A-2 quadrangle, Alaska: U.S. Geological Survey Geologic Quadrangle Map GQ-808, 1 sheet, scale 1:63,360.

Wahrhaftig, C., 1970b, Geologic map of the Fairbanks A-4 quadrangle, Alaska: U.S. Geological Survey Geologic Quadrangle Map GQ-810, 1 sheet, scale 1:63,360.

Wahrhaftig, C., 1970c, Geologic map of the Fairbanks A-5 quadrangle, Alaska: U.S. Geological Survey Geologic Quadrangle Map GQ-811, 1 sheet, scale 1:63,360.

Wahrhaftig, C., 1970d, Geologic map of the Healy D-3 quadrangle, Alaska: U.S. Geological Survey Geologic Quadrangle Map GQ-805, 1 sheet, scale 1:63,360.

Wahrhaftig, C., 1970e, Geologic map of the Healy D-4 quadrangle, Alaska: U.S. Geological Survey Geologic Quadrangle Map GQ-806, 1 sheet, scale 1:63,360.

Wahrhaftig, C., 1970f, Geologic map of the Healy D-5 quadrangle, Alaska: U.S. Geological Survey Geologic Quadrangle Map GQ-807, 1 sheet, scale 1:63,360.

Wahrhaftig, C., 1958, Quaternary geology of the Nenana River valley and adjacent part of the Alaska Range, *in* Wahrhaftig, C. and Black, R.F. eds., Quaternary and Engineering geology in the Central Part of the Alaska Range, U.S. Geological Survey Professional Paper 293, Washington D.C., p. 1-73.

Wahrhaftig, C., 1987, The Cenozoic section at Suntrana, Alaska: Centennial Field Guide Volume 1: Cordilleran Section of the Geological Society of America, v. 1, p. 445-450.

Wahrhaftig, C., Turner, D.L., Weber, F.R., and Smith, T.E., 1975, Nature and timing of movement on Hines Creek strand of Denali fault system, Alaska: Geology, v. 3, no. 8, p. 463-466.

Wang, K., and Hu, Y., 2006, Accretionary prisms in subduction earthquake cycles: The theory of dynamic Coulomb wedge: Journal of Geophysical Research, v. 111, p. B06410.

Wegner, W.W., 1972, The Denali fault (Hines Creek strand) in Northeastern Mt. McKinley National Park, Alaska [M.S. thesis]: University of Wisconsin Madison, 72 p.

Westgate, J.A., Preece, S.J., Froese, D.G., Walter, R.C., Sandhu, A., and Schweger, C.E., 2001, Dating Early and Middle (Reid) Pleistocene Glaciations in Central Yukon by Tephrochronology: Quaternary Research, v. 56, no. 3, p. 335-348.

Whipple, K.X., and Meade, B.J., 2006, Orogen response to changes in climatic and tectonic forcing: Earth and Planetary Science Letters, v. 243, no. 1-2, p. 218-228.

Chapter IV

Athey, J., Newberry, R., Werdon, M., Freeman, L., Smith, R., and Szumigala, D., 2006, Bedrock geologic map of the Liberty Bell area, Fairbanks A-4 Quadrangle, Bonnifield mining district, Alaska: Alaska Division of Geological & Geophysical Surveys Report of Investigation 2006-2 v. 1.0.1, 98 p., 1 sheet, scale 1:50,000.

Bemis, S.P., 2004, Neotectonic framework of the north-central Alaska Range foothills [M.S. Thesis]: University of Alaska Fairbanks, 142 p.

Bemis, S.P., and Wallace, W.K., 2007, Neotectonic framework of the north-central Alaska Range foothills, in Ridgway, K., Trop, J., Glen, J., and Fisher, M. eds., Tectonic Growth of a Collisional Continental Margin: Crustal Evolution of Southern Alaska, Geological Society of America Special Paper 431, p. 549-572.

Bemis, S.P., Weldon, R.J., and Benowitz, J.A., 2006, Does Thrust Belt Width Affect Hinterland Height?: EOS Transactions, AGU Fall Meeting Abstracts, v. 44, p. 03.

Carter, L.D., 1980, Tertiary tillites(?) on the northeast flank of Granite Mountain, central Alaska Range, *in* Alaska Division of Geological & Geophysical Surveys, Short Notes on Alaskan Geology: 1979-1980, Alaska Division of Geological & Geophysical Surveys Geologic Report 63E, p. 23-27.

Carver, G., Plafker, G., Metz, M., Cluff, L., Bemis, S.P., Roddick, J., Redington, J., and Sorenson, S., 2006, Late Quaternary growth of thrust faults and associated folds in the eastern part of the Northern Foothills Fold and Thrust Belt, central Alaska Range, Alaska, *in* AGU Chapman Conference on Active Tectonics and Seismic Potential of Alaska, Girdwood, Alaska.

Carver, G.A., Bemis, S.P., Solie, D.N., and Obermiller, K.E., 2008, Active and potentially active faults in or near the Alaska Highway corridor, Delta Junction to Dot Lake, Alaska: Alaska Division of Geological & Geophysical Surveys Preliminary Interpretive Report 2008-3D, 32 p.

Crone, A.J., Personius, S.F., Craw, P.A., Haeussler, P.J., and Staft, L.A., 2004, The Susitna Glacier Thrust Fault: Characteristics of Surface Ruptures on the Fault that Initiated the 2002 Denali Fault Earthquake: Bulletin of the Seismological Society of America, v. 94, no. 6B, p. S5-22.

Cross, R.S., and Freymueller, J.T., 2008, Evidence for and implications of a Bering plate based on geodetic measurements from the Aleutians and western Alaska: Journal of Geophysical Research, v. 113, p. B07405.

Csejtey, B., Mullen, M., Cox, D., and Stricker, G., 1992, Geology and geochronology of the Healy Quadrangle, south-central Alaska: U.S. Geological Survey Miscellaneous Investigations 1191, 63 p., 1 sheet, 1:250.000 scale.

Eberhart-Phillips, D., Haeussler, P.J., Freymueller, J.T., Frankel, A.D., Rubin, C.M., Craw, P., Ratchkovski, N.A., Anderson, G., Carver, G.A., Crone, A.J., Dawson, T.E., Fletcher, H., Hansen, R., Harp, E.L., Harris, R.A., et al., 2003, The 2002 Denali Fault Earthquake, Alaska: A Large Magnitude, Slip-Partitioned Event: Science, v. 300, p. 1113-1119.

Fitzgerald, P.G., Sorkhabi, R.B., Redfield, T.F., and Stump, E., 1995, Uplift and denudation of the central Alaska Range: A case study in the use of apatite fission track thermochronology to determine absolute uplift parameters: Journal of Geophysical Research (Solid Earth), v. 100, no. B10, p. 20,175-20,191.

Foster, H.L., 1970, Reconnaissance geologic map of the Tanacross quadrangle, Alaska: U.S. Geological Survey Miscellaneous Investigations 593, 1 sheet, scale 1:250,000.

Freymueller, J.T., Woodard, H., Cohen, S.C., Cross, R., Elliott, J., Larsen, C.F., Hreinsdóttir, S., and Zweck, C., 2008, Active Deformation Processes in Alaska, Based on 15 Years of GPS Measurements, *in* Freymueller, J.T., Haeussler, P.J., Wesson, R., and Ekström, G. eds., Active Tectonics and Seismic Potential of Alaska, American Geophysical Union Geophysical Monograph Series 179, p. 1-42.

Haeussler, P.J., 2008, An overview of the neotectonics of interior Alaska: Far-field deformation from the Yakutat Microplate collision, *in* Freymueller, J.T., Haeussler, P.J., Wesson, R.L., and Ekstrom, G. eds., Active Tectonics and Seismic Potential of Alaska, American Geophysical Union Geophysical Monograph Series 179, p. 83-109.

Haeussler, P.J., Saltus, R.W., Ruppert, N.A., and Karl, S.M., 2008, Evidence for Pliocene to present thrust faulting on the south side of the Alaska Range in the vicinity of the Peters Hills piggyback basin: EOS Transactions, AGU Fall Meeting Abstracts, v. 44, p. 08.

Haeussler, P.J., Schwartz, D.P., Dawson, T.E., Stenner, H.D., Lienkaemper, J.J., Sherrod, B., Cinti, F.R., Montone, P., Craw, P.A., Crone, A.J., and Personius, S.F., 2004, Surface Rupture and Slip Distribution of the Denali and Totschunda Faults in the 3 November 2002 M 7.9 Earthquake, Alaska: Bulletin of the Seismological Society of America, v. 94, no. 6B, p. S23-52.

Hamilton, T., 1994, Late Cenozoic glaciation of Alaska, *in* Plafker, G. and Berg, H. eds., The Geology of Alaska, Boulder, Colorado, Geological Society of America, Geology of North America, v. G-1, p. 813-844.

Holmes, G., and Pewe, T.L., 1965, Geologic map of the Mount Hayes D-3 Quadrangle, Alaska: U.S. Geological Survey Geologic Quadrangle Maps 366, 1 sheet, scale 1:63,360.

Lesh, M.E., and Ridgway, K.D., 2007, Geomorphic evidence of active transpressional deformation in the Tanana foreland basin, south-central Alaska, *in* Ridgway, K.D., Trop, J., Glen, J., and Fisher, M. eds., Tectonic Growth of a Collisional Continental Margin: Crustal Evolution of Southern Alaska, Geological Society of America Special Paper 431, p. 573-592.

Lowey, G.W., 1998, A new estimate of the amount of displacement on the Denali Fault system based on the occurrence of carbonate megaboulders in the Dezadeash Formation (Jura-Cretaceous), Yukon, and the Nutzotin Mountains Sequence (Jura-Cretaceous), Alaska: Bulletin of Canadian Petroleum Geology, v. 46, no. 3, p. 379-386.

Mackey, K.G., Fujita, K., Gunbina, L.V., Kovalev, V.N., Imaev, V.S., Koz'min, B.M., and Imaeva, L.P., 1997, Seismicity of the Bering Strait region: Evidence for a Bering block: Geology, v. 25, no. 11, p. 979-982.

Matmon, A., Schwartz, D., Haeussler, P.J., Finkel, R., Lienkaemper, J., Stenner, H., and Dawson, T., 2006, Denali fault slip rates and Holocene-late Pleistocene kinematics of central Alaska: Geology, v. 34, no. 8, p. 645-648.

Mériaux, A., Sieh, K., Finkel, R.C., Rubin, C.M., Taylor, M.H., Meltzner, A.J., and Ryerson, F.J., 2009, Kinematic behavior of southern Alaska constrained by westward decreasing postglacial slip rates on the Denali Fault, Alaska: Journal of Geophysical Research, v. 114, p. B03404.

Nokleberg, W.J., Jones, D.J., and Silberling, N.J., 1985, Origin and tectonic evolution of the Maclaren and Wrangellia terranes, eastern Alaska Range, Alaska: Geological Society of America Bulletin, v. 96, no. 10, p. 1251-1270.

Page, R.A., Plafker, G., and Pulpan, H., 1995, Block rotation in east-central Alaska: A framework for evaluating earthquake potential?: Geology, v. 23, no. 7, p. 629-632.

Plafker, G., Gilpin, L., and Lahr, J., 1994, Neotectonic Map of Alaska, *in* Plafker, G. and Berg, H. eds., The Geology of Alaska, Boulder, Colorado, Geological Society of America, Geology of North America, v. G-1, plate 12, 1:2,500,000.

Reed, J.J., 1961, Geology of the Mount McKinley quadrangle, Alaska: U.S. Geological Survey Bulletin 1108-A, p. A1-A36, 1 sheet, scale 1:250,000.

Richter, D.H., and Matson, N.A., 1971, Quaternary Faulting in the Eastern Alaska Range: Geological Society of America Bulletin, v. 82, no. 6, p. 1529-1540.

Ridgway, K.D., Trop, J.M., Nokleberg, W.J., Davidson, C.M., and Eastham, K.R., 2002, Mesozoic and Cenozoic tectonics of the eastern and central Alaska Range: Progressive basin development and deformation in a suture zone: Geological Society of America Bulletin, v. 114, no. 12, p. 1480-1504.

Ruppert, N.A., 2008, Stress Map for Alaska From Earthquake Focal Mechanisms, *in* Freymueller, J.T., Haeussler, P.J., Wesson, R., and Ekström, G. eds., Active Tectonics and Seismic Potential of Alaska, Geophysical Monograph Series 179, American Geophysical Union, p. 351-367.

Ruppert, N.A., Ridgway, K.D., Freymueller, J.T., Cross, R.S., and Hansen, R.A., 2008, Active Tectonics of Interior Alaska: Seismicity, GPS Geodesy, and Local Geomorphology, *in* Freymueller, J.T., Haeussler, P.J., Wesson, R., and Ekström, G. eds., Active Tectonics and Seismic Potential of Alaska, Geophysical Monograph Series 179, American Geophysical Union, p. 109-133.

Seitz, G.J., Haeussler, P.J., Crone, A.J., Lipovsky, P., and Schwartz, D.P., 2008, Eastern Denali Fault Slip Rate and Paleoseismic History, Kluane Lake Area, Yukon Territory, Canada: Eos (Transactions of the American Geophysical Union), v. 89, no. 53, p. Abstract T53B-1947.

Sherwood, K.W., and Craddock, C., 1979, General geology of the central Alaska Range between the Nenana River and Mount Deborah: Alaska Division of Geological and Geophysical Surveys Open-File Report 116, 24 p., 3 sheets, scale 1:63,360,

St. Amand, P., 1957, Geological and geophysical synthesis of the tectonics of portions of British Columbia, the Yukon Territory, and Alaska: Geological Society of America Bulletin, v. 68, no. 10, p. 1343-1370.

Taylor, M.H., Leprince, S., Avouac, J., and Sieh, K., 2008, Detecting co-seismic displacements in glaciated regions: An example from the great November 2002 Denali earthquake using SPOT horizontal offsets: Earth and Planetary Science Letters, v. 270, p. 209-220.

Thoms, E.E., 2000, Late Cenozoic unroofing sequence and foreland basin development of the central Alaska Range: Implications from the Nenana Gravel [M.S. Thesis]: University of Alaska Fairbanks, 221 p.

Thorson, R.M., 1986, Late Cenozoic glaciation of the northern Nenana River valley, in Hamilton, T., Reed, K., and Berg, H. eds., Glaciation in Alaska—The Geologic Record, Alaska Geological Society, Fairbanks, Alaska, p. 99-122.

Triplehorn, D.M., Drake, J., and Layer, P.W., 2000, Preliminary 40Ar/39Ar ages from two units in the Usibelli Group, Healy, Alaska: New light on some old problems: Alaska Division of Geological and Geophysical Surveys, Short Notes on Alaskan Geology, Professional Report 119, p. 117-127.

Wahrhaftig, C., 1987, The Cenozoic section at Suntrana, Alaska: Centennial Field Guide Volume 1: Cordilleran Section of the Geological Society of America, v. 1, p. 445-450.

Chapter V

Carver, G.A., Bemis, S.P., Solie, D.N., and Obermiller, K.E., 2008, Active and potentially active faults in or near the Alaska Highway corridor, Delta Junction to Dot Lake, Alaska: Alaska Division of Geological & Geophysical Surveys Preliminary Interpretive Report 2008-3D, 32 p.

Page, R.A., Plafker, G., and Pulpan, H., 1995, Block rotation in east-central Alaska: A framework for evaluating earthquake potential?: Geology, v. 23, no. 7, p. 629-632.

Appendix A

Bemis, S.P., and Wallace, W.K., 2007, Neotectonic framework of the north-central Alaska Range foothills, *in* Ridgway, K., Trop, J., Glen, J., and Fisher, M. eds., Tectonic Growth of a Collisional Continental Margin: Crustal Evolution of Southern Alaska, Geological Society of America Special Paper 431, p. 549-572.

Dortch, J.M., 2006, Defining the timing of glaciation in the central Alaska Range using terrestrial cosmogenic nuclide and optically stimulated luminescence dating of moraines and terraces [M.S. thesis]: University of Cincinnati, 77 p.

Thorson, R., 1979, Recurrent late Quaternary faulting near Healy, Alaska: Alaska Division of Geological and Geophysical Surveys, Short Notes on Alaskan Geology - 1978, Geologic Report 61C.

Wahrhaftig, C., 1970, Geologic map of the Healy D-4 quadrangle, Alaska: U.S. Geological Survey Geologic Quadrangle Map GQ-806, 1 sheet, scale 1:63,360.

Appendix B

Balco, G., Stone, J.O., Lifton, N.A., and Dunai, T.J., 2008, A complete and easily accessible means of calculating surface exposure ages or erosion rates from 10Be and 26Al measurements: Quaternary Geochronology, v. 3, no. 3, p. 174-195.

Bronk Ramsey, C., 2008, Deposition models for chronological records: Quaternary Science Reviews, v. 27, no. 1-2, p. 42-60.

Bronk Ramsey, C., 2001, Development of the radiocarbon calibration program OxCal: Radiocarbon, v. 43, no. 2A, p. 355-363.

Bronk Ramsey, C., 1995, Radiocarbon calibration and analysis of stratigraphy: The OxCal program: Radiocarbon, v. 37, no. 2, p. 425-430.

Burgette, R.J., 2008, Uplift in response to tectonic convergence: The Kyrgyz Tien Shan and Cascadia subduction zone [Ph.D. dissertation]: University of Oregon, 242 p.

Marrero, S.M., Borchers, B., Aumer, R., Akkan, H., and Phillips, F.M., 2009, Depth-profile calculator for interpretation of cosmogenic chlorine-36 and beryllium-10 profiles, *in* Geological Society of America Abstracts with Programs, p. 649.

Reimer, P., Baillie, M.G.L., Bard, E., Bayliss, A., Beck, J.W., Bertrand, C.J.H., Blackwell, P.G., Buck, C.E., Burr, G.S., Cutler, K.B., Damon, P.E., Edwards, R.L., Fairbanks, R.G., Friedrich, M., Guilderson, T.P., et al., 2004, IntCal04 Terrestrial Radiocarbon Age Calibration, 0-26 Cal Kyr BP: Radiocarbon, v. 46, no. 3, p. 1029-1058.

Stuiver, M., and Polach, H.A., 1977, Discussion: Reporting of 14C Data: Radiocarbon, v. 19, no. 3, p. 355-364.

Thorson, R.M., and Bender, G., 1985, Eolian deflation by ancient katabatic winds: A late Quaternary example from the north Alaska Range: Geological Society of America Bulletin, v. 96, no. 6, p. 702-709.